Multi-Objective Optimisation of Building Geometry for Energy Consumption and View Quality

By

Zack Xuereb Conti

Supervised by

Dr. Paul Shepherd
Prof. Paul Richens

A thesis submitted for the degree of Master of Philosophy

The University of Bath

Department of Architecture and Civil Engineering

October 2013

Acknowledgements

I would like to sincerely thank Dr. Paul Shepherd and Prof. Paul Richens for their fantastic supervision, for sharing new knowledge but most of all for granting the opportunity to pursue the course. I would also like to show my appreciation towards my colleague and friend Will Pearson for his help, especially during the first few months of this course.

Finally, I would like to dedicate this dissertation to my parents whose love and support contribute to my motivation and passion for the subject.

Abstract

Property developers' strict monetary-yielding objectives are pressuring architects to only prioritise the design variables that directly affect these objectives. The conflicting consequences of their design decisions are being ignored as a result of the shift in priorities and rigid time budgets.

This dissertation tackles the conflict between the design of large glazed facades for maximised vistas, hence increased property value and the consequences of energy consumption. The conflicting objectives are treated as a multi-objective optimisation problem in search for solutions of optimal energy consumption and view quality. This is achieved in the form of an interactive software tool allowing users to modify and constrain the building geometry, simulate the cooling load and assign view values. A view-scoring method is developed in order to quantify and score a view according to the quality of its contents. An interactive evolutionary optimisation tool was implemented within the same software to search for building geometries of reduced cooling loads and high view values.

Table of Contents

Table of Figures

Table of Tables

1. Introduction

1.1. Introduction

An architectural project involves a number of stakeholders ranging from the consultants to the client. Each of these stakeholders put forward several criteria to be satisfied. These criteria affect each other in either a conflicting or complimentary manner depending on the objectives of the design problem. Traditional design processes have long employed the 'dominating-architect' approach whereby the rest of the stakeholders contribute at later stages of the design process and are then constrained within the design parameters set by the architect's dominant 'vision'. This dominant position is also an issue when occupied by the client.

The real-estate developer has established a dominant but restrictive role in the above-mentioned hierarchy of the design process by which the architect is constrained to satisfy their strict and limiting criteria. These criteria generally involve satisfying the minimum required legal-planning requirements yet yielding the maximum profit potential of the site.

This dissertation will deal with a reoccurring scenario of this nature in Mediterranean regions where the client's objective involves maximising the rentable potential value by exploiting the view quality of the site. Such a relationship commonly prompts the architect to design large areas of glazing in order to take full advantage of the view regardless of its orientation. This will in turn increase the rentable value of the property drastically thus satisfying the client's strict criteria. However, this approach ignores the fundamental consideration of the implications on the cooling load of the building caused by the conflicting orientation of the view. Malta will be used throughout this dissertation as a case study region.

Multi-criterion situations are sometimes too complex for the human cognitive process to handle and optimise effectively (Kahneman 2011). This dissertation explores computational methods as potential solutions to the conflicting objectives of view quality and cooling load of a block of apartments as opposed to the traditional approach discussed above. The aim is to achieve a number of solutions which maximise both objectives and which in turn still yield a high rental value for the apartments.

1.2. Research Objectives

The main aim of this research is to achieve optimal apartment building geometries that satisfy maximised view quality yet minimise peak summer cooling loads. It proposes an integrated genetic framework which involves the generation of building solutions, the simulation of the solutions and the search for the optimal solutions which satisfy best the objectives. This involves:

1. Parameterising building geometry into a set of variables.
2. Developing the solar simulation in order to provide the direction of the sun's rays based on location, time and orientation.
3. Developing thermal simulation to calculate the cooling loads in the peak summer months. This also includes the simulation and calculation of projected shadows on windows.
4. Developing a novel method for assessing and quantifying the view quality through each window.
5. Selecting and developing a fast search optimisation algorithm which searches for the best trade-offs between multiple objectives.

The conflicting objectives discussed in Section 1.1 deal with apartment block building typologies. Since the aim of this dissertation is to propose optimal solutions to the conflicting objectives, the parameters will be restricted to this building typology. Parameterisation of any building typology will not be difficult as the framework discussed above is widely applicable. This dissertation will produce an interactive software tool capable of the following:

1. Interactive variables controlling the building geometry.
2. Controllable solar geometry.
3. Real-time mapping of solar radiation on the building mesh
4. Real-time cooling load calculations in the model environment
5. Real-time shadow raytracing
6. Real-time rental value calculation based on habitable area and view quality.
7. Simulation and assessment of the view through the windows from various eye positions in each apartment.

8. Interactive genetic optimiser displaying the plotted solutions for view quality versus cooling load and indicating the Pareto front solutions with the capability to visualise the corresponding building geometries of any plotted solutions.

1.3. Chapter Overview

Chapter 2 will discuss and review past proposals on generative frameworks which involve the optimisation of building envelopes and fenestration geometry with the conflicting objective of minimising energy loads. The simulation components of the proposed generative framework are discussed in Chapter 3 and Chapter 4. The former will discuss the theoretical aspect of calculating the building cooling load whilst the latter discusses the theoretical aspect of the method developed to score and quantify the view quality from each window and it's derivation. Chapter 5 discusses the optimisation component in detail. The generative framework was implemented as a software tool, whose computational framework is discussed in Chapter 6. The software tool is then applied to a case study in Chapter 7. Finally, Chapter 8 concludes this research by discussing how the objectives have been satisfied.

2. Existing Literature

2.1. Introduction

As discussed in Chapter 1, the aim of this research involves two objectives: to minimise the energy consumption and to maximise the view quality from the fenestration of a building. This chapter discusses approaches to optimising the former however there have been no attempts by others to optimisation of the latter to the author's knowledge, particularly in a multi-objective context. The calculation and quantification of the view quality is discussed in Chapter 5.

Section 2.2 will review two main geometric models for optimisation: the optimisation of both the building geometry and the fenestration geometry (Approaches A-B) (2.2.2), and that of the fenestration geometry only (Approaches D-F) (2.2.3). It is a fact that the fenestration geometry has a significant effect on the energy consumption of a building due to the amount of direct solar radiation transmitted through the glazed area (Wright and Mourshed 2009).

Despite the lack of literature on the maximisation of view quality, the objectives considered in the literature are still applicable for comparison due to their conflicting nature with the objective of minimising the energy consumption. The objectives considered include maximising illuminance (daylight) (Caldas and Norford 2003; Shea *et al.* 2006; Gagne and Andersen 2010; Lartigue *et al.* 2013), minimising glare (Gagne and Andersen 2010) and minimising cost (Shea *et al.* 2006; Wright *et al.* 2013).

2.2. Literature Review

2.2.1. Generative Design System (GDS)

The application of natural biological processes in problem solving by computational means has now become a widely researched paradigm (Coello *et al.* 2007). A further step involved integrating this generative design paradigm within larger design frameworks which allowed solutions to evolve to satisfy certain specified criteria.

Caldas & Norford (2002) set a foundation for the integration of performance simulation and evolutionary methods within a generative framework, mainly for the search of optimal low-energy solutions. They presented a Generative Design System (GDS) (Figure 1) which combines a Genetic Algorithm (GA) and building energy simulation software (DOE2.IE) to generate varied solutions (Caldas and Norford 2003). This was eventually developed in the form of a generative software tool known as GENE_ARCH (Caldas 2008).

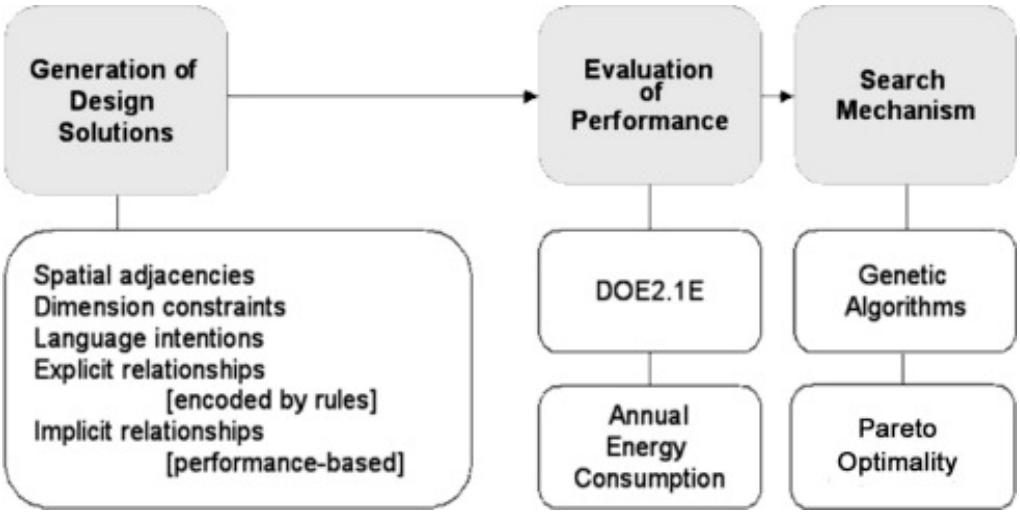

Figure 1: Proposed Generative Design System (Caldas and Norford 2003)

Another example of the integration of an evolutionary solver within a simulation framework is the Thermal Optimisation Program (TOP) proposed by Bouchlaghem (2000). This is discussed further in 2.2.2, Approach B.

This dissertation proposes a similar integrated framework discussed further in 6.1. The following three components are common to all approaches: the selection of the variables, the performance simulation method and the optimisation method.

2.2.2. Building Envelope Optimisation and Fenestration Geometry

This section summarises two approaches (*A* and *B*) by different research teams to reduce the energy consumption by means of the optimisation of both the building envelope and fenestration geometry.

*Approach **A***

Caldas & Norford (2002) first apply their new integrated approach to the placement and sizing of windows to optimise the lighting, heating and cooling performance in an office using a Genetic Algorithm (GA). This research is further developed to deal with multi-objective scenarios and optimisation using a Pareto search GA (Caldas and Norford 2003). The aim was a building shape generator as opposed to fenestration optimisation only. One of the scenarios tested entailed the minimisation of energy consumption for lighting (corresponding the maximising daylight) and the minimisation of energy consumption for heating. The GDS presented by Caldas & Norford (2003) suggests that the designer/user provides the system with a basic layout, the constraints and the relationship between the adjacent spaces (topological information) as opposed to providing the building's exact geometry. Figure 2 visualises the problem set of topological information and constraints which consists of 44 independent variables and generates about 350 dependent variables. What seems to be a simple set of rules can produce a large variety of combinations as displayed in Figure 3.

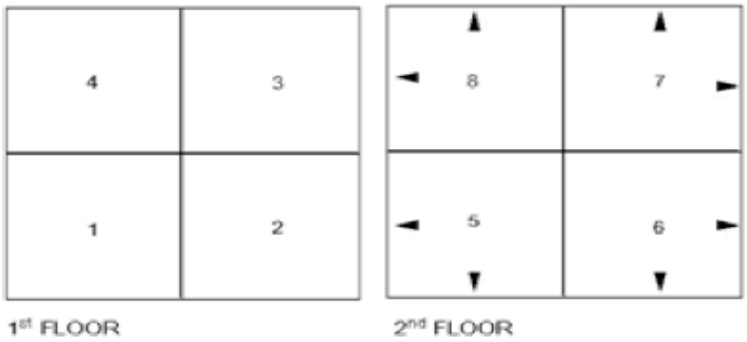

Figure 2: Basic layout for 1st and 2nd floors. Arrows show possible roof tilts. (Caldas and Norford 2003)

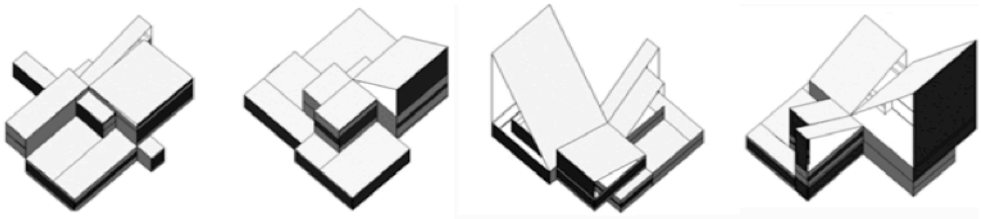

Figure 3: Randomly generated combinations. (Caldas and Norford 2003)

The second GDS component integrates the energy simulation software, DOE2.IE in order to evaluate the generated solutions and return energy and daylight performance feedback to the system. Chicago climatic data was used during the simulation as this provoked an interesting challenge for the GDS to handle due to the conflicting objectives. The conflict would occur when the system would try to enlarge the windows for adequate daylighting and solar gains, however they would be a major source of heat loss during severe winter (Caldas and Norford 2003).

The third component of the GDS searches for Pareto optimality in a population of generated solutions by means of a Genetic Algorithm. This is capable of handling multi-objective optimisation problems such as the one being considered in this dissertation. Pareto Genetic Algorithms avoid the assignment of weighting factors to the objectives and instead look for the best possible trade-offs between the conflicting objectives (Caldas and Norford 2003). GENE_ARCH produced a uniformly sampled, continuos Pareto Front (Figure 4). Figure 4 displays the optimal solution for daylighting on the left, and the optimal solution for minimised heat losses on the right.

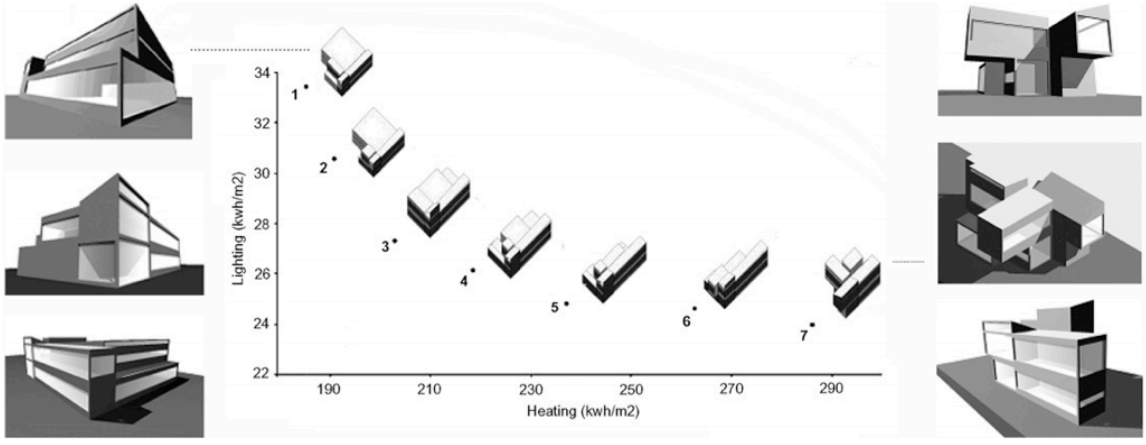

Figure 4: Generated Pareto solutions. (Caldas and Norford 2003)

*Approach **B***

An interesting approach by Bouchlaghem (2000) attempts to achieve optimal thermal comfort by employing numerical optimisation techniques such as the simplex method (Nelder and Mead, as cited in Bouchlaghem 2000) in order to optimise the choice of variables defining the building geometry, the material properties, glazing properties and shading parameters. Bouchlaghem (2000) combines an analytical method for the thermal optimisation and simulation together with a graphical method which deals with the shadowing of the windows. There exist many thermal behaviour prediction models however as stated by Bouchlaghem (2000), "One of the disadvantages of these models is that they are intended for the analysis of a predetermined design solution, not for synthesis of an optimum solution". The thermal optimisation program (TOP) developed by Bouchlaghem is visualised in Figure 5.

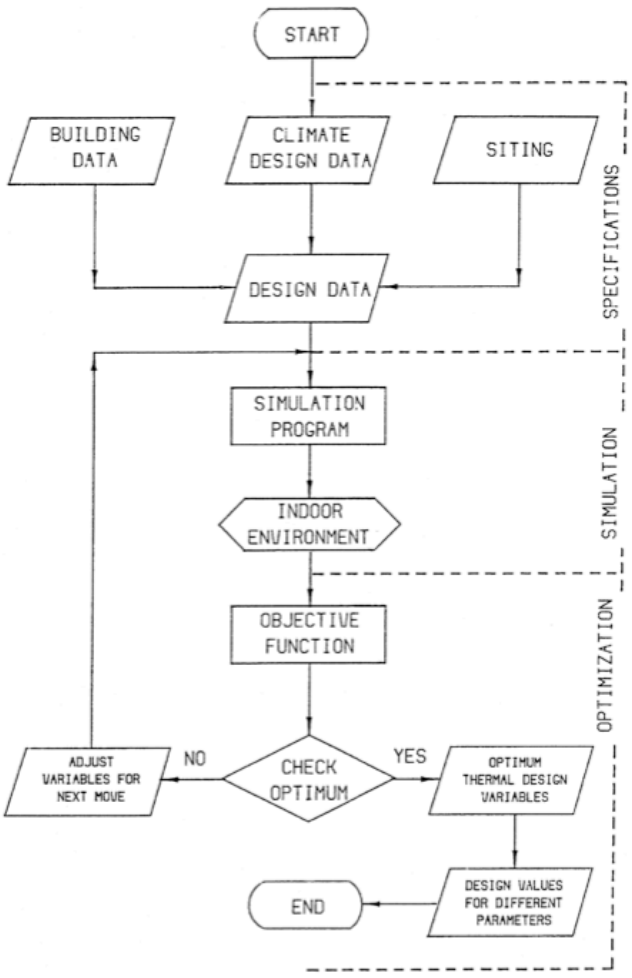

Figure 5: TOP workflow (Bouchlaghem 2000)

The framework is similar to the GDS presented by Caldas & Norford (2003), which is also composed of three main stages: specification, simulation and optimisation. However the optimisation adopted by Bouchlaghem (2000) adjusts the selection of variables when iterating between simulation and optimisation. This is done until the minimum degree of discomfort is reached. Several possible objective functions listed in Table 1 were tested and two were selected based on minimisation criteria and lEast computational expense criteria.

The six objective functions which were tested and compared
D = degree of discomfort. t_{res} = dry resultant temperature (comfort index). t'_{res} = peak dry resultant temperature. t_c = comfort temperature. Δt = comfort band. n = number of coordinates ($n = 24$).

Function	Description
$D_1 = (1/n)\Sigma 24((\lvert t'_{res} - t_c \rvert)/(\Delta t))$	Mean absolute deviation from the comfort level
$D_2 = (1/n)\sqrt{\Sigma_{24}(t_{res} - t_c)^2}$	Root-mean-square deviation
$D_3 = \exp(D_1)$	Exponential of D_1 to emphasize large deviations
$D_4 = \Sigma\{(t_{res} - t_c)^{summer}\}^a + \Sigma\{(t_c - t_{res})^{winter}\}^a$	Separate summations for summer and winter conditions
$D_5 = (1/n)\Sigma(t_{res} - t_c)^3$	Mean of cube deviation
$D_6 = t'_{res} - t_c$	Difference between peak value of t_{drt} and comfort temperature

[a]Only positive values taken.

Table 1: Potential objective functions. (Bouchlaghem 2000)

Bouchlaghem (1996) developed a small program to define the shape of the shadow cast on a window due to overhangs or shading devices. This method was purely geometrical and was not capable of incident radiation calculation (Dubois and Science 1997). Bouchlaghem (2000) later developed a tool known as SUN-SHADE (Bouchlaghem 2000) which was capable of superimposing the window outline on a sunpath diagram for those specific hours of penetration of the sun's rays inside a room.

2.2.3. Fenestration Geometry Optimisation Only

This section summarises four approaches (*C-F*) by different research teams to reduce the energy consumption by means of the optimisation of the fenestration geometry only.

*Approach **C***

Shea et al. (2006) attempt to optimise the energy consumption of the building design by proposing a computational and optimisation tool that facilitates the optimisation for lighting, energy, cost and architectural criteria. However, Shea et al. (2006) focus on maximising lighting performance and minimising cost of panelled building envelopes. The configuration of the envelope is optimised where each panel can have different light transmission properties. Different lighting performance at difference reference points in different spaces can be achieved. The objectives in this scenario also formulate a multi-objective problem similar to the aforementioned approaches. However Shea et al. (2006) employ a Multi-criteria Ant Colony Optimisation (MACO) algorithm as the search and optimisation method. Figure 6 explains the overall workflow. The software Radiance was used for the daylight simulation and calculations. Daylight and sun hours data for each panel on the surface are precompiled,

collected into matrices and used as an input into the optimisation algorithm. The lighting calculations are performed once provided that the geometry of the building envelope does not change.

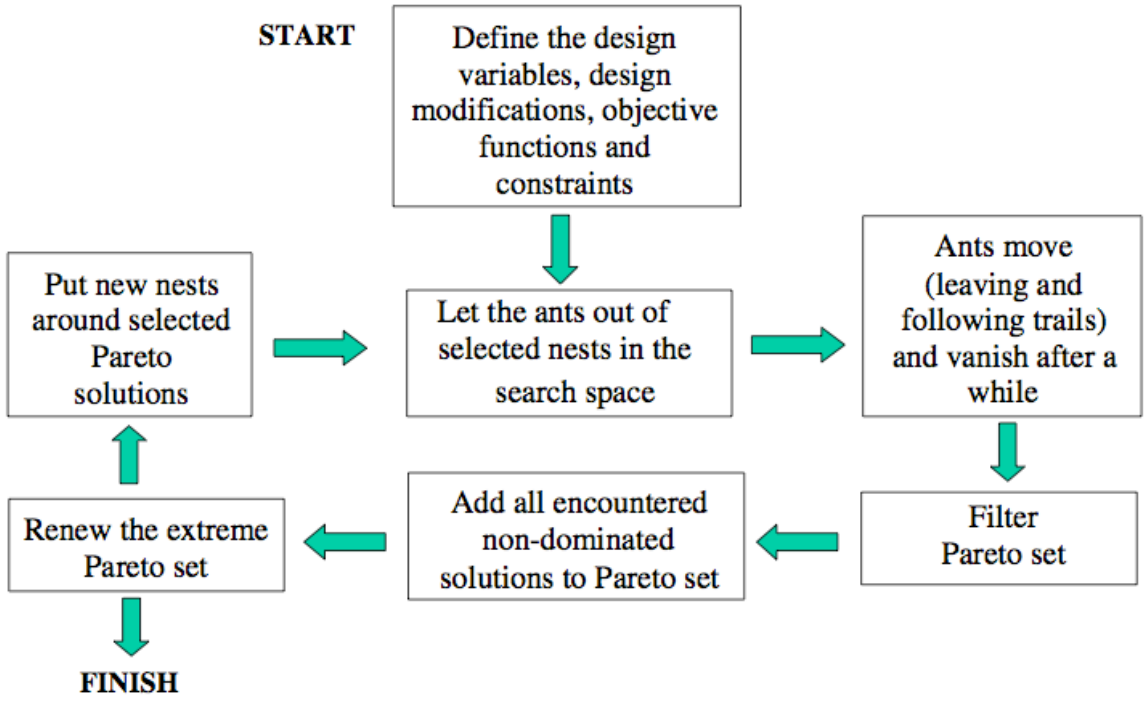

Figure 6: Multi-criteria Ant Colony Optimisation (MACO) algorithm (Shea *et al.* 2006)

The MACO was applied to a case study (Figure 7) consisting of a space subdivided into several internal rooms, all with different lighting requirements to satisfy. The roof and wall panels were subdivided into 1m x 1m panels. The material of each panel can either be opaque, clear glass, diffusing glass or shaded glass. Four types of materials indicated a large number of possible solutions. A reference point (P1-P5) was placed in each room (Figure 8, right). Each reference point required to satisfy different combinations of objectives. For example, P3 required to maximise the daylight factor and minimise the afternoon direct sun in summer. On the other hand, P4 required to maximise daylight factor, maximise the view and also minimise the afternoon direct sun in summer. The view is calculated as an independent criterion. Predefined matrices score the view from the individual reference points (P4 & P5) to a particular object a certain distance away. This will indicate the need for clear glass through the relevant panels in the direction of the view. The conflict occurs when an added window to satisfy the view would also affect the daylight factor. The average daylight factor across all reference points versus total sun hours versus cost solution space was plotted as shown in Figure 8.

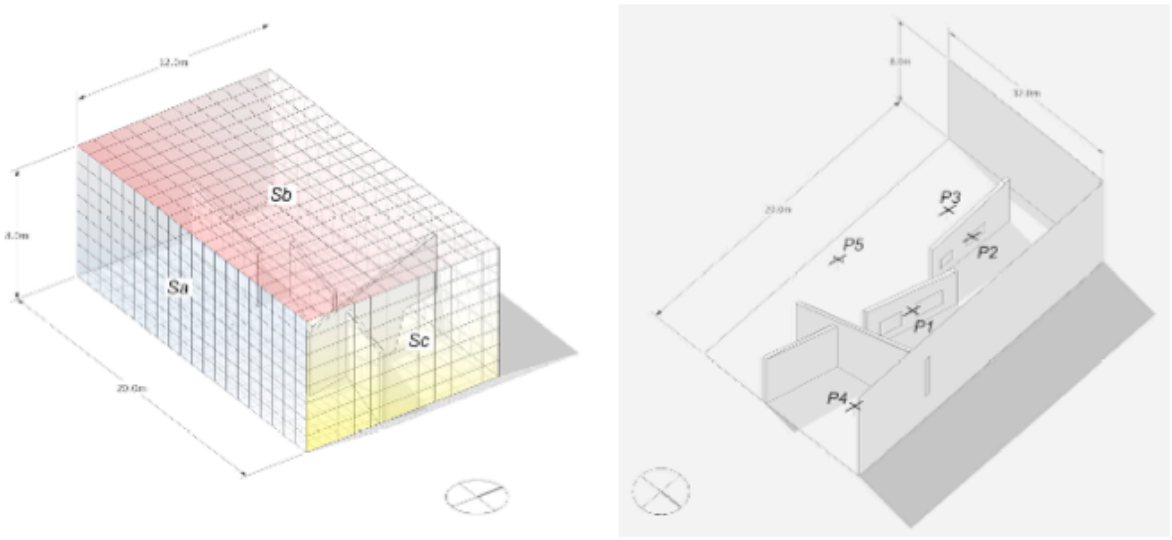

Figure 7: Case study test. (Shea *et al.* 2006)

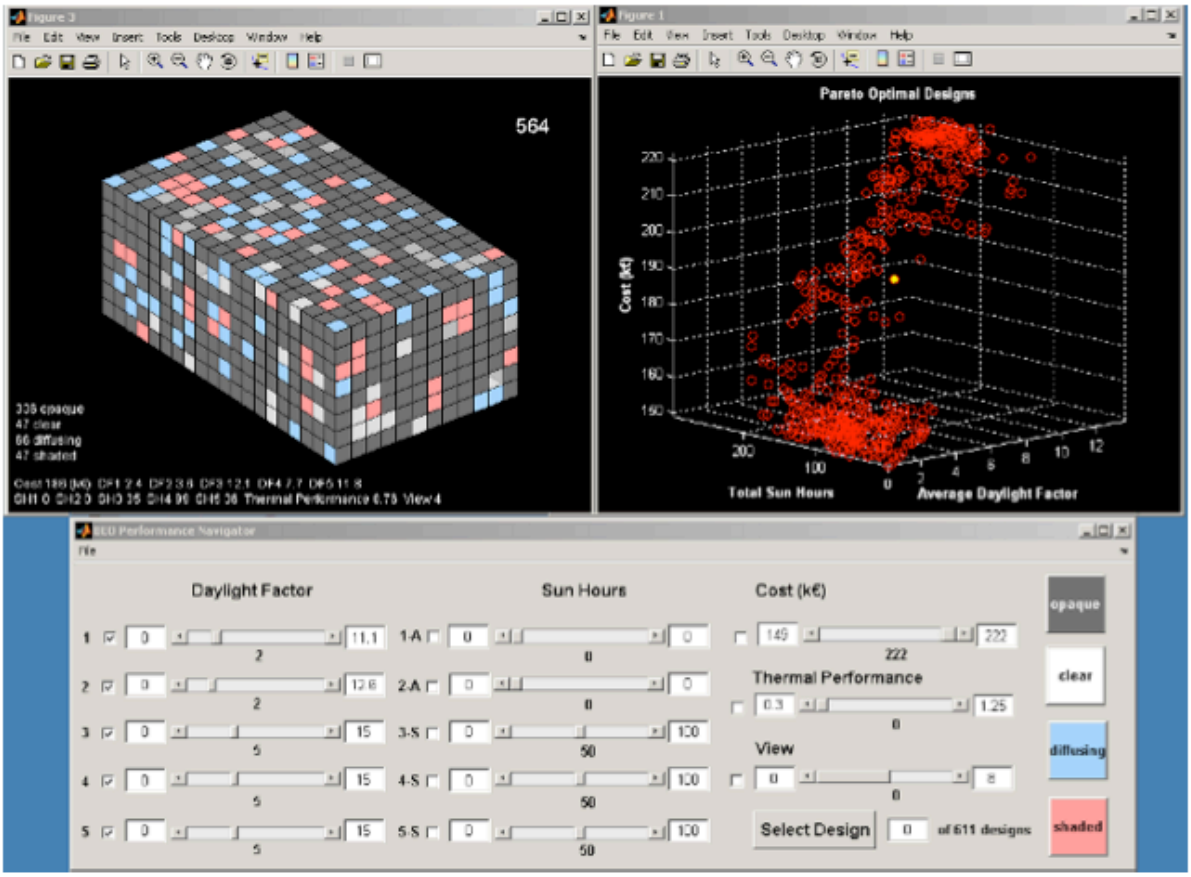

Figure 8: GUI for building envelope optimisation and visualisation of the Pareto solutions. (Shea *et al.* 2006)

Approach ***D***

Wright & Mourshed (2009) achieve an almost free-form fenestration geometry by means of a cellular subdivision method. The authors developed a novel method of allowing more flexibility in the geometry with the aim of optimising energy-use. The number of variables is equivalent to the number of cells where each cell could have one of two states, solid wall construction or transparent glazing (window). Five window constraints were developed in order to give the user more control over the solutions. These consisted of the number of windows, the window area, the window aspect ratio, the window density and the location of the window (indicated with a red cross in Figure 9). EnergyPlus (version 2.0.0.25; Crawley et al. 2001, as cited in Wright and Mourshed 2009) was used to simulate and evaluate the energy-use of each solution. A binary encoded Genetic Algorithm (GA) was employed as the optimisation approach. This suited the nature of the binary encoded variables perfectly.

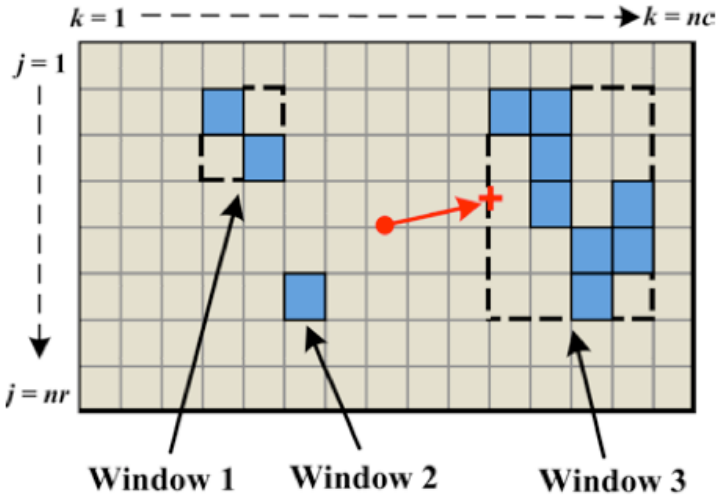

Figure 9: Cellular window facade (Wright and Mourshed 2009)

In later research, Wright et al. (2013) adopted the same cellular approach to dealing with a multi-criterion problem. They attempt to search for optimal fenestration configurations with the objectives of minimising energy consumption and also minimising the construction costs. Their research focuses on searching for optimal solutions of the conflicting objectives by means of a GA. Wright & Mourshed (2009) showed that a GA was able to find near optimal results when applied to a minimisation problem. Wright et al. (2013) discuss the use of Non-dominated Sorting Genetic Algorithm II (NSGA-II) algorithm (Deb *et al.* 2002) as having the best performance in solving multi-objective problems of this nature. As discussed, this

approach is similar in concept to (Shea *et al.* 2006) however lacking the capability of constraining the overall window shape and application of overhangs for shading.

The building energy-use (kWh) takes the annual heating, cooling and electrical use into account whilst the capital cost of the facade is calculated by taking the cost of the opaque construction, the glazed cost and the cost of the overhang into account.

Seeding the initial population of the NSGA-II with feasible solutions resulted in having a positive effect in the case of unconstrained variables.

*Approach **E***

An approach by Gagne & Andersen (2010) allows the user to upload a massing model as an input (Figure 10) together with the desired performance goals thus not requiring the user to have any programming skills. This approach deals with facade optimisation in terms of facade and shading. They first explore a single-objective problem with the objective of maximising illuminance and then proceed onto a multi-objective problem with the objectives of maximising illuminance and minimising glare. The variables considered are visualised in Table 2.

Façade Parameter	Min	Max	Step
Window-to-Wall Ratio	0.1	0.8	0.1
Number of Windows	1	8	1
Aspect Ratio*	Thinnest	Widest	-
Vertical Location*	Lower Bounds	Upper Bounds	-
Horizontal Location*	Right Bounds	Left Bounds	-
Window Distribution*	Windows Touching	Far Apart	-
Overhang	No	Yes	-
Fins	No	Yes	-
Length of Shading Devices	0.5ft	4ft	0.5ft
Total Glass Transmissivity	10%	85%	5%
Percent (Specular) Transmission	0%	100%	12.5%
** Absolute values of max and min for these parameters will depend on user-defined geometry*			

Table 2: List of considered variables (Gagne and Andersen 2010)

A simulation engine known as Lightsolve Viewer (LSV) is adopted to assess the daylight and glare metrics based on sensors placed inside the 3D model as seen in Figure 10. This is similar to the method adopted by Shea et al., (2006). The LSV combines forward raytracing with radiosity and shadow volumes rendering (Cutler et al., as cited in Gagne and Andersen 2010).

A GA-based search method with was adopted for both cases.

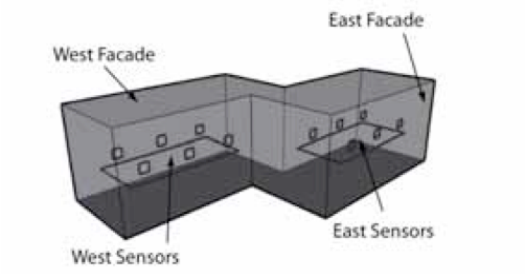

Figure 10: Input 3D massing model. (Gagne and Andersen 2010)

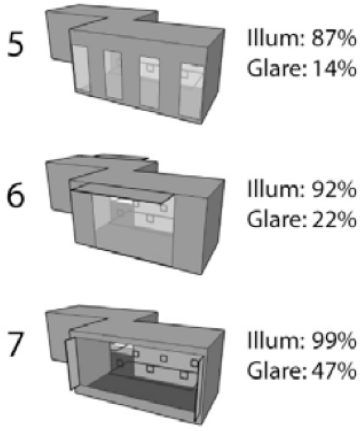

Figure 11: 3 solutions from the Pareto front. (Gagne and Andersen 2010)

This approach is capable of understanding the building information of the input model such as it's location, geometry, orientation and material. The system 'understands' what the role of each face is by specific material names specified by the user. For example, the planes that are to be manipulated by the GA have a specifically labelled material name "GA_WALL" (Gagne and Andersen 2010).

After running the GA for a few generations, the multiple objectives proved to be conflicting, however several solutions came close to satisfying both goals. Figure 11 visualises the resulting variety within a small subset of the Pareto front.

*Approach **F***

An approach by Lartigue, Lasternas, & Loftnes (2013) shares the common, energy consumption optimisation goals as the above approaches A to D. However it deals with three objectives simultaneously: heating loads, cooling loads and daylight duration. The authors claim that daylight and energy consumption are rarely studied simultaneously.

The heating and cooling load objectives were simulated and evaluated respectively by means of the energy simulation software known as TRNSYS (Magnier L & Haghighat F., as cited in Lartigue *et al.* 2013). The daylight objective is presented in the form of the annual daylight duration. Daylight was evaluated as the illuminance flux incident on a surface per unit area by

means of simulation software Dayism. Dayism computes the Radiance algorithm for annual weather data.

The type of window (discrete variable) and the window to wall area ratio (WWR) (continuos variable) were considered as variables (Lartigue *et al.* 2013). These two variables proved to cause conflict between the energy and daylight objectives during the summer months. Increasing the WWR maximises the daylight and solar radiation transmitted to the space during the winter. However it causes unwanted heat-gains during the summer, thus increasing the cooling load. This conflicting situation called for a Pareto approach in search for the best combination of objective values. A posteriori method would then be used to select a singular solution (Lampinen J. as cited in Lartigue *et al.* 2013).

2.2.4. Reflection on The Approaches Reviewed

Generally, such approaches and methods are applied on larger scale projects and most likely employed by non-traditional architecture firms. Traditional firms are most likely to employ the widely used, standard CAD packages only to aid their drafting needs. The same firms will most likely not involve performance consultants on their projects due to time and budget reasons. Some of the literature reviewed in this section involves the development of a software tool, one of which is even applicable to users with no programming skills (Gagne and Andersen 2010). This dissertation not only proposes and explores optimised solutions to the conflicting energy and view objectives but also bridges the applicability of this computational approach for smaller, perhaps more traditional firms. This is reinforced by the fact that the conflict this research is attempting to solve stems from a problem commonly encountered in small projects by small traditional firms.

2.3. Reflection on a Potential Approaches

Although the discussed approaches do not deal with view quality as an objective, they are still very relevant to this dissertation because they still deal with objectives that conflict with minimising energy consumption.

2.3.1. Variables

This dissertation optimises both the fenestration geometry and the building envelope with the aim of exploring the possibilities of self-shaded building geometry. This will further optimise the cooling loads as opposed to post-installed overhangs or shading devices. This research explores the effects of shaded windows (Figure 12) over tilted facades (Figure 13) which produce a larger solar incident angle on the window face. The requirement of self shading thus dictates the geometrical variables to be selected (discussed further in 6.3). The proposed variables allow floors to overhang and facades to incline in either direction provoking shading opportunities.

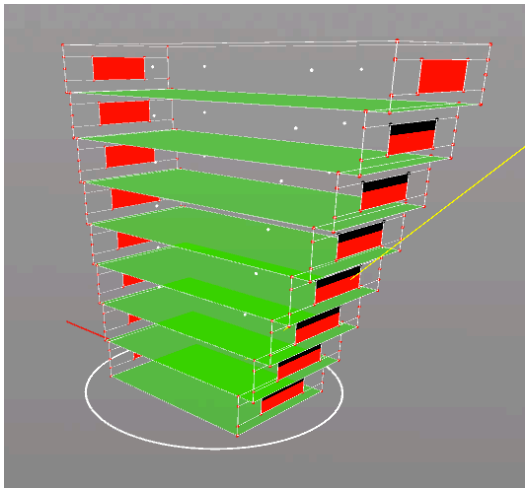

Figure 12: Partially shadowed windows via overhangs.

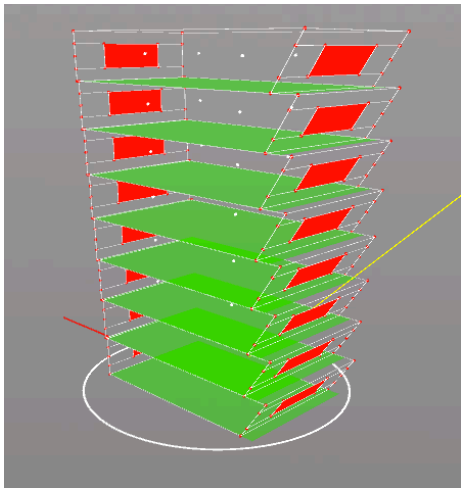

Figure 13: Inclined facades to produce low incident solar angle.

2.3.2. Simulation

This dissertation emphasises on the fact that accurate simulations are not necessary at the early stages of design therefore simplified energy calculations are proposed to be coded and executed within the same environment as opposed to calculations in external simulation packages such as in the case of the afore-discussed publications. This has an advantage to the computational efficiency of the optimisation algorithm. Lower computational efficiency allows near real-time performance calculations as the user interacts with the building geometry and solar position.

2.3.3. Optimisation

This dissertation proposes to adopt a Non-dominated Sorting Genetic Algorithm (NSGA-II) (Deb *et al.* 2002) to search for Pareto solutions, as this has proved to be ideal for multi-objective conflicting scenarios (Wright *et al.* 2013). The NSGA-II avoids the issue of assigning weighting values to an objective function (Caldas and Norford 2003). The latter, is a method adopted in the weighted sum approach. NSGA-II deals with the objectives in their true nature. The weighted sum approach was considered for this dissertation however the two approaches are compared and discussed further in Chapter 5.

3. Thermal Objective

3.1. Introduction

This chapter will discuss the theoretical aspect of obtaining the thermal fitness. One of the objectives being considered in this dissertation minimises the energy consumption of a building during the peak summer months in Malta. Generally, no heating is required during these months because the outdoor temperature is never less than the approximate comfort indoor temperatures, resulting in no heat-loss. The solar intensity is highest during these months. This, will therefore cause conflict when windows are required to maximise South-Eastern and Southern views.

The ultimate goal of the proposed software tool is to aid the user with a real-time idea of the performative consequences as they interact with the variable to vary the building geometry according to their requirements. This may be achieved by reducing the amount of information required and considered to perform the calculations by eliminating redundant information not necessary for early stage design. A simpler calculation method will allow for quicker iterations during the optimisation since each solution in each generation requires to calculate the cooling load. The true priority in the early stage design is quick feedback on the user's decisions rather than accurate calculations.

In this light, the proposed method only considers the transmission of the incident solar radiation into the building as the main contributor to the cooling load, thus ignores loads from casual gains.

3.2. Review of Calculation Methods

Several methods for calculating the cooling load are documented in this section. The criterion for the selection of the appropriate method is based on the requirement for the least tabulated data possible.

3.2.1. Cooling Load Temperature Difference Method (ASHRAE Method)

The cooling load temperature difference calculation method CLTD/CLF (ASHRAE 1979) which was eventually revised to CLTD/SCL/CLF method (Spitler *et al.* 1993) is a simplified version of the transfer function method (TFM) (Spitler & McQuiston 1992, cited by Spitler *et al.* 1993) for calculating cooling load due to heat transfer. The method makes use of a large number of predetermined tabulated data based on a number of variables such as material type, day of the year, time of day, orientation of the surface, wall face orientation of the surface and many more (Spitler *et al.* 1993). This method uses different equations depending for which building element the heat transfer is being calculated.

Heat transfer through walls and roofs uses tabulated predetermined CLTD values derived from the cooling loads of 36 types of roofs and 96 different wall construction types using the TFM. Heat transfer through fenestration was divided into the conductive part and the solar radiation part. Determination of the conductive also uses tabulated predetermined CLTD values for heat transfer in standard conditions. The solar radiation part was calculated uses SCL values (Spitler *et al.* 1993) which take into account the solar heat gain coefficient SHGF and the cooling load factor CLF (ASHRAE 1979).

Although simplified, the method is not ideal for embedding within a software tool due to the large amount of tabulated data. However, this indicated that since the proposed software tool is also capable of calculating the solar position, the cooling load may be determined as a function of the latitude and global solar radiation.

3.2.2. Degree Days

Degree days are calculated as an integral of the difference between the outdoor temperature and an internal base temperature over a specific time interval where,

$$\hat{E} = \lambda \int (\theta_{ao} - \theta_b) dt$$

$$\text{for } \theta_{ao} > \theta_b$$

where $\hat{E}$ is the Degree-day estimated energy demand (kWh)

θ_{ao} is the external temperature

θ_b is the base temperature

(Day *et al.* 2000)

Degree days are segmented into heating degree days and cooling degree days. Naturally, the cooling degree days (CDD) method was considered for the application of this dissertation. As discussed by Prek & Butala (2010) the most accurate method for calculating CDD is by,

$$CDD = \frac{\sum_{j=1}^{24} \left(T_{e,j} - T_b\right)_{\left((T_{e,j} - T_b) > 0\right)}}{24}$$

using hourly outside temperature data $T_{e,j}$ and integrating directly using the base temperature T_b. However, one of the main problems with the degree days approach is that of the base temperature T_b. T_b can be defined as external temperature above which the building does not require heating. It is generally assumed as a general value for buildings. For example, the T_b value in the UK is of 15.5°C. This value was derived by assuming that buildings are generally heated to 19°C subtracted by an average internal heat gain of 3.5°C. This however is misleading and can lead to erroneous assumptions because different buildings require different temperatures and also because internal heat gains vary from building to building varying with number of occupants and equipment depending on the function of the building. The calculations and assumptions in this dissertation are based on the Maltese climate.

3.2.3. LT Method

The LT method is an easy to use manual energy-design tool, eventually compiled into a software (Baker and Steemers 1996). This method is based on passive zones which lie at a maximum distance from the perimeter wall of the floor plan. The zones cater for the positive or negative gains through the fenestration. The LT method presents predetermined values of Annual Primary Consumption per m^2 from the LT Curves for lighting, heating and cooling and also applying any correction factors due to shading devices. Different curves for different orientations are also presented.

The LT method is applicable mostly to office buildings as the curves were derived by assessing large amounts of one building typology. Although simple, the LT method is not suitable for the software tool presented here due to the large amount of predetermined data (LT-curves). The derivations of these curves are not available.

3.2.4. Admittance Method (CIBSE Method)

This method derives and tabulates several data such as the sol-air temperature and the admittances (Y-values) based on conditions (such as solar radiation, outdoor temperature, etc.) that fluctuate sinusoidally over a period of 24 hours (idealistic conditions).

The sol-air temperature is a concept representing the combined effect of radiation and convective heat exchange on the outer surface of the building fabric being considered (Ruivo *et al.* 2013). O'Callaghan & Probert (1977) conclude that relying on pre-determined tabulated sol-air temperatures may be dangerous because meteorological data, behaviour of individual structures in terms of their surface properties may vary thus varying the heat transfer coefficients.

The calculation for the cooling load is composed of two steps: mean heat gains from all sources are calculated separately from the mean internal environmental temperatures. An adapted version of this method is implemented in 3.4.

Essentially, the estimation of the cooling load for a space always involves assessing the heat gains on the various surfaces, the radiation transmitted into the room by heat transfer

and convection. This principle is common to both the CIBSE method and ASHRAE methods.

3.3. Calculation of Global Solar Radiation

This section will explain how the global solar radiation is calculated in terms of its components. The direction of the beam is determined in order to determine its intensity at the specific location and time as well as for the raytracing shadow calculations.

3.3.1. Direction of Beam Radiation

The direction of the beam radiation is first determined by calculating the **elevation angle** α and the **azimuth angle** γ_s (Figure 14).

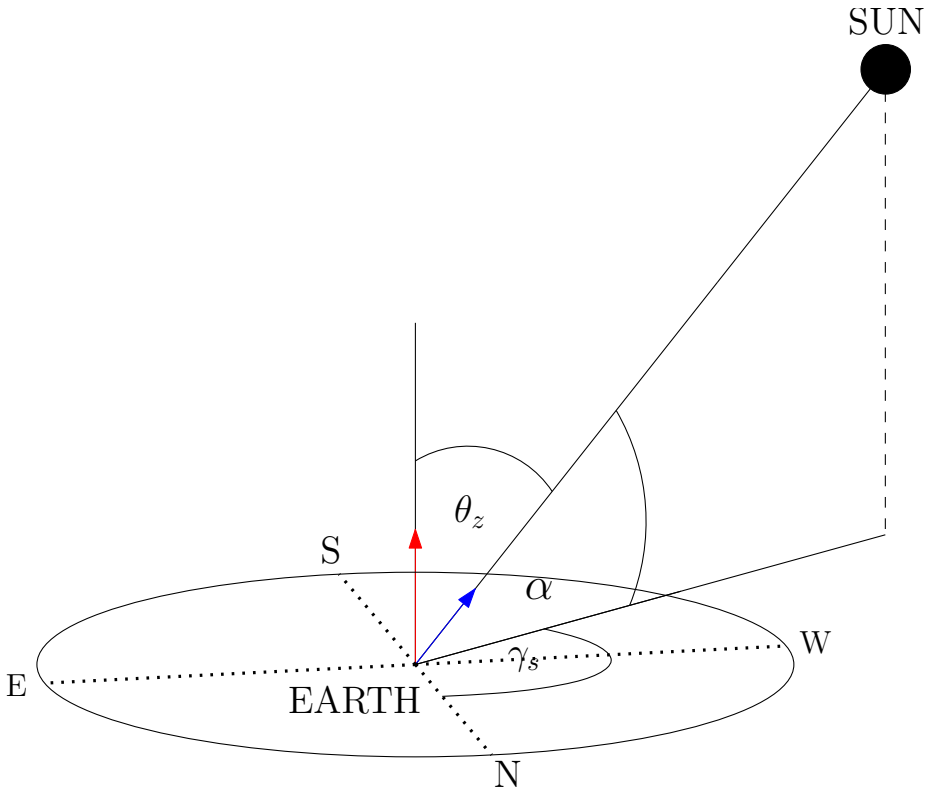

Figure 14: Azimuth and elevation to calculate solar position.

The calculation details are explained in Appendix A. The direction vector $\vec{D}$ of the sun can therefore be defined as the following:

$$\vec{D} = \sin\gamma_S i + \cos\gamma_S j + \sin\alpha k$$

3.3.2. Global Solar Radiation

The global solar radiation incident on a surface I_{SG} is composed of three main components. I_{SG} can be defined as,

$$I_{SG} = I_B \cos\theta + I_S + I_R$$

where,

I_B is the direct beam radiation

I_S is the sky radiation

I_R is the reflected ground radiation

θ is the angle of solar incidence between the direction of sun's rays (direct beam) to the normal of a horizontal surface

Further detail to the calculation of the global solar radiation is given in Appendix A.

3.4. Proposed Cooling Load Calculation

This dissertation implements an adapted version of the CIBSE Admittance method (CIBSE 2006) for the calculation of the cooling loads. The following assumptions are taken:

1. Maltese climate is being considered for the simulation,
2. The cooling loads for June, July, August (peak) are being considered in which the solar radiation is most intense.
3. The average outdoor temperature during these months never goes below 20 °C , thus avoiding the need to calculate for any heat loss (MaltaWeather.com n.d.).
4. Causal gains from lighting and people are being ignored because this research is focusing on the optimisation of the building envelope and the fenestration geometry only.
5. Ventilation gains and heat transfer through walls are not being considered in order to simplify the simulation calculations for early stage design.

The CIBSE Admittance method was developed as a cyclic model. This is a dynamic model in which the parameters are repeated at regular intervals (CIBSE 2006, Chapter 5, pp. 5). The weather data used in the Admittance method is assumed to be sinusoidal with a period of 24 hours. This dissertation however, adapts the Admittance method (CIBSE 2006, Chapter 5, pp. 15) to a non-sinusoidal set of temperatures to assume a realistic change in the outdoor temperature typical to Maltese climate. A range of recorded hourly temperatures (Freemeteo 2012) for Malta, during the peak months being considered were passed as parameters.

The dominant source contributing to the cooling load of a building is that of the solar radiation incident on the fenestration, thus implying that the fenestration geometry and orientation have a large impact. The CIBSE cyclic model calculation method for summertime temperatures also takes the internal heat gains into account. However, as discussed in 3.1, a simplified cooling load calculation for early stage design calls for considering only the sources of heat gain that have most significant impact, hence the following:

1. Solar gain transmitted through the glazing , Q_{SG}
2. Sensible transmission through the glazing, Q_G
3. Heat gain through the roof, $Q_{Q+f\ Roof}$

The roof of a floor can be exposed either if the floor is the top floor of the building or if the above floor is recessed to terracing of the building. Although a small contribution to the cooling load of the room, the heat gain through the roof was considered in order to allow the area of a floor to effect the cooling load.

The total cooling load Q_T can be defined as,

$$Q_T = Q_W + Q_{Q+f\ Roof}$$

Q_W is the total heat gain through the window and $Q_{Q+f\ Roof}$ is the total heat gain through the roof. This also caters for the case of terracing of floors. Each floor knows of a part of its roof is exposed to solar radiation. The area of the floor-plate of the above floor is subtracted from the ceiling area of the current floor to obtain the area of the exposed roof.

Calculating Q_W

The total heat gain through a window Q_W is composed of the heat gain Q_G due to sensible transmission through the glazing from the ambient radiation and the heat gain Q_{SG} due to the incident direct solar radiation on the window, therefore Q_W can be defined as,

$$Q_W = Q_G + Q_{SG}$$

where,

Q_G calculates the heat transfer from the outside to the internal space based on the U-value of the glazing type U, the total glazed area A_T and the the external and internal temperature. Q_G is defined as,

$$Q_G = UA_T\left[T_E - T_R\right]$$

The equation used for calculating Q_{SG} as suggested by the CIBSE method (CIBSE 2006, Chapter 5, pp. 16, Chapter 15, pp. 17) is defined as,

$$Q_{SG} = S.q_{SG}.A_T$$

where,

S is the mean solar gain factor at the environmental node or air node from CIBSE Guide A (2006) Table 5.7.

q_{SG} is tabulated cooling load from CIBSE Guide A (2006) Table 5.19 to 5.24 (W/m^2)

A_T is the total glazed area of a window

This equation requires large amounts of tabulated data to be stored for pre-calculated values of q_{SG} for various locations. The radiation $q_{SG}.A_T$ can be replaced by the incident solar radiation values I_{SG} already calculated in 3.3 and explained in 6.4.1, which already takes the non-shaded area of the window into account.

The solar gain factor S can be defined as the ratio of the components of the heat gain through the window to the incident solar radiation on the window (CIBSE 2006, Chapter 5, pp. 88). This is the fraction of solar radiation that enters the building due to the glazing properties. The tabulated solar gain factors in CIBSE Guide A, Table 5.7 (CIBSE 2006) are values for combined glazing and shading from blinds. Since this dissertation obtains glazed facades that do not require shading through blinds in order to take full advantage of the view quality at all times, the solar gain factor S needs to be adjusted accordingly. Since S is the same as the air-node coefficient F_C multiplied by the shading coefficient F_S (CIBSE 2006), the solar gain factor S can be replaced by F_C to eliminate the factoring for shading.

The transmitted heat due to solar gain may therefore be defined as,

$$Q_{SG} = F_C I_{SG}$$

The total heat gain through a window can therefore be defined as,

$$Q_W = UA_T \left[T_E - T_R \right] + F_C I_{SG}$$

Calculating $Q_{Q+f\ Roof}$

The heat gain through the roof $Q_{Q+f\ Roof}$ is made up of the mean gain through the roof Q_Q and takes into account the variation from that mean Q_f and can be defined as,

$$Q_{Q+f\ Roof} = Q_Q + Q_f$$

where, Q_Q is the product of the surface area of the roof fabric and the corresponding transmittance over the surface through which heat flow occurs (Wk^{-1}).$T_{SA\ mean} - T_R$ is the swing in mean sol-air temperature (^{o}C) which is determined by subtracting the constant dry resultant temperature (^{o}C) (room dry bulb) T_R from the mean sol-air temperature $T_{SA\ mean}$ (CIBSE 2006, Section 5.8.1.1). Q_Q/A is the steady-state rate of heat transfer per unit area (O'Callaghan and Probert 1977). Q_Q can therefore be defined as,

$$Q_Q = A\,.U\left(T_{SA\ mean} - T_R\right)$$

Q_f determines the effective heat input due to fabric heat gain (CIBSE 2006, Section 5.8.1.5) as follows.

$$Q_f = A\,.U\,.f(T_{SA} - T_{SA\ mean})$$

where, the decrement factor f is defined as " the ratio of the rate of flow of heat through the structure to the environmental temperature in the space for each degree of deviation in external temperature about its mean value, to the steady state rate of flow of heat (U-value)." (CIBSE 2006, Chapter 3, pp. 25).

O'Callaghan & Probert (1977) define T_{SA} as follows.

$$T_{SA} = T_E + R(\alpha I_{SG} - \varepsilon I_L)$$

where,

T_E is the exterior temperature (^{O}C).

R is the thermal resistance of the external surface/air interface ($Wm^{-2}K^{-1}$).

R is equivalent to the reciprocal of the surface heat transfer coefficient h which is commonly assumed as 17 Wm^{-2} (Ruivo *et al.* 2013).

α and ε are the absorptivity for solar radiation and emissivity respectively.

I_{SG} is the direct solar radiation incident on the roof at time t-f, where f is the time lag tabulated for several materials (CIBSE 2006, Table 3.49 to 3.55).

I_L is the intensity of long-wave radiation from a thermally black body of temperature T_E.

I_L is sometimes referred to as δR. ASHRAE (as cited in Ruivo *et al.* 2013) define δR as "the difference between long-wave radiation incident on surface from sky and surroundings and radiation emitted by blackbody at the temperature of outdoor air ". δR is generally assumed to be 63 Wm^{-2} for horizontal surfaces such as roofs and 0 Wm^{-2} for vertical surfaces such as walls (Ruivo *et al.* 2013).

The mean solar air temperature $T_{SA\,mean}$ is calculated by iterating through 24 hours and each time adding the sol-air temperature to a total. The total is then divided by 24 to obtain the mean.

The heat gain through the roof $Q_{Q+f\ Roof}$ can therefore be defined as,

$$Q_{Q+f\ Roof} = AU\left[\left(T_{SA\,mean} - T_R\right) + \left(T_{SA} - T_{SA\,mean}\right)\right]$$

since,

$$Q_T = Q_W + Q_{Q+f\ Roof}$$

The total cooling load Q_T can therefore be written as,

$$Q_T = \left(U_{Glazing} A_{T\ Glazing} \left[T_E - T_R\right] + F_C I_{SG}\right) + \left(U_{Roof} A_{T\ Roof} \left[\left(T_{SA\ mean} - T_R\right) + \left(T_{SA} - T_{SA\ mean}\right)\right]\right)$$

The cooling load objective is valued as a monthly energy consumption therefore an average cooling load is calculated by iterating through hourly external temperatures (read from an excel sheet), for each day of the peak months being considered (June, July, August) and adding the calculated cooling load Q_T each time to a total. The total is then divided by three to obtain the monthly average cooling load Q_T .

The cooling cost can easily be obtained by multiplying the cooling load Q_T (kWh) by the electricity rate which is generally given per kWh however this dissertation will deal with the cooling load in it's true units (kWh).

4. View Quality Objective

4.1. Introduction

It is important to define the quality of a view by questioning what makes a good view. The answer is a subjective one. However in order to assess its conflict with the energy consumption, the view quality needs to be objectified. The view quality in the real estate sector is somehow rationalised and objectively rated. This indicates that a good quality view can indeed be distinguished from an inferior quality view. The scenario being studied in this dissertation involves the real estate developers' lack of consideration of the consequences of the thermal performance of a particular building typology due to a focus on the rental value as opposed to the running cost. Therefore, a rational approach to scoring a view based on the real-estate approach can be derived for the purposes of this research.

Section 4.2 discusses previous approaches in evaluating the quality of a view for real estate purposes. No literature on the quantification of the view for use in multi-objective optimisation exists to the author's knowledge however there were several attempts at the quantification of the view for real estate purposes.

Section 4.3 discusses the logic adopted in objectifying the quality of a view in the real estate context. This approach demonstrates that although the judgement of a view is a subjective one, there is an element of objectivity in it which can be used a general view-ranking method.

The implementation of the proposed approach is discussed in terms of how the value of the view was derived and used in a comparative study. A view scoring system is also presented and explained.

4.2. Review of view estimation methods literature

4.2.1. Hedonic Regression

The hedonic pricing method (Gundimeda 2005) is generally employed in real estate as a method of property evaluation. This method achieves the values of the individual components composing the total property value such as location, amenities, bedroom size, number of bedrooms etc., by estimating the Hedonic Price Function of the property by which the prices of various properties in the same area are related to the individual components. The function could result in a linear or non-linear relationship (Gundimeda 2005). The differentiation of the price function will therefore yield the value of the individual components. The prices obtained by means of this analysis are then regressed against those derived from people's subjective desires.

4.2.2. Quantification and Evaluation of The View

Whilst there have not been any known attempts at the quantification of the quality of the view in the context of a multi-objective problem, there have been several attempts in evaluation of a view for general, real-estate purposes.

Shellard (2006) reviews several publications that have dealt with the quantification of a view most of which employ hedonic regression analysis discussed in 4.2.1 (Shellard 2006). Lake et al., (1998) and Yu et al., (2007) present an evaluation method using a GIS model by obtaining data and statistics of the surrounding amenities available in the GIS model. In both cases, the "viewshed" function available in the GIS package is used to determine the visibility of a view from various observation positions.

Yu et al., (2007) use the viewshed function in order to determine the value of a dummy variable to indicate whether the sea is visible or not. The viewshed is the portion of the terrain mesh in the GIS software visible from the observation point. The GIS terrain model uses geospatial data thus knowing what land-use is contained within the viewshed boundary (Figure 15). A viewshed index is derived as a proportion of the visible mesh cells to the total number of cells on the terrain mesh to determine the extent of the view. The viewshed variable and 'seaview' variable (dummy variable) were constructed with ArcGIS 3-D Analyst (Yu *et al.* 2007).

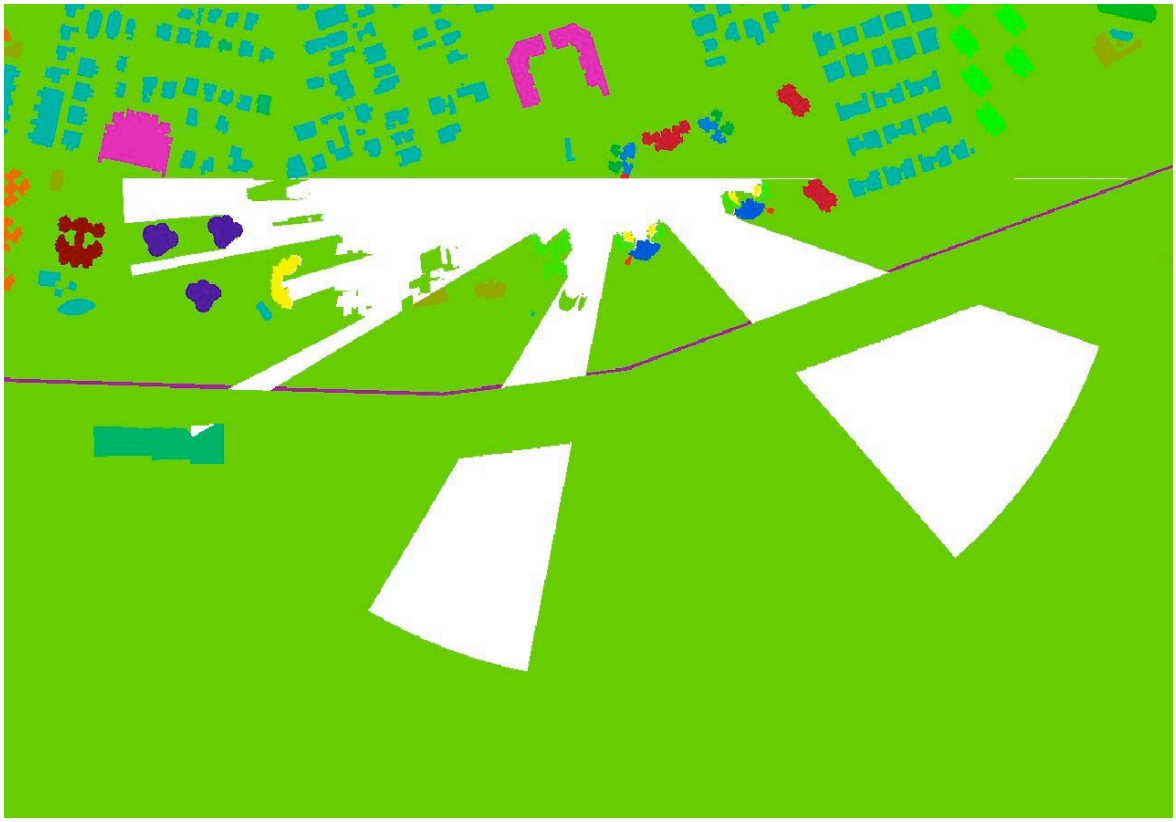

Figure 15: The viewshed from the particular observation point is displayed in white. Note the effect of the obstructing neighbouring buildings.

The index should reflect the effects of the height of the observer, the obstructing neighbouring buildings the orientation of the building and the type of view.

Yu et al., (2007) apply the presented approach in order to maximise the visibility of the sea view for a high-rise project by proposing an 'optimised' floor plan. This is done manually, through several simulations of different floor layouts and orientations. As a result, the value of the property increases.

This dissertation proposes a similar yet simplistic hedonic approach (discussed in 4.4.1) whereby the real value of a few properties with and without views, within the same condominium, are compared and simplistic regression determines the linearity of the relationship between the view component values and the view type.

4.3. Quantification of a View

The view quality in real estate can be defined as a property characteristic contributing significantly to the rental value of the property. A “good” view is therefore one that will yield profit whilst “no” view is one that is not factored into the property value. Using this logic, the first image in Figure 16 would be regarded as a “good” view because it will contribute heavily to the property value whilst the last image in Figure 16 would be regarded as “no” *view* because the view of the street in the balcony will not contribute at all to the value of the property.

The rental value of a property is also dependent on several other factors such as location, and floor area. The value of a property is derived through several estimation methods. The most common one being the comparative method where the property is compared to several other very similar properties of the same typology, in the same location. The property development scene in Malta, categorises the property view types into a simple number of types. These range from direct sea view, direct country view, side sea view, side country view, open views (such as town squares and townscapes) and no view at all (Bartoli 2013).

1)

2)

3)

4)

Figure 16: 1) Sea and skyline view, 2) country view, 3) sea view , 4) no *view*
(Images: Airbnb.co.uk, Tripadvisor.co.uk)

4.4. Proposed Approach

The proposed approach must therefore fuse the derivation of the value of the view together with a calculation method.

To frame a good view or parts of one, a cellular fenestration approach such as Wright & Mourshed (2009) or Shea, Sedgwick, & Antonuntto (2006) would be suitable. However independent window geometries would require independent variables for each window. One of the criterion set by this dissertation for selecting the fenestration geometrical system was to minimise the amount of variables as possible to avoid lengthy optimisation iterations.

A more geometrical fenestration approach was adopted however still allows the possibilities of fully glazed facades, which is one of the fenestration configurations this research explores.

There is need of a relationship between the view type and the property value in order to rationalise for optimisation. This can be assessed by performing a comparative study of several properties of same building typology and location, and plotting the results for each view type and corresponding property value. It is important that besides the typology, the finishes, number of bedrooms etc are similar to ensure a fair comparison.

4.4.1. Derivation of The Value of The View

A recently constructed luxury condominium in Malta was selected (Figure 17) and a few identical pairs of apartments with extreme view types, within the same complex, were compared.

A condominium offers the perfect characteristics for such a study because the best possible view can immediately be identified and because the comparison will be fair due to the identical common finishes and location. The best view of the selected condominium can be viewed in Figure 17. The view type is of a direct sea view. In addition, the skyline of Valletta, the capital city of Malta and world heritage site, contributes heavily to the value of the property enjoying this view. Vassallo (2013) stated that when the development was

constructed, the proportion in property value of properties with a direct sea and skyline view compared to those with no view was double. He also stated that since the properties have now been handled by various owners and real estate agents, this proportion may not longer exits however the following work by the author has shown that the assumption is still valid.

Figure 17: Tigne Point Condominium, Malta.

Two ‘direct sea and skyline’ view apartments (properties A & B) and one ‘view-less’ apartment (property C) within this condominium were selected from a real-estate agency website (FrankSaltRealEstateMalta 2013, Ref:026516, Ref: 705975 & Ref: 024642) in order to assess the relationship between the area and property value, and secondly, to deduce the actual property value, typical of this condominium. The ‘direct sea and skyline’ view is regarded as the best view type in this condominium by the property agencies (Frank Salt Real Estate Malta 2013). Properties A and B are also compared to property C in order to also assess whether the floor area value rate is applicable to all apartment types in the condominium, even those with no view.

Table 3 deduces the view value rate of the best view for A & B, where the monthly rental value is divided by 2 to obtain the view components, assuming the suggested double proportion (Vassallo 2013). The floor area value rate for A, B & C is also determined. This comparison indicates an approximate equivalency in the figures thus confirming a consistency in both the area value rate and view value rate for all properties. This exercise also confirmed that the assumption of double proportion is still valid.

	Unit	A	B	C
View		Direct Sea & Skyline	Direct Sea & Skyline	None
Area	m^2	330	200	180
Rental V	€/month	7000	4000	2000
View V	€/month	3500	2000	0
View V	€/month/m^2	10.6	10	0
Floor Area V	€/month/m^2	10.6	10	11.1

Table 3: Property comparison.

The average monthly floor area value rate may be deduced by taking the average floor area value rate of A, B and C. Therefore,

$$\frac{10.6+10+11.1}{3} = €10.56/\text{month}/m^2$$

Once the floor area value rate and the maximum view value rate were defined based on the above properties, the linearity of the view value rate needs to be assessed. Therefore, by now comparing A and C to a property with direct sea views and side skyline views (Side DS&S) in the same condominium, D (JKGroup 2013, Ref: 240101030-341), D should lie at the midpoint of A and C, based on the above linear logic. Property D has a monthly rental value of € 5,500 with a floor area of 330 m^2 .

This time, to obtain the rate of the view value, we first need to deduce the expected monthly floor area value which is the product of the condominium average rate deduced above and the floor area:

$$€10.56 * 330m^2 = €3484.8/\text{month}/m^2$$

Therefore, the monthly floor area value of property D is subtracted from the actual monthly rental value to obtain the monthly view value:

$$€5,500 - €3484.8 = €2015.2/\text{month}$$

The monthly view value is therefore divided by the area in order to obtain the monthly view value rate.

$$\frac{€2015.2/\text{month}}{330m^2} = \quad €6.10/\text{month}/m^2$$

The same procedure is applied for property E, one with views of the plaza within the same condominium (open views). The results were plotted (Figure 18). The scale of the 'View Type' axis in Figure 18 is only a representation of proportion.

	Unit	A	D	C	E
View		DS &S	Side DS&S	None	Open Views
Area	m^2	330	330	180	200
Rental V	€/month	7000	5500	2000	2300
View V	€/month	3500	2015.2	0	188
View V	€/month/m^2	10.6	6.10	0	0.94
Floor Area V	€/month/m^2	10.6	10.56	11.1	10.56

Table 4: View type comparison.

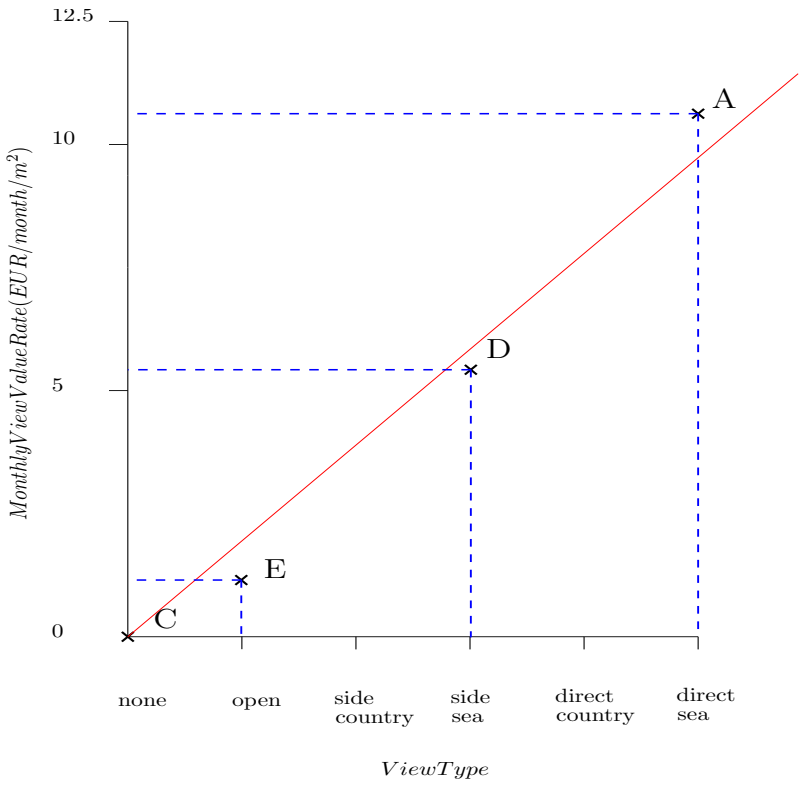

Figure 18: Plotted Value rate vs. View type comparison.

The graph indicates that the type of the relationship between the view types and the estimated monthly view value rate is of a linear nature, thus verifying that the deduced monthly floor area value rate and monthly best view value rate are correctly assumed.

The monthly property value of an identical property, with a similar direct sea view, in a different location, varies. Assuming the linear proportionality obtained as an example, the location element may be factored in the equation as a weighting constant.

Figure 19 visualises an **assumptive** linear relationship between the view type V_T and the view value V_V of several properties in different locations L. The gradient of the graph, a value between 0 and 1, indicates the quality of the location. With reference to Figure 19, the monthly view value rate of a property with a side country view in location L1 is higher than an identical property with the same side country view in location L3. This is represented by the difference in slope.

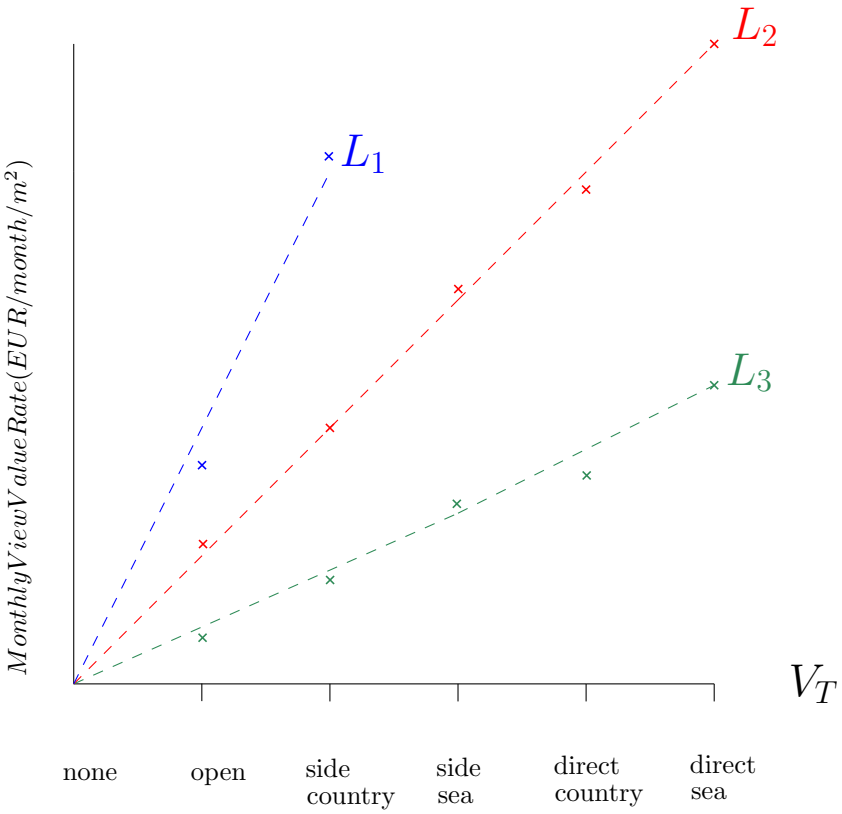

Figure 19: Assumptive linear example of varying gradient with location.

This relationship can therefore be represented in the form of a simple equation.

$$V_V = L \,.\, V_T$$

A major factor also affecting the view component of the property value is the fenestration. The glazing to wall ratio has a direct effect on the value. To put it simply, a window-less facade with a potential sea view is equivalent to one with no view. Therefore, the glazing percentage A_F is introduced as a weighting of V_V. Since this derived relationship is derived from the real-estate's view value, it is being assumed that the real-estate approach of evaluating a view is a generalisation of the view. This means that it does not take into account exactly what is visible through the windows. By means of this assumption, the area is assumed to be linear with the view type, assuming that a glazing to wall ratio of 1 is equivalent to the estate agent's view value. Therefore,

$$V_V = L \,.\, A_F \,.\, V_T$$

4.4.2. Calculation

The above equation, based on the linearity of the view value rate assumes a view of uniform view quality. When the view component is factored into the property value by the real estate agencies, the view is assessed for its general quality but not for its individual content. Despite weighting the view value based on the glazed ratio, the linear relationship deduced is a simplification of the actual view thus not being true to the actual contents of the view. This calls for a smarter method of assessing the view by developing a scoring system whereby a window score represents the total of the individually and appropriately scored 'items' in the view.

The quality of a view relative to an apartment does not only depend on the view itself and the area of glazing but also on the visibility of its contents from various positions inside an apartment. This fact is also ignored when the value of a property with a view is estimated by real estate agencies.

This dissertation therefore proposes a view scoring method where the floor-plate area is subdivided into four sub-areas and a position at eye level (1.6m) at the centroid of each sub-area is set as an eyeball test position (Figure 20). The view from each of these eyeball positions is scored based on the relative field of view, which is explained further in 6.4.2. The scores from each eyeball position are added and a total is assigned to the window. This is done for each window on a floor, thus assigning a total score for the floor, and then further added to assign a total score to a building.

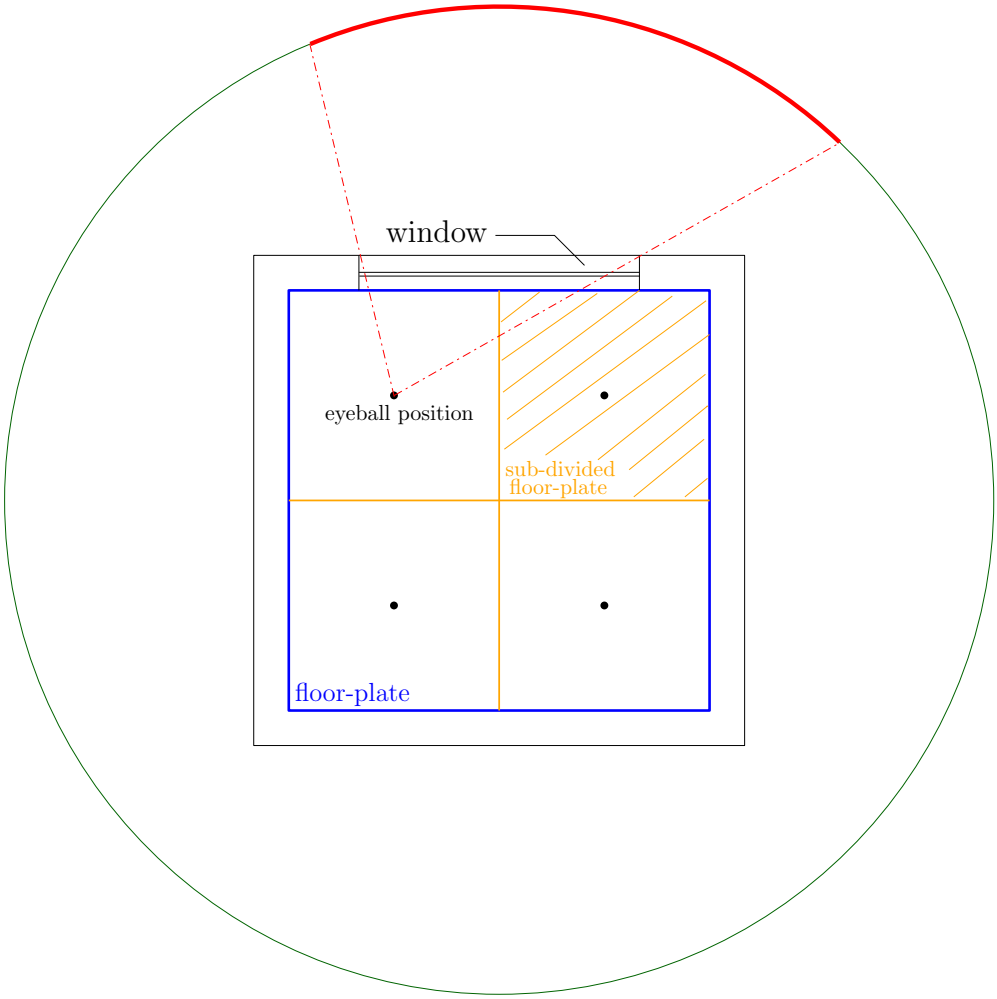

Figure 20: The eyeball positions at the centroid of each sub-area of the floor-plate.

The condominium discussed in 4.4.1 was set as a realistic base scenario as a means for exploring the conflicting objectives. The best view (direct sea & Valletta) offered by the condominium is oriented in the South direction (Figure 21) thus provoking conflict of solar gain and the large fenestrations required to satisfy the view objective.

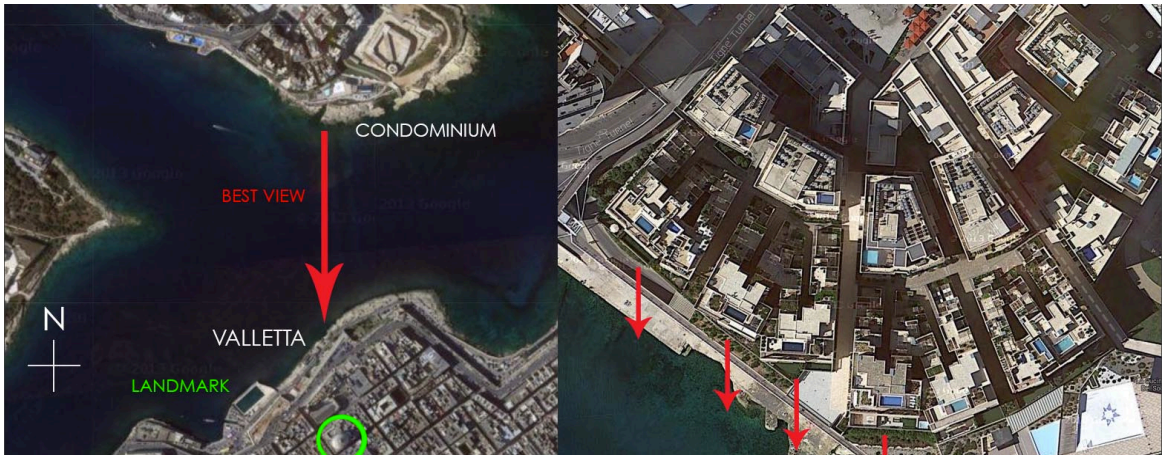

Figure 21: Condominium site on a peninsula (left). Site plan of condominium oriented towards the view (right).

Since a *view type* has no units, its evaluation as an independent variable is not possible. Evaluating the view in terms of it's real estate value was well suited to the purpose of this dissertation due to the context of the issue being tackled being, prioritisation of money itself (Chapter 1).

This research proposes a method where the contents of the view are scored by means of a pixel scoring system. A score range is represented by 255 greyscale tones where: 0 = 6 points, 50 = 5 points, 87 = 4 points, 162 = 3 points, 209 = 2 points, 255 = 1 point. The user, digitally assigns a grey tone, to each pixel in the image of the view prior to running any simulation (Figure 20 (bottom)). The image is eventually uploaded via the user-interface. The tones are assigned based on the user's or the client's subjective judgement. One scored point is equivalent to €0.001209304875. This was calculated by simulating the view that is visible through the fully glazed facade of a property facing the Valletta skyline, from the condominium (Frank Salt Real Estate Malta 2013, Ref: 027733) (Figure 22 (top)). The simulation was done by means of the developed software tool. This view is regarded as the best view in the condominium. Figure 22 (bottom) displays the corresponding grayscale image of the view, indicating the high view value of the Valletta World Heritage skyline (pixels of greyscale tone 0). The corresponding total pixel score is 2480764. This property is listed as having a monthly rental value of €6,000 whilst the view rental value is assumed to be €3,000 based on the assumption verified in 4.4.1. The view rental value of one scored point for properties in this condominium can therefore be deduced by dividing €3000 by 2480764 points.

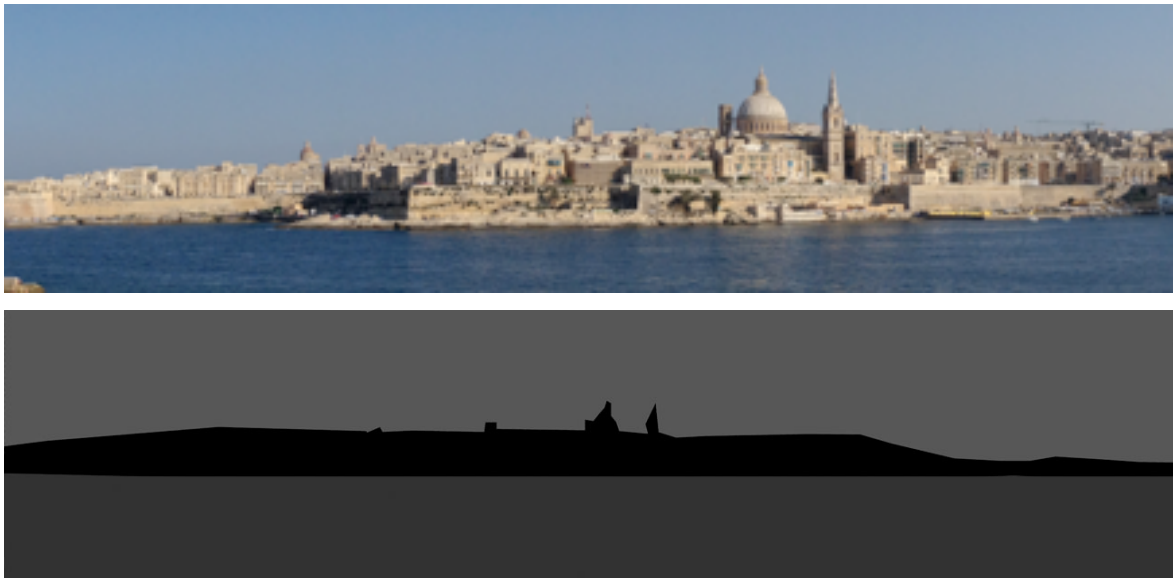

Figure 22: Original image (top). Shaded image by user (bottom).

Figure 23 (top & middle) visualises the view from a property with a side view of the skyline. As expected, the total pixel score is lower than that of the previous example. The greyscale version of this view (Figure 22 (bottom)) was adapted from the previous example due to the difficulty of obtaining access to the property. The simulation of this example (Figure 24) obtained a score of 1991232 corresponding to a rental view value of €2,408 when multiplied by the deduced rental value per score. The small visible tower was given a grey tone of 87 because it has got historical value whilst the nearby surroundings are deemed lower in value when compared to the sea, hence the lowest score.

Figure 23: View from the apartment (top & middle). Scored image by user (bottom). (JKGroup 2013)

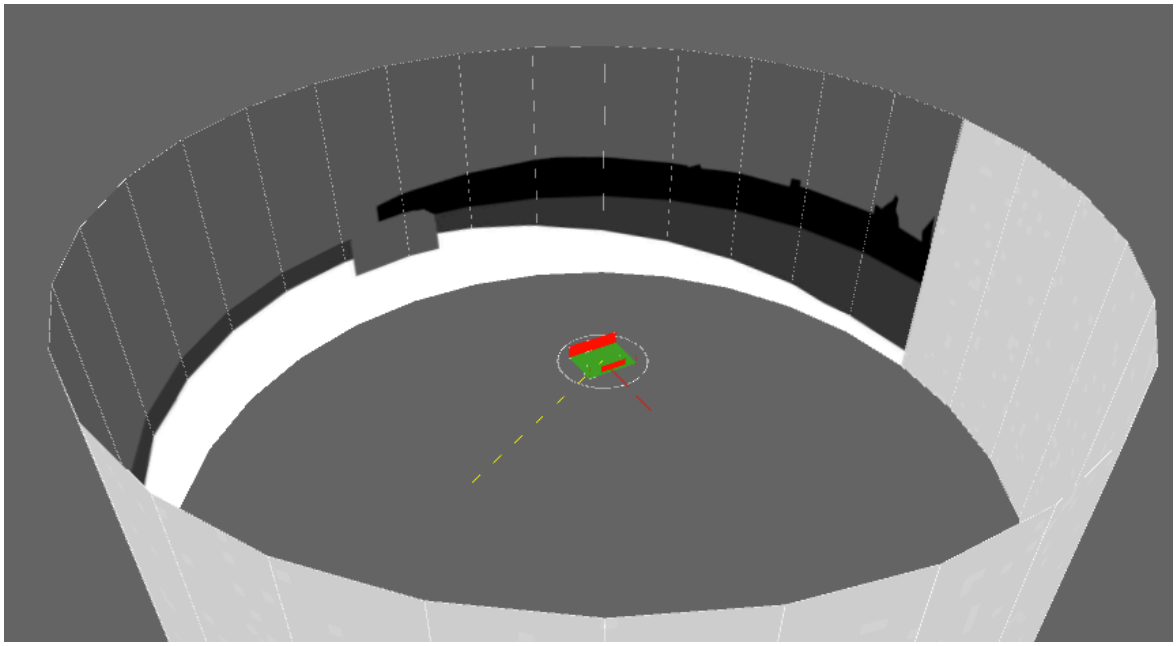

Figure 24: The simulation environment.

During the research for rationalising the quality of a view, other approaches were briefly discussed such that very distant objects in a view may not necessarily contribute negatively to the view quality. This occurs when an on object becomes part of a ‘distant skyline’. Distant skylines are generally a positive quality in a view. Figure 25(top) shows a direct view of the cooling towers of a nearby nuclear plant. This is a view which is generally regarded as negative quality. However, when they form part of the distant skyline such as in Figures 25(bottom) and Figure 26, thus contribute somewhat interestingly to the skyline. An avenue for further research would be to explore the potentials of deriving a relationship between objects in a view and distance either by means of GIS packages or sterephotogrammetry. Such a method could possibly replace the manual scoring by the user or integrate into a hybrid method of subjective scoring and ‘smart’ scoring based on distance but it is outside the scope of this project.

Figure 25: Direct view (top) (Haddock 2013). Distant view (bottom) (Brizlincot Parish Council 2009).

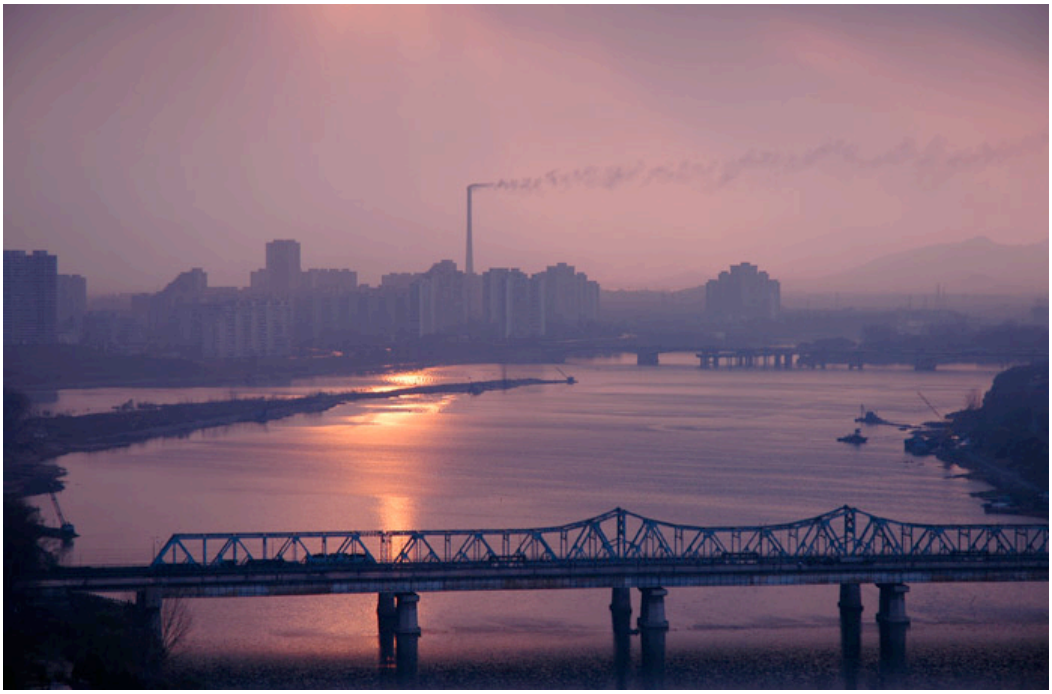

Figure 26: Pyongyang skyline (Baldwin 2013)

5. Optimisation

5.1. Introduction

The optimisation component of the proposed generative framework deals with searching for the best possible solutions that offer the best combination of the objectives being considered. The simulation of the cooling load and the view value are represented as an objective vector whereby,

$$\vec{O} = (Q_c, Q_v)$$

where,

Q_c = cooling load, KWh

V_v = view cost, €

The intention is to obtain the lowest possible Q_C and the highest possible Q_V values. The nature of the relationship between the two objectives is dependant on the orientation of the building, the orientation of the view and the direction of sun. When the orientation of the sun and orientation of the view coincide, the nature of the objectives becomes a conflicting one. To achieve the best minimisation of the cooling load value as a singular objective optimisation problem, minimal glazed area would be yielded, where as to achieve the best maximisation of the view value as a singular objective optimisation problem fully glazed walls would be yielded. In the case of a multi-objective scenario, the attempt to increase the glazed area to maximise the view value, yet decrease the glazed area to minimise the cooling load is clearly conflicting. Therefore, the introduction of new variables to cause overhanging floors will give the opportunity to achieve the minimisation of the cooling load yet maximisation of the view value simultaneously due to shading. The minimisation of the cooling load also becomes dependable on the new variables causing the overhangs.

5.2. Optimisation Search Methods

Multi-objective problems have to be solved non-linearly due to the competing objectives. Evolutionary algorithms are commonly employed as a means for search optimisation. The use of Evolutionary Algorithms (EA) in multi objective optimisation has been documented several times such as Coello, Lamont, & Van Veldhuisen (2007). Genetic Algorithms (GA) are the most common type of EA adapted and applied to multi objective optimisation searches. GA are founded on a population-based evolutionary approach, which searches for different areas in the solution space simultaneously. The Non-dominated Sorting Genetic Algorithm-II (NSGA- II) (Deb *et al.* 2002) and the Strength Pareto Evolutionary Algorithm 2 (SPEA-2) (Zitzler *et al.* 2001) have become the standard approaches. A good overview of the application of GA in multi-objective optimisation was given by Deb (2001) and more recently by Konak, Coit & Smith (2006).

5.2.1. Weighted Sum Approach

The weighted-sum approach (Goldberg and Holland 1988) is one of the earliest methods developed to solve such conflicting problems. In the weighted-sum approach, the objective functions are combined and scalarised to form a single composite function.

Generally, the objective values are scaled to a range between 0 and 1 based on maximum objective values. Determining the maximum objective value is not a very reliable approach because it is highly dependable on the effect of each individual variable on each of the objectives. This effect is not always intuitable therefore, requires to be assessed manually via manual hill climbing. This is done by manually iterating through the variables and manually incrementing the values to determine their effects on the individual objective fitnesses. It is important that the maximum objective value is assessed as a common maximum to all solutions to ensure a fair comparison between solutions.

A weighted average of the objective fitnesses is then calculated to obtain one fitness value. The aim of the optimiser is to maximise this fitness value. However, weightings must be assigned to the individual objective functions prior to running the GA. These weightings reflect a set of fixed priorities, consequently constraining the set of solutions (Todd, 1997). Selecting the appropriate weighting to an objective is the main issue with adopting a

weighted sum approach mainly due to the decision maker's lack in knowledge on the subject. Even so, it is still not an easy task for an expert in the field of the objective to assign a weighting because of lack in knowledge of the dependancy and relationship type with the other objectives being considered in the function. There have been attempts at developing smarter weighting assignment methods such as Murata and Ishibuchi (1995). Dynamic weighting assignments method have also been presented by Liu & Wang (2008). Ismail, Yusof, & Khalid (2011) propose a dynamic weighting assignment method for multi-objective optimisation, which avoids knowledge in the subject by means of a cascade GA optimisation process where the weightings are optimised using a GA inside an inner loop.

5.2.2. NSGA-II

Deb et al., (2002) developed a GA based search method that employs elitism. Elitism ensures that the best solutions of a generation are retained for the next generation and replaced only if they become dominated. This also ensures a cheaper computational expense. A random initial population of solutions is randomly generated and it's offspring is generated by crossing over and mutating the current population. The parent and child population are combined and sorted according to non-domination. This is done by comparing each solution to the rest of the combined set and assigning a rank index to each of the solutions corresponding to their dominance. This way, the dominance rank indicates the number of solutions a solution is dominated by. A rank index of zero corresponds to a Pareto solution as it is not dominated by any other solution. An implementation of NSGA-II is explained in detail in 5.5.

5.3. Proposed

The weighted sum was first considered as an optimisation approach in the early stages of this research. A common element is required in order to scalarise the objectives into one function. The cooling load fitness is evaluated in kWh however it can be converted to Euro based on known energy consumption rates. The value of the view is already calculated in Euro, as discussed and explained in Chapter 4. At this stage, the maximisation of the total habitable floor area was also being considered as a third objective. The value of the habitable floor area is equivalent to the total rental value subtracted by the value of the

view (Chapter 4). The habitable floor area is the area whose floor-to-ceiling height does not exceed the minimum set by planning regulations.

Since the objectives fitnesses at this stage were measured in the common unit, Euro, it was possible to directly derive a rental value (*RValue*) in Euro and avoid calculating any maximum values by,

$$Area + View - Cooling = RValue$$

The research progressed from a weighted mean optimisation approach towards a true multi-objective optimisation approach where an NSGA-II (Deb *et al.* 2002) was later implemented as a means of exploring Pareto solutions and avoid assigning weights to the objectives.

Solutions that are dominated by the same number of solutions lie on what is known as a 'front'. All Pareto solutions are not dominated by any other solution hence why they lie on a common front known as a 'Pareto front'.

The cooling load and view value are traded off in their true units, hence in kilowatt-hour (kWh) and in Euro (€), respectively. This was implemented as explained in 5.2.2 and in more detail in 6.5.2. The non-dominated solutions (Pareto solutions) are visualised as the red plotted squares in Figure 27 and have a dominance index value of 0. The index value increases as the solutions are dominated by other solutions, thus forming fronts of solutions having common ranks. The solution fronts in Figure 27 are visualised in the various colours. The user may select a mutation factor by which the non constrained variable values will mutate to a random value and within the range of each respective variable.

Some test generations were run to explore the effects of mutation and population size. This exercise also aided to test for elitism by ensuring that the newer dominated fronts are not dominated by any past solutions (white / faded solutions) (Figure 27).

The view value on the y-axis has been inverted in order to display a more familiar Pareto curve. The maximum view value and the minimum cooling load value of a generation are situated at the origin of the axes. The inversion is only a graphical manipulation.

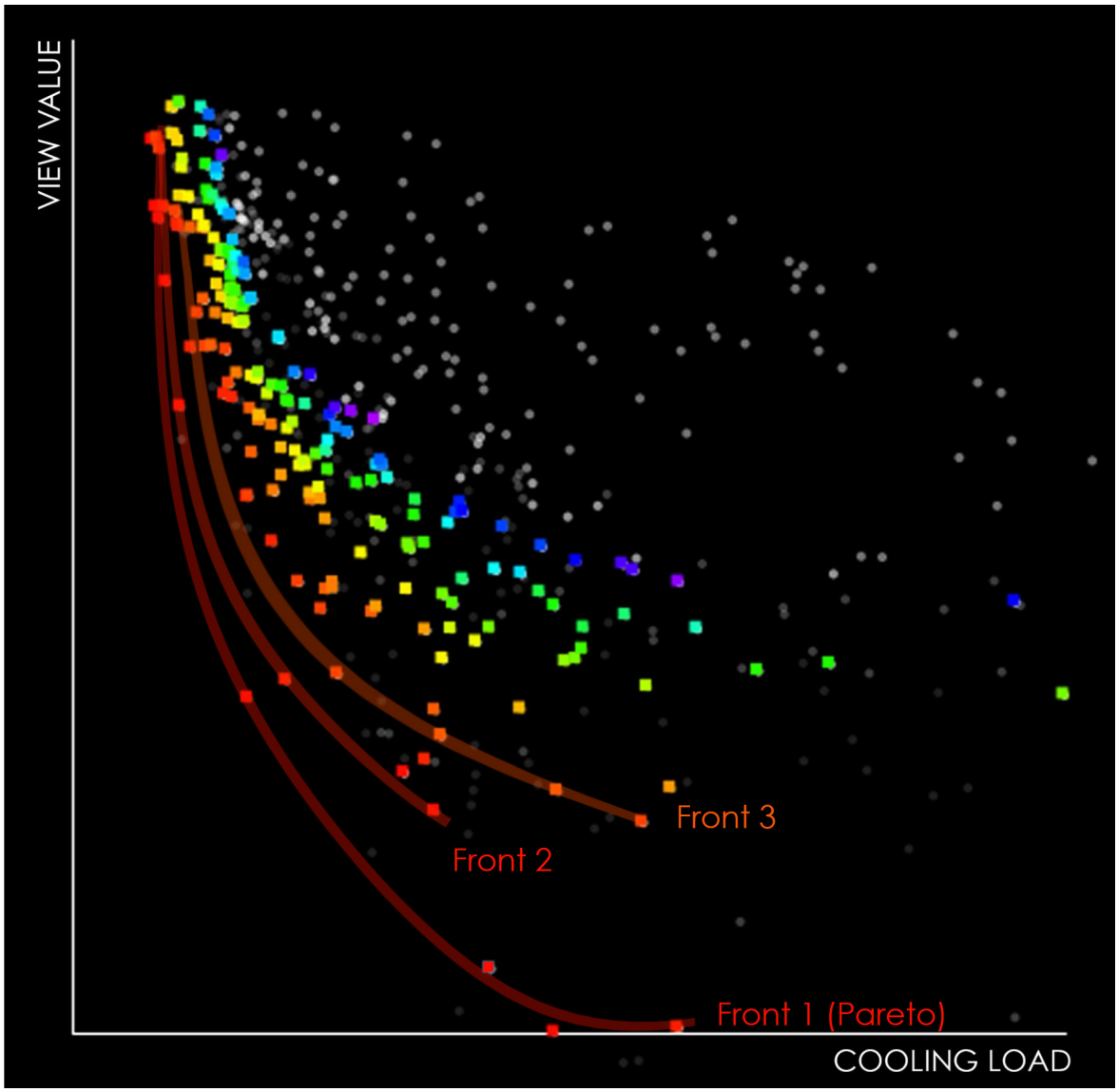

Figure 27: Example of a typical generation. The outermost plotted solutions represent the non-dominated Pareto front. The grey plotted dots represent the past generations. The opacity of the grey dots is relative to the age of the solution, where the lowest opacity represents the oldest solutions.

5.4. Reflection on Optimisation Techniques

The effect of the population size seems to have an effect on the variety of the solutions on the Pareto front. In the case of complimentary objectives a small population size does not yield enough variation as the results are too similar. This was demonstrated during the test for the North facing view where a good view in the North orientation provokes large glazed walls on the North windows. In the case of conflicting objectives, shaded windows via overhangs on a South face are introduced. This yields a larger number of combinations for reducing the cooling load. A larger population is therefore required to allow the exploration of a larger number of non-dominated combinations.

The Pareto front offers a variety of solutions. There is not only one optimal result but many as each of them are not dominated by any other solution in the population. The position of a solution on the Pareto front gives an indication of the objective weightings. Most commonly, the solution nearest to the origin is selected as being the one with the lowest of both objectives however this is not necessarily correct. Such a decision implies that the decision maker is attempting to assign “equally-weighted” objectives. The intention of the Pareto front is one to aid at understanding the relationship between the objective and help make the decision maker to make a more informed decision when eventually assigning weightings to such conflicting objectives.

6. Software Structure

6.1. Introduction

This chapter will explain in depth how the integrated generative framework was built. Such a framework was written in an object oriented programming environment which benefitted the reuse of certain complex routines. Figure 28 visualises an exploded representation of the classes involved in composing the framework. The classes are grouped into three components which reflects the parent structure of the integrated generative framework. These are: the building geometry, simulation and optimiser.

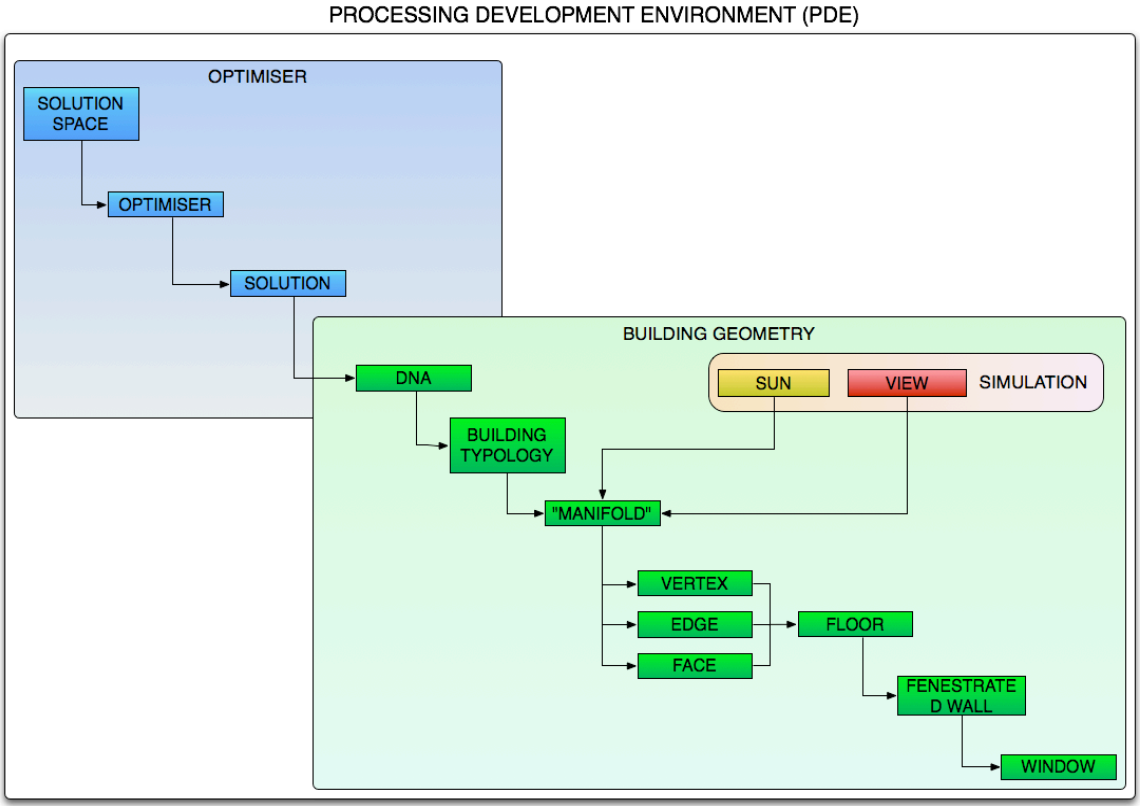

Figure 28: Classes of the proposed generative framework.

6.2. PDE

“Processing” was selected as a programming environment (Fry and C.Reas 2004). Processing is a Java (Oracle 2011) based, open source platform. Several libraries have been developed within Processing. The software tool developed in this dissertation makes use of the controlP5 library (Schlegel 2012) and peasycam libraries (Feinberg 2012). ControlP5 is a graphical user-interface library for Processing whilst peasycam provides a mouse controlled camera.

6.3.Building Geometry

The geometric variables were dictated by the problem being tackled. This dissertation deals with one building typology. As discussed in 2.3.1, the selected variables must allow overhangs in order to cast shadows on the windows. These variables were implemented in the form of sliders by means of ControlP5 library (Schlegel 2012) to allow for interaction. The proposed interactive approach also allows the user to constrain any of the variables by locking the sliders. As mentioned earlier, it is important to select the least possible number of variables to increase the efficiency of the GA. This difficulty was reflected in the parametricisation of both the overhang geometry and also the fenestration geometry. The optimality of the combination of selected variables can only truly be known once some results are achieved. In fact, this resulted in a lengthy process, such that the window and overhang variables were re-adjusted up till the final development stages of this software tool due to issues based on feedback from the optimiser.

The building geometry for a block of flats was written in the form of a method of the building class. The intention is to easily add further building typologies and geometries in the future. The flats building geometry is mainly composed of floor objects which in turn are composed of carpets, ceilings, walls and fenestrated walls which in turn contain windows (Figure 29). The geometry of a floor is mainly a manifold of vertices, edges and faces. A building is therefore a group of manifolds.

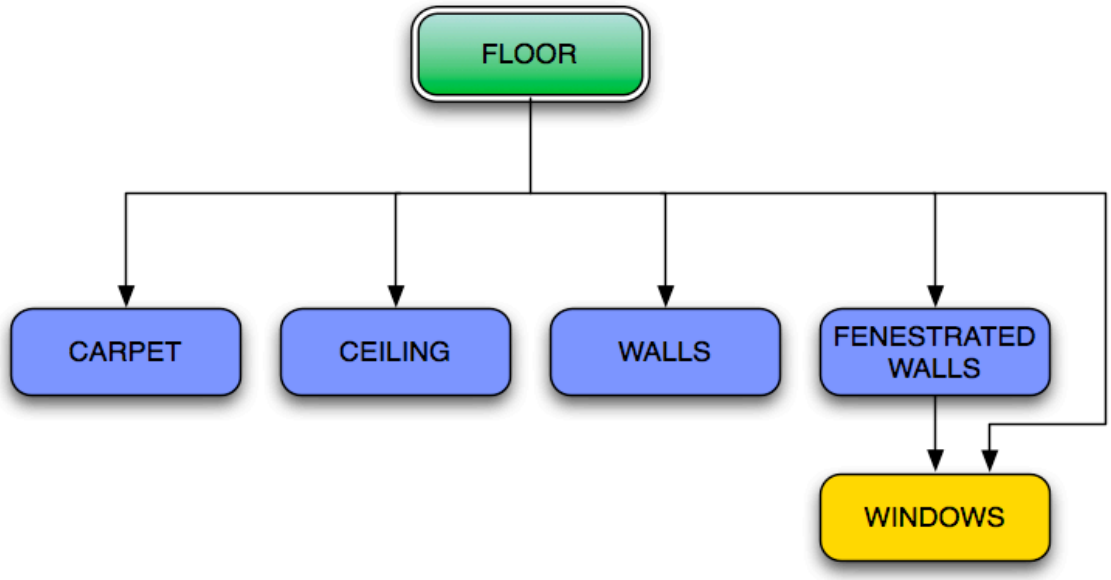

Figure 29: Floor hierarchy

The following is a list of the selected variables:

Variable	Notation	Parameters
Floor to ceiling height	***FH***	3m ≦ ***FH*** ≦ 4m
Overall building height	***BH***	3m ≦ ***BH*** ≦ 27m
Site length	**S***y*	0m ≦ **PL** ≦ 35m
Site width	**S***x*	0m ≦ **PW** ≦ 15m
Front facade inclination *x* direction	**IF***x*	-2m ≦ **IF***x* ≦ 2m
Front facade inclination *y* direction	**IF***y*	-2m ≦ **IF***y* ≦ 2m
Back facade inclination *x* direction	**BF***x*	-2m ≦ **BF***x* ≦ 2m
Back facade inclination *y* direction	**BF***y*	-2m ≦ **BF***y* ≦ 2m
Top floor relative length	**T***y*	-3m ≦ **TL** ≦ 6m
Top floor relative width	**T***x*	-3m ≦ **TW** ≦ 6m
Offset floors *x* direction	**Off***x*	-3m ≦ **Off***x* ≦ 3m
Offset floors *y* direction	**Off***y*	-3m ≦ **Off***y* ≦ 3m
Front facade number of windows	**FW***n*	1 ≦ **FW***n* ≦ 6
Front facade window height	**FW***h*	0 ≦ **FW***h* ≦ 1
Front facade window width	**FW***w*	0 ≦ **FW***w* ≦ 1
Back facade number of windows	**BW***n*	1 ≦ **BW***n* ≦ 6
Back facade window height	**BW***h*	0 ≦ **BW***h* ≦ 1
Back facade window width	**BW***w*	0 ≦ **BW***w* ≦ 1

The number of floors is deduced from **FH** and **BH**. **BH** was chosen as a variable rather than the number of floors variable to allow the option to ‘fit’ as many apartments in a stipulated building height as is done in realistic projects.

S*y* and **S***x* allow the user to specify the dimensions of the ground floor which reflect the dimensions of the site.

The facade inclination variables **IF*x*, IF*y*, BF*x*, BF*y*** allow inclination of the front facades in the direction of the x-axis, the front facades in the direction of the y-axis, the back facades in the direction of the x-axis and the back facades in the direction of the y-axis respectively. The inclination towards the direction of the x-axis has been constrained for this research as the focus lies on blocks of flats with shared neighbouring walls. The inclinations of the front facades and the back facades are independent of each other. The inclinations will either decrease the incidence angle of the sun's rays on the facade (Figure 30 (2)) or allow shading of the windows (Figure 30 (3)). This is done by updating the location of all the ceiling vertices causing an overall inclination of all front or back facades as **IF*x*, IF*y*, BF*x*, BF*y*** are relative to **S*y*** and **S*x***. When the facade is inclined inwards (Figure 30 (3)), the habitable area of each floor is recalculated and updated as it decreases due to the floor to ceiling height constraint.

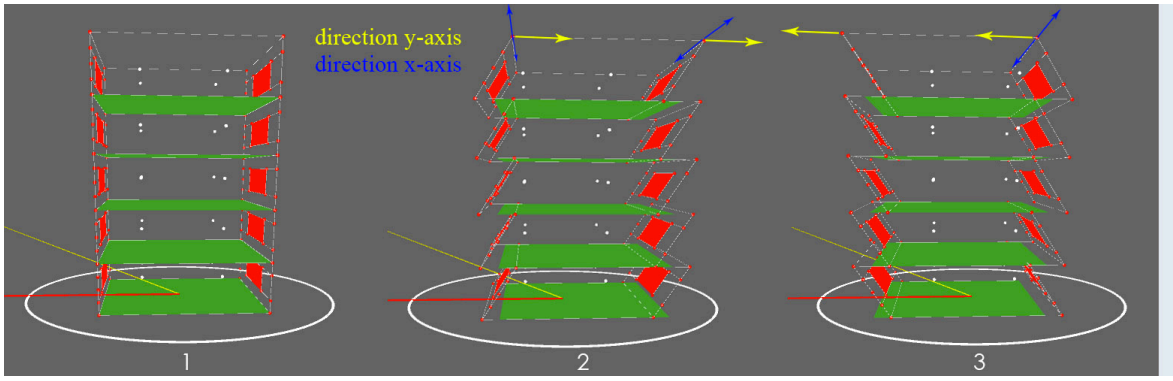

Figure 30: 1) IFy = 0m & BFy = 0m, 2) IFy = 2m & BFy = 2m, 3) IFy = -2m & BFy = -2m

T*y* and **T*x*** update the vertices of the top floor as they are relative to the **S*y*** and **S*x***. The translation of the facade vertex locations of the floors between the top floor and the ground floor are interpolated between these two floors, consequently causing overhangs. **Off*x*** and **Off*y*** offset the top floor vertices to shift the overhang to one side (Figures 31, 32 & 33).

Various methods for parametricising the fenestration were assessed including Wright & Mourshed's cellular approach (2009). The initial aim of the fenestration was to frame the view components of high value and avoid the lower quality parts. The cellular approach suits such an irrational window arrangement however it involves a large amount of variables which cause a lengthier optimisation. A more geometrical method with fewer

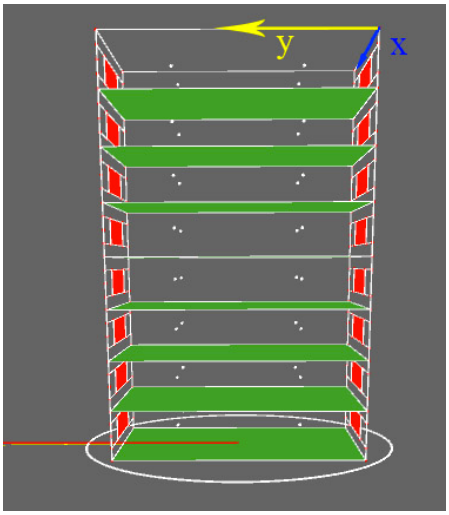

Figure 31: T*y* = 0m, T*x* = 0m, Off*x* = 0m, Off*y* = 0m

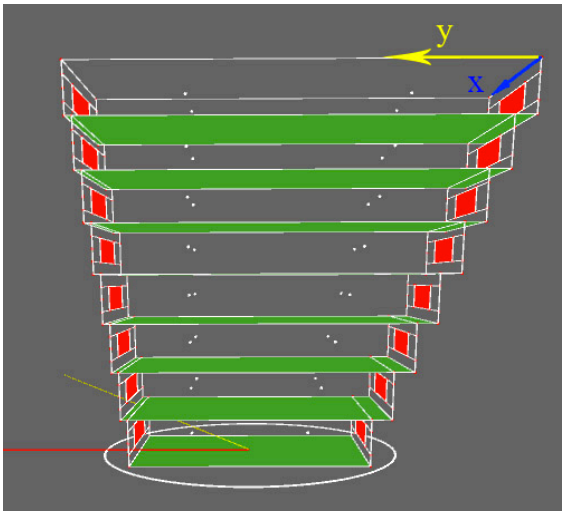

Figure 32: T*y* = 6m, T*x* = 0m, Off*x* = 0m, Off*y* = 3m

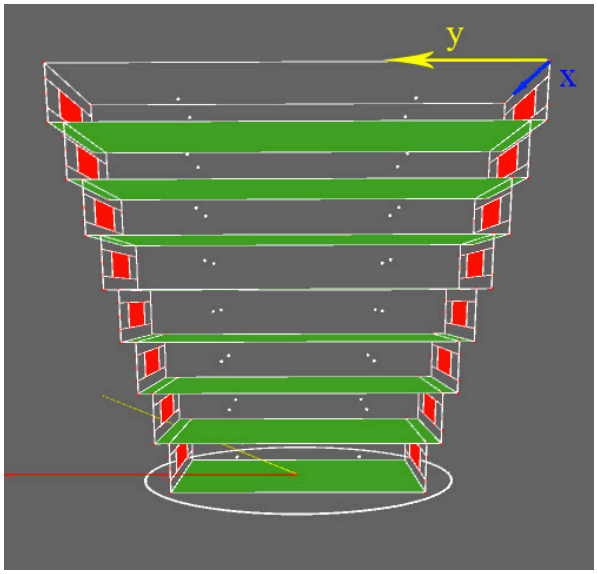

Figure 33: T*y* = 60m, T*x* = 0m, Off*x* = 0m, Off*y* = 0m

variables was therefore selected. The selected method allows window arrangements ranging from fully glazed walls to multiple individual windows whose height and width can be individually controlled.

A fenestrated wall (Figure 34) takes a wall face as a parameter which it will replace. The centre of the windows are positioned depending on $\mathbf{FW}^n$, $\mathbf{BW}^n$ and the width of the wall. The windows vertices are drawn around the central positions in an anti-clockwise manner, such that their normals face outwards. This is important due to calculation of the solar incidence. The fenestrated wall is made up of a lintel $FDAE$, a sill $GBCH$, left panel GE $w_{0v2}w_{0v3}$ and right panel $w_{nv1}w_{nv0}$ HF as visualised in Figure 34. The panels in between the windows are created by lacing up window vertices $w_{nv1}w_{nv0}w_{(n+1)v3}w_{(n+1)v2}$. Since the chosen

variables will allow inclination of planar walls, the fenestrated vertices, edges and faces are all relative to local wall plane UV (Figure 35). **FW**w and **BW**w control the width of the windows as a proportion of the width of the wall whilst **FW**h and **BW**h and height of the windows as a proportion of the height of the wall.

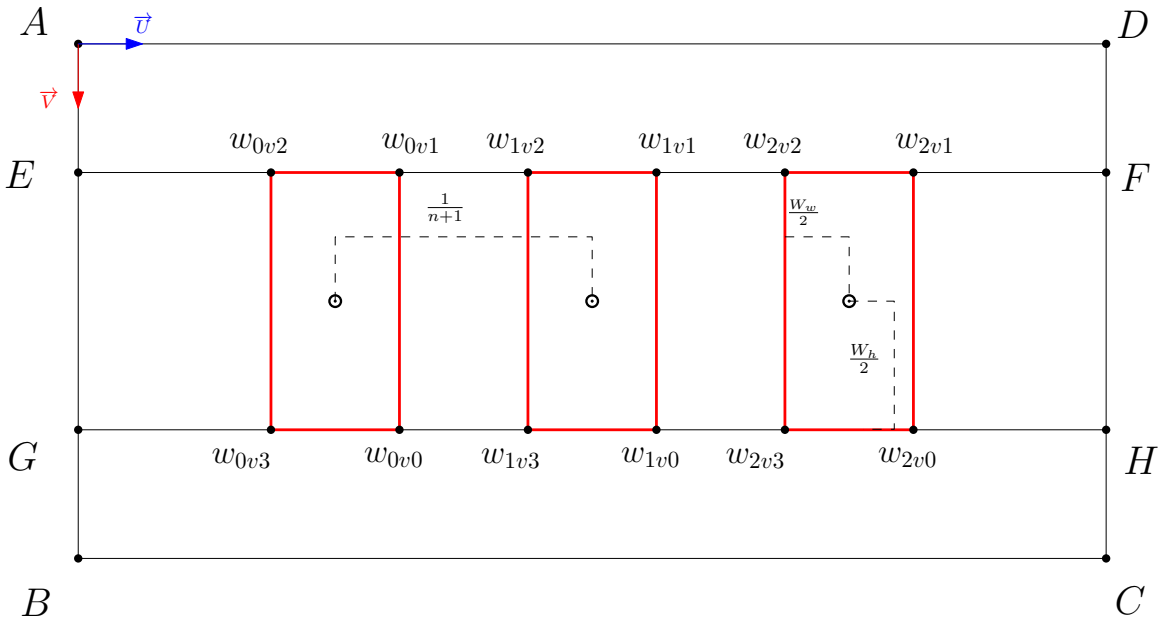

Figure 34: The geometry of the fenestrated wall.

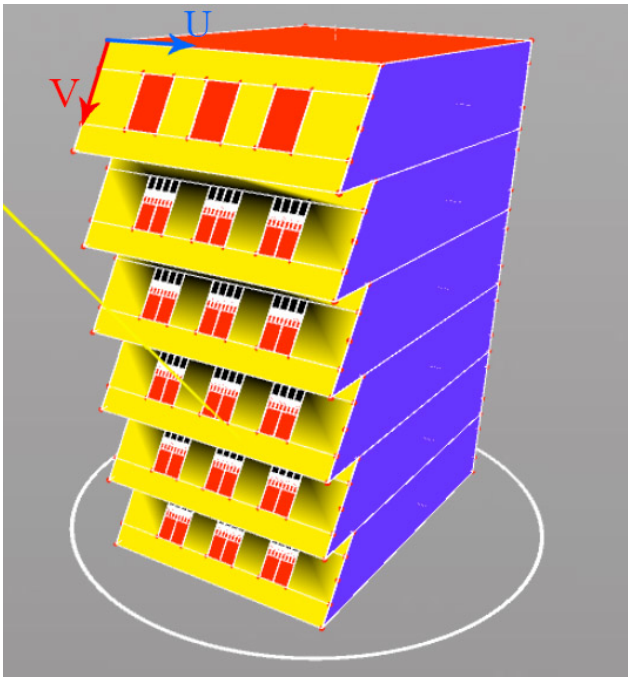

Figure 35: Inclined fenestrated wall.

The values of each variable are stored as a DNA object, which will eventually be used in the optimisation process. The DNA is visualised as a user interface in the form of interactive sliders (Figure 36). This allows the user to manually input their choice of values and visualise the corresponding geometry and simulation in a real time manner.

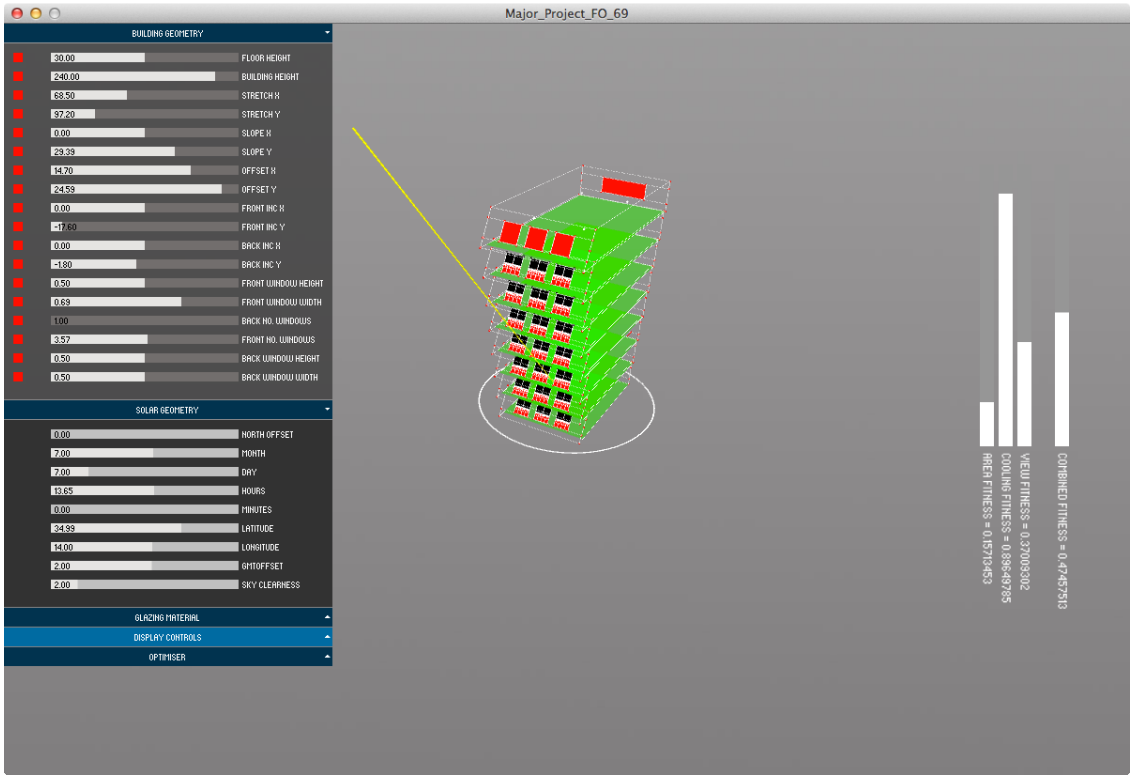

Figure 36: The interactive user-interface. DNA sliders are in the top left

6.4. Simulation

6.4.1.Solar Radiation

The global solar radiation incident on a window is calculated inside the window class. This first calculates the *solar incidence* by means of the dot product of the window face normal $\vec{n}$ and the sun direction $\vec{D}$.

$if\left(\vec{n}\bullet\vec{D}\le 0\right)$ the window face is definitely in total shadow because the solar incidence angle is greater than 90°, meaning that the sun direction is behind or parallel to the face. Incident solar radiation = 0Watts (W)

$$solar\ incidence = \vec{n}\bullet\vec{D}$$

$if\left(\vec{n} \bullet \vec{D} > 0\right)$ the window face is either totally exposed, fully shaded by means of overhangs or partially shaded by means of overhangs. The corner vertices of the window face are therefore ray-traced to determine if they are in shade. A ray path (1) originating from each window vertex v_n location, in the direction of the sun direction $\vec{D}$ is tested for intersection with any of the above floors (Figure 37).

$$\vec{X} = \vec{v_n} + \vec{D}t \qquad \text{... (1)}$$

$$\text{where } \vec{v_n} = v_1, \ldots, v_4$$

The distance *t* between the window vertex v_n and intersection $\vec{X}$, is calculated using,

$$\vec{P} \bullet \vec{N} = -d \qquad \text{... (2)}$$

$$t = \frac{-d - \vec{v_n} \bullet \vec{N}}{\vec{D} \bullet \vec{N}} \qquad \text{... (3)}$$

where,
d is the distance from the origin
$\vec{P}$ is a point on the floor plane

and then substituted back into (1) resulting in the intersection position vector $\vec{X}$.

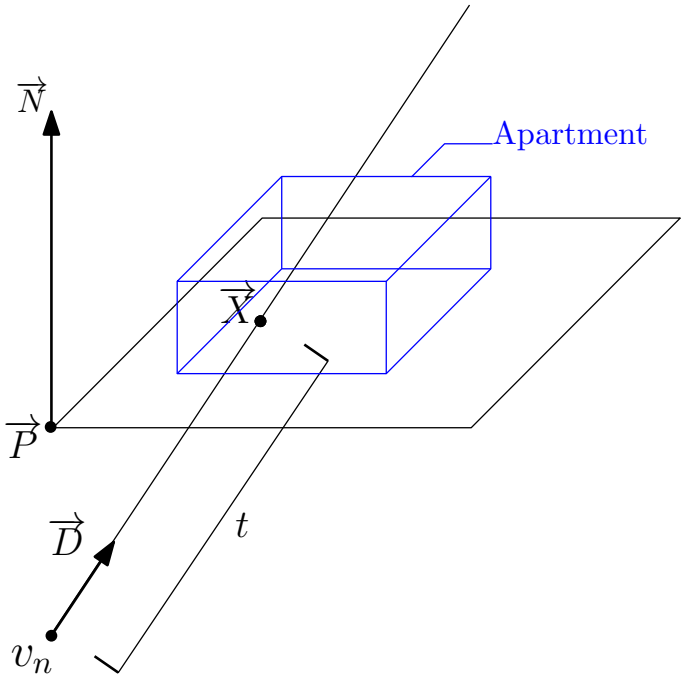

Figure 37: Ray intersection with a plane diagram.

It needs to be determined whether, the intersection $\vec{X}$ lies **inside** any of the above floor faces or outside. This is done by determining the dot product of the cross product of the edge vectors connected to each vertex ($v_0,\ldots,v_3$) with the cross product of one edge vector and intersection vector $\vec{X}$ (Figure 38).

$$\vec{N_n} = \vec{B} \times \vec{C}$$

$$\vec{V_n} = \vec{A} \times \vec{X}$$

$$if\left(\vec{N_n} \bullet \vec{V_n} \geq 0\right) \text{ for } \left(v_0,\ldots,v_3\right),\ \vec{X} \text{ is inside.}$$

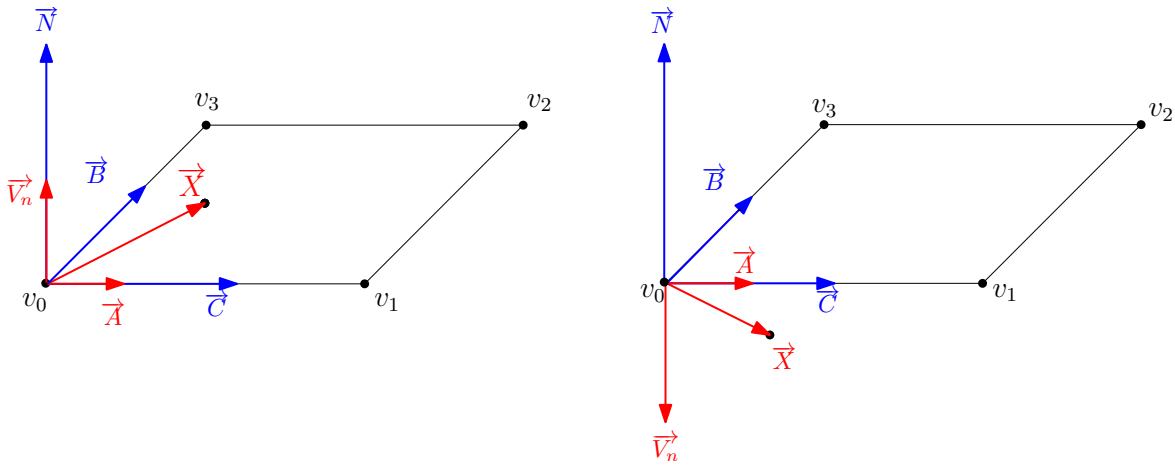

Figure 38: Intersection point inside(left). Intersection point (right).

The global solar radiation is stored in a '*radiation'* variable, which is a property of the window class. If none of the window vertices are in shade, the global solar radiation is calculated for the total window area (Figure 39, left). If the window vertices are all in shade nothing is added to '*radiation'*. If only some of the window vertices are in shade, then the window face is subdivided once into four faces using the midpoint of the window and the new faces are stored in a list of window faces (Figure 39, right). The same radiation calculation function is called again and the new subdivided faces are passed as parameters.

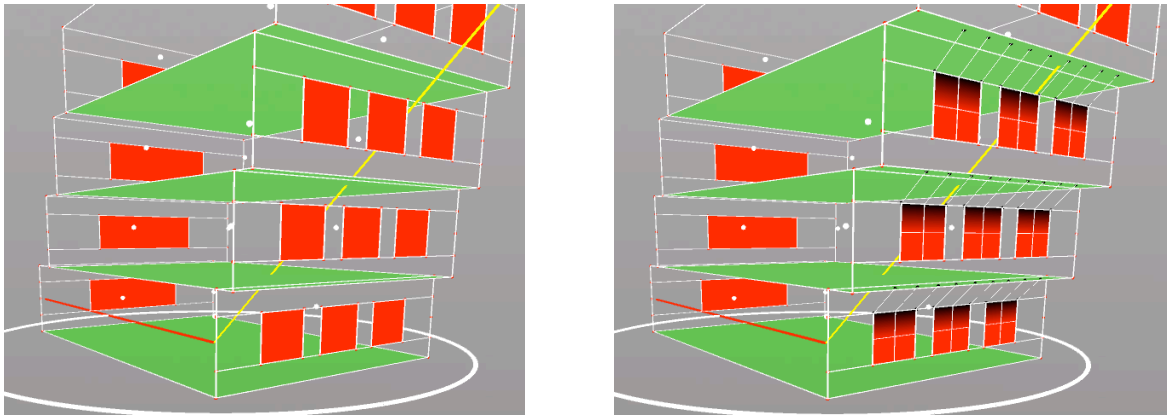

Figure 39: No intersection (left). Ray - floor face intersection(right).

The function recurses until the face diagonal reaches a threshold length, dynamically subdividing the window faces each time (Figure 40) and a proportion of the total global solar radiation is added to *'radiation'*, based on the ratio of shaded to non-shaded vertices of the last face.

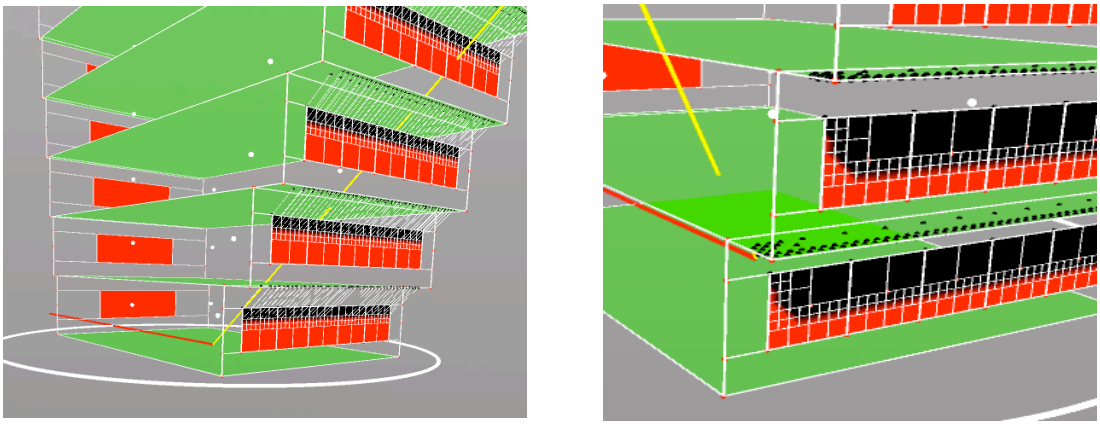

Figure 40: Dynamic subdivision to accurately obtain cast the shadow.

The total radiation obtained is then used to calculate the transmitted radiation through the glazing into the space.

6.4.2.View Score

The window class is capable of the view quality calculation of a view visible through the window. The geometry of the apartment, the geometry of the window and the image of the view itself have a direct effect on the view score. Since the geometry of each floor varies differently when causing overhangs it is important for the window class to know of the geometry of the floor it belongs to. The floor geometry determines the eyeball positions $\vec{E}$.

The model presented in Figure 40 assumes an image ‘wrapped’ around the circumference of a cylinder. Since the field of view of the camera which took the image is unknown, the distance of the observer away from the landscape cannot be calculated. An infinite distance is therefore assumed. This assumption further assumes parallelism between the vector $\vec{A}$ (Figure 41) and radius of the cylinder. This method avoids the requirement for the distance between the *view* and the *eyeball* position $\vec{E}$ and assumes the cylinder is of infinite radius. These assumptions cause visual inaccuracies when displaying the A’B’ boundary because of the fact that geometry with an assumed infinite radius is being represented with finite dimensions.

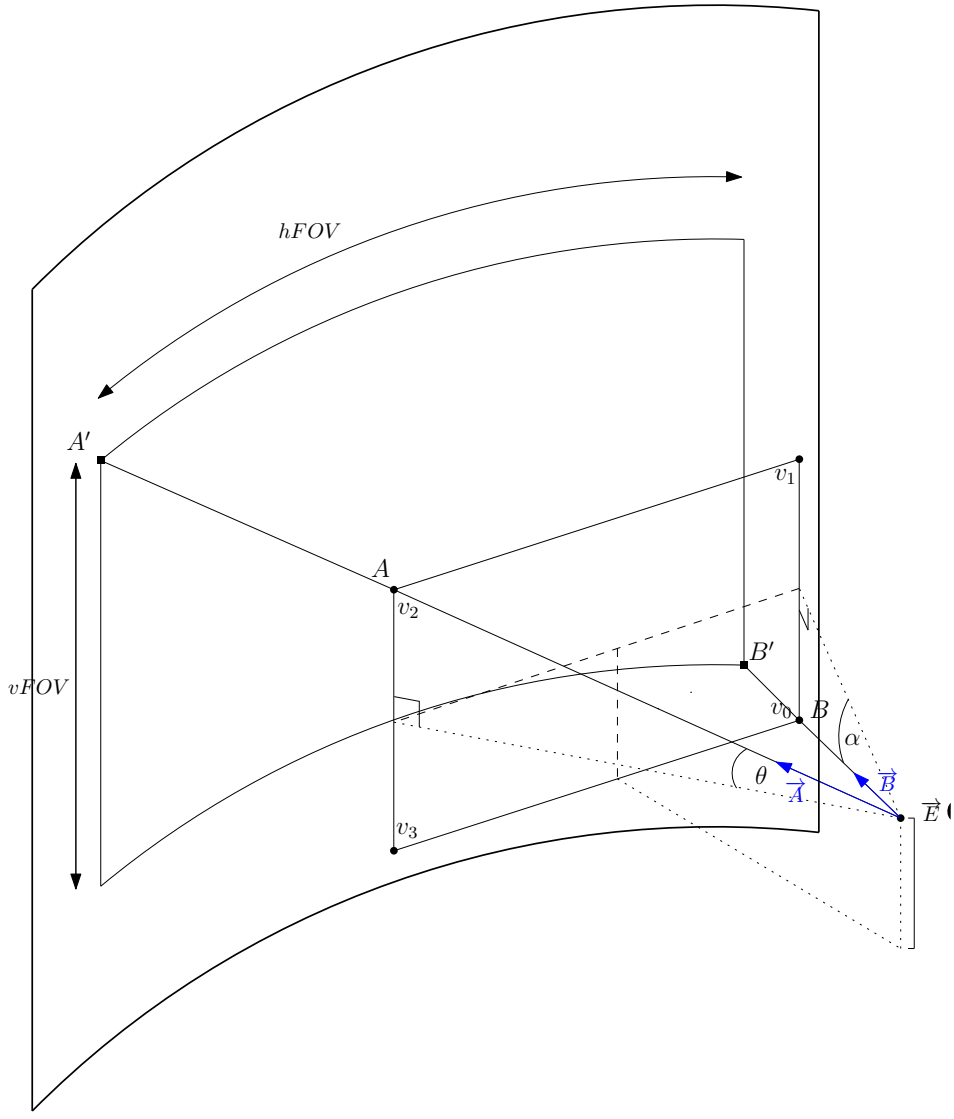

Figure 41: The proposed model for determining the corresponding pixels bounding the FOV.

The aim of this exercise is to project the boundary of the window AB onto the wrapped image to obtain the bounding pixel coordinates $A'B'$. The image pixels within the projected boundary $A'B'$ are visible through the window at the particular eyeball position $\vec{E}$. These pixels are required at a later stage in order to be scored.

Method

The floor-plate area of each floor is subdivided into four sub areas as explained in 4.4.2. (Figure 42). Two vectors $\vec{A}$ and $\vec{B}$ are extended towards the window diagonal corners A and B. Two vectors provide enough information to obtain the bounding coordinates assuming that the window geometry is always rectangular. These vectors are unitised and used to determine the horizontal and vertical field of view (*hFOV* and *vFOV* respectively) (Figure 41).

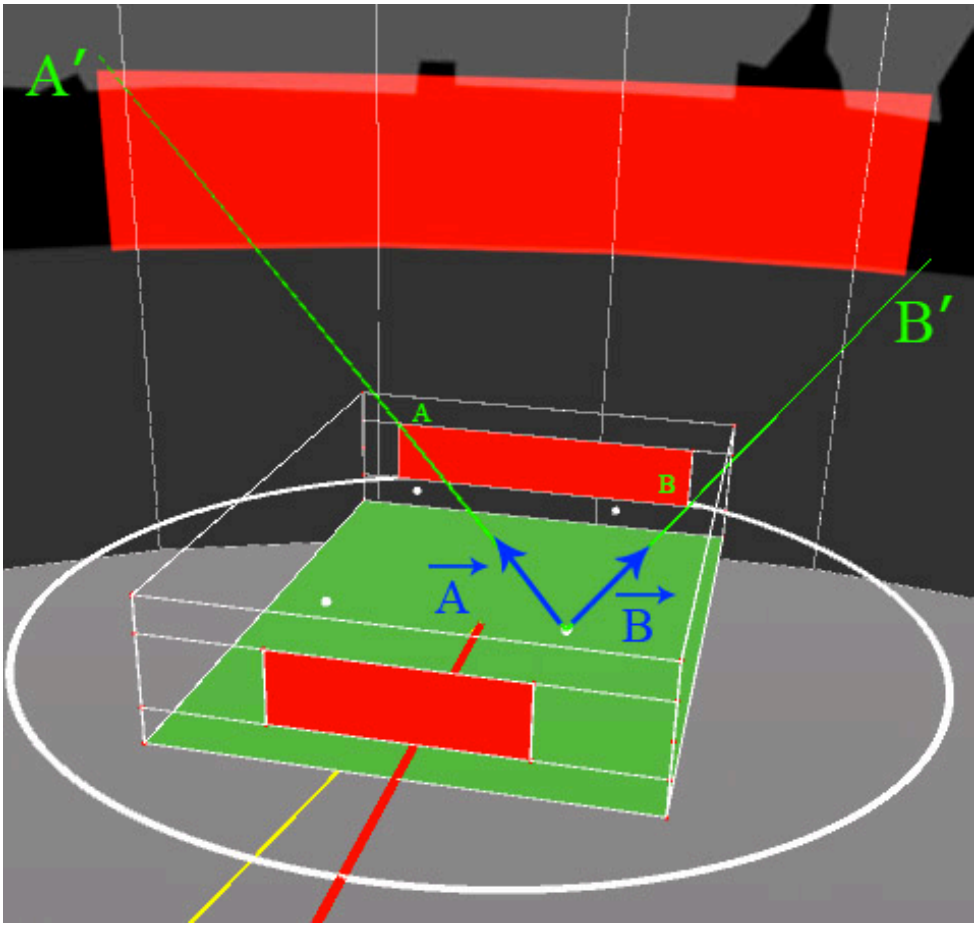

Figure 42: Vectors $\vec{A}$ & $\vec{B}$ extended from all eyeball positions.

Determining $hFOV$:

$hFOV = A'_U - B'_U$

where,

A'_U and A'_U are the U-components of the UV coordinates of the upper left most pixel and lower right most pixel of the projected boundary, respectively. W represents the width of the image whilst h represents the height of the image (Figure 43).

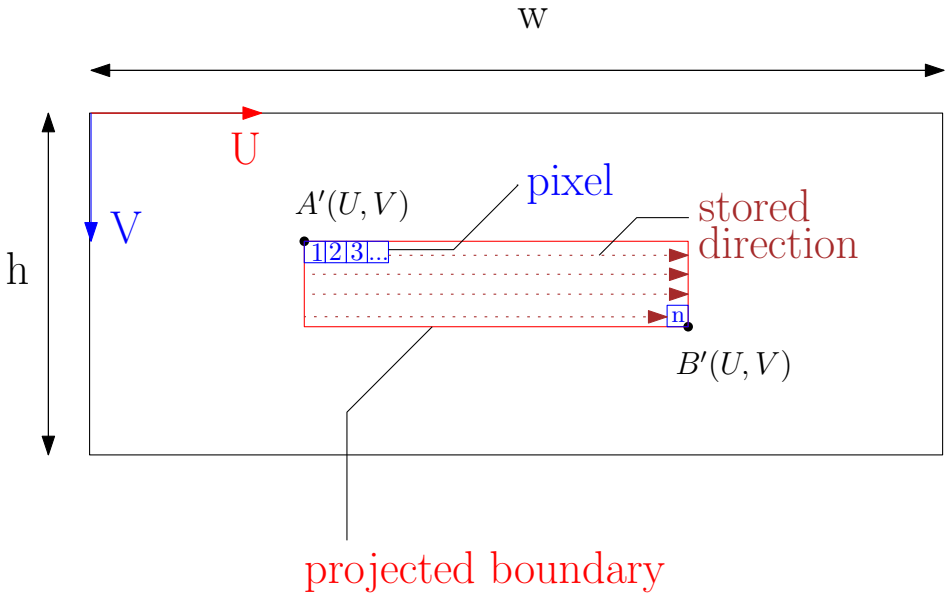

Figure 43: Local UV coordinate system of the 'unwrapped' cylindrical image, explained.

Angles ϕ and φ represent the horizontal azimuths of unit vectors $\vec{A}$ and $\vec{B}$ respectively. These are measured from the positive horizontal x-axis are needed in order to determine A'_U and B'_U . Angles are measured between $-\pi$ and π when using built-in processing function atan2 (Figure 44). The direction of measure of the azimuth angle corresponds to the direction in which the pixels are stored in.

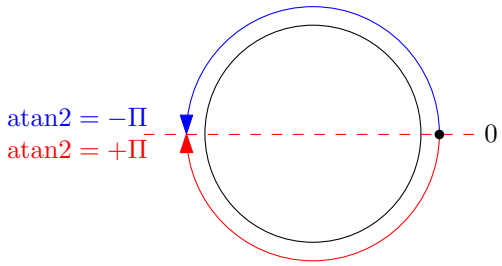

Figure 44: atan2 **direction of measure.**

$$\left.\begin{aligned}\text{azimuth } \varphi &= \text{atan2}\left(B_y, B_x\right)\\ \text{azimuth } \phi &= \text{atan2}\left(A_y, A_x\right)\end{aligned}\right\}\text{Figure 45, right}$$

where, A_x, A_y are the components of unit vector $\vec{A}$ and B_x, B_y are the components of unit vector $\vec{B}$.

$$\left.\begin{aligned}if\left(\varphi<0\right) &\Rightarrow \text{azimuth } \varphi = 2\pi-\varphi\\ if\left(\phi<0\right) &\Rightarrow \text{azimuth } \phi = 2\pi-\phi\end{aligned}\right\}\text{Figure 45, left}$$

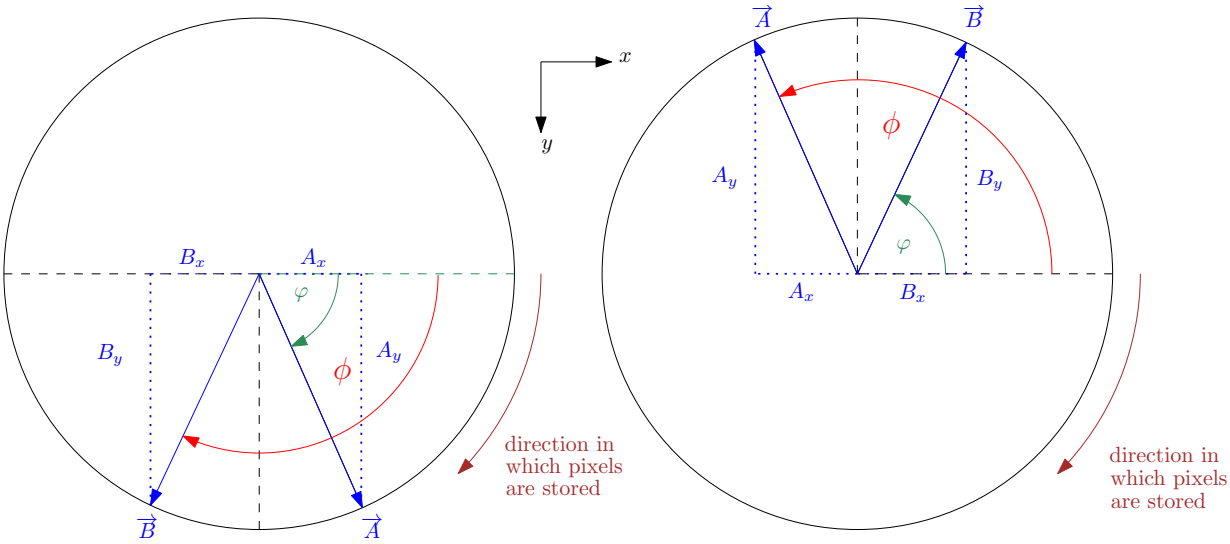

Figure 45: Plan view. Calculation of the horizontal

Since the image is wrapped around the circumference, 2π is equivalent to the number of pixels in the width of the image therefore,

$$A'_U = \frac{\text{azimuth } \varphi * W}{2\pi} \qquad B'_U = \frac{\text{azimuth } \phi * W}{2\pi}$$

Determining *vFOV* **:**

$vFOV = A'_V - B'_V$

A'_V and B'_V are the V-components of the local coordinates of the upper left most pixel and lower right most pixel of the projected boundary, respectively.

The vertical angles θ and α are determined in order to find A'_V and B'_V respectively (Figure 46).

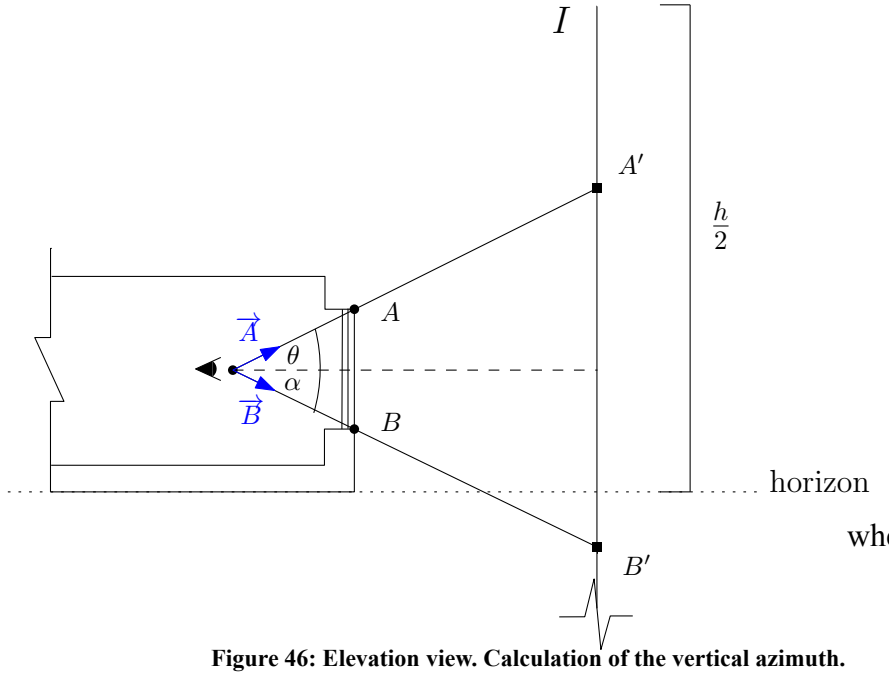

$$\theta = \sin^{-1}(A_z)$$

$$A'_V = \left(\frac{h}{2} - \frac{\theta * W}{2\pi}\right)$$

$$\alpha = \sin^{-1}(B_z)$$

$$B'_V = \left(\frac{h}{2} + \frac{\alpha * W}{2\pi}\right)$$

where, I = image

h = image height

Figure 46: Elevation view. Calculation of the vertical azimuth.

Now, since A' and B' have coordinates (A'_U, A'_V) and (B'_U, B'_V) respectively, the bounding limits are known and the pixels inside the boundary may be scored as by means of a nested loop as discussed in Chapter 4. Figure 47 visualises the projected pixel boundary in red.

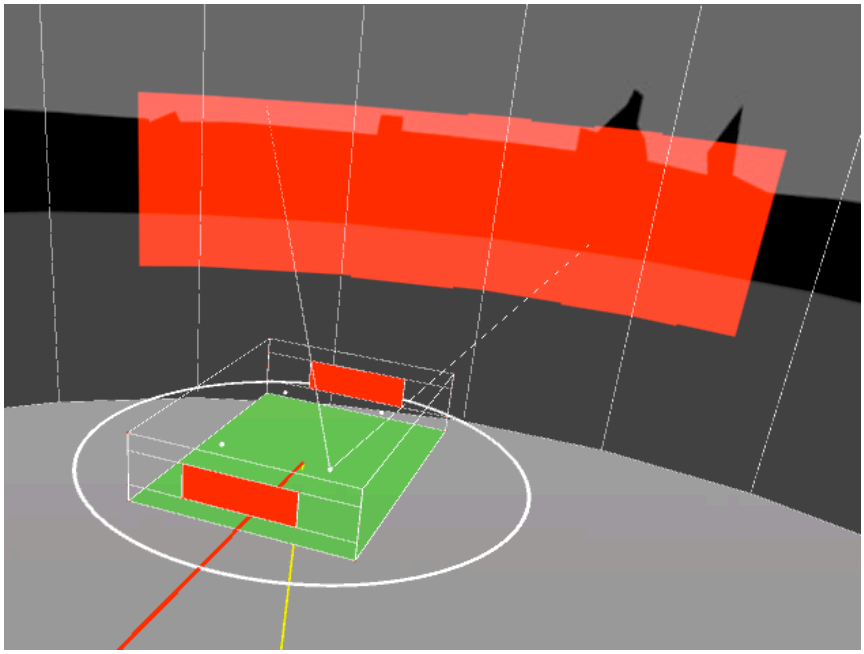

Figure 47: Visualised projection on the image.

While looping through the pixels within the boundary, a method that scores a pixel based on its grayscale value, is called for each pixel. Scores ranging between 6 and 1 are assigned to 6 shades of grey ranging from 0 (black) to 255 (white), respectively. The view image is 'shaded' according to the user's preference as explained in Chapter 4 prior to running the software. The score of each pixel is summed and it's final total returned as the view score for that window.

An overhang may be visible through a window and thus obstruct a view. Figure 48 visualises such a scenario where,

θ is the elevation angle of vector A'

φ is the elevation angle of the unit vector extended from the eyeball position E in the direction of one corner of the overhang O (Figure 48)

$if\,(\varphi \geq \theta)$ an overhang is not visible through the window

$if\,(\varphi < \theta)$ an overhang is visible through the window therefore obstructing the view. In the case of an overhang obstructing the view, the obstructive number of pixels is determined by the following:

$$\text{number of obstructed pixels} = \frac{(\theta - \varphi) * W}{2\pi}$$

The obstructive number of pixels are then added to the A'_V coordinate (Figure 48). The pixels obstructed by the overhang are assigned the lowest score of 1.

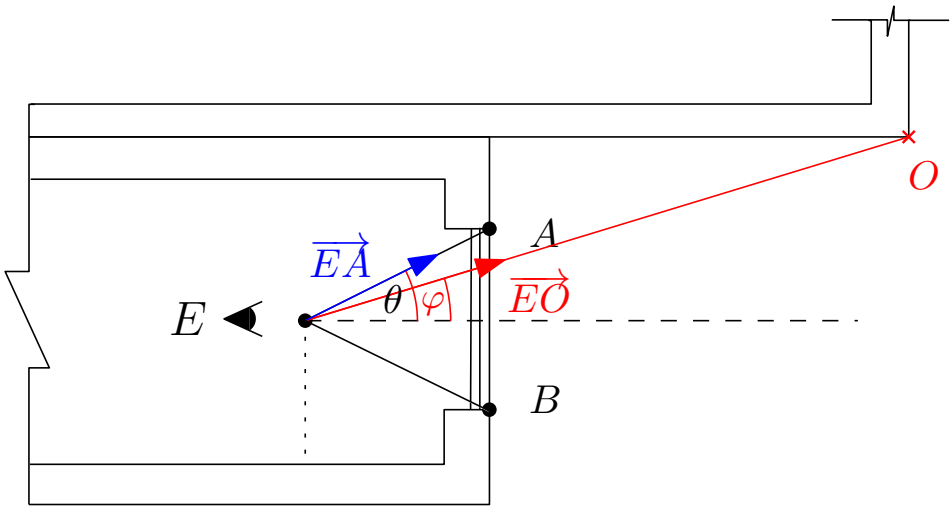

Figure 48: Sectional elevation of an obstructed view scenario.

6.5. Optimisation

6.5.1. User Interface (UI)

The aim of an interactive UI for the building geometry was also extended to the optimisation component of the proposed integrated framework. A second window was created to display the population of plotted solutions in the solution space bounded by the cooling load objective on the x-axis and the view cost objective on the y-axis (Figure 49). The solutions are plotted as selectable buttons which when pressed, display the geometry corresponding to the DNA stored within that solution.

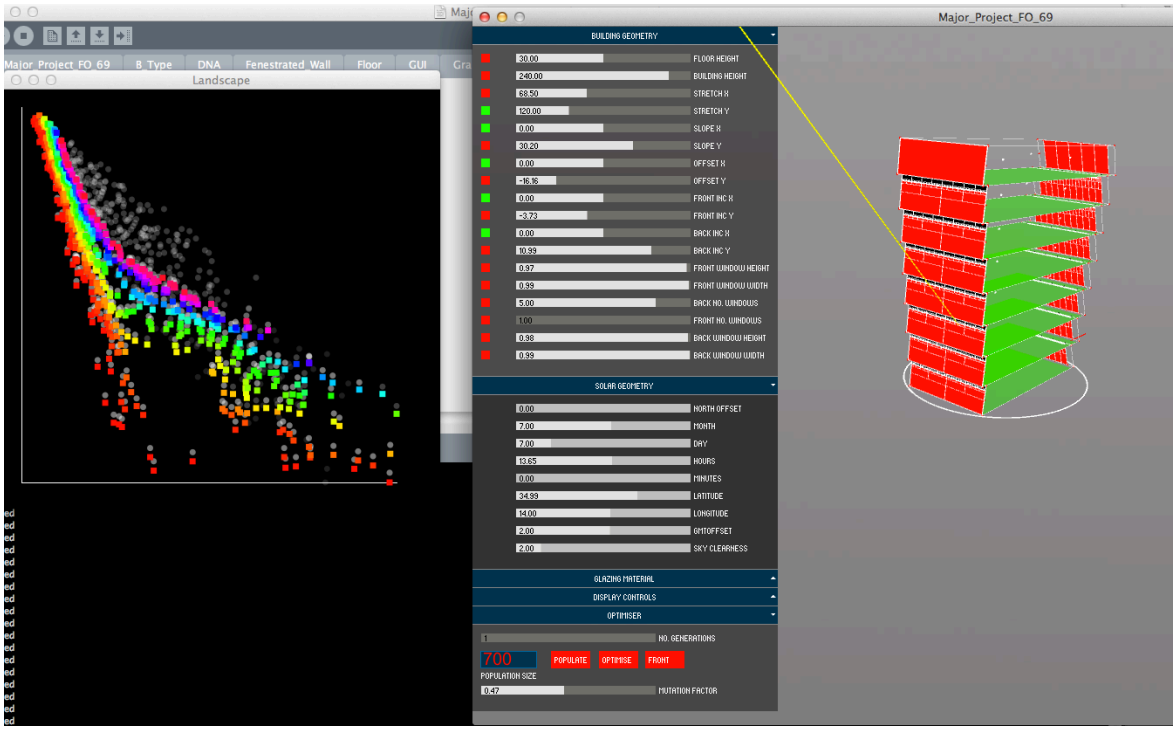

Figure 49: Second window displaying the objective space.

6.5.2. Generative Framework

The *Optimiser* class contains all the functions involved in the GA. An *Optimiser* object passes a list of *Solution* objects as an argument. This list is ranked based on each solution's objective function, crossed over and mutated.

The proposed generative framework implements a Non-dominated Sorting Genetic Algorithm (NSGA-II) (Deb *et al.* 2002). The main steps involved in the algorithm consist of the following in order:

when ($t = 0$) :

1. Initialise random population P_0

when ($t \geqq 0$) :

2. Select parents
3. Crossover and mutate P_t
4. Combined P_t and Q_t
5. Sort combined population R_t
6. Fill new population Q_{t+1}

where, t = number of generations

I. Initialise random population P_0

For each member of the population, a DNA object with random argument values is instantiated and the simulation functions are called in order to form the objective vector. The objective vector is defined as,

$$\vec{O} = (Q_c, Q_v)$$

where,

Q_c = cooling load, *KWh*

Q_v = view cost, €

II. Select parents

Binary tournament (Miller and Goldberg 1996) is performed in order to select two random parents, S_A and S_B for crossing over. S_A is determined by randomly selecting two random solutions, comparing them and selecting the fittest. This is repeated to select S_B.

III. Crossover and mutate P_0

Once the parents are selected, they are crossed over to form a new offspring S_{child} of the same amount of variables as the parents'. In many GA applications, a single-point cross over is used (Agrawal *et al.* 1994). A probability value p ($0 \leq p \leq 1$) is generated randomly. p determines the probability of selecting a variable from parent S_B otherwise

they are selected from S_A . A second random value q ($0 \leq q \leq 1$) is generated. The child's 'empty DNA' is looped through and for each empty variable slot V_n , variable V_n from parent S_A is selected if q ≥ p, otherwise V_n is selected from S_B . The cooling load and view value of S_{child} are then calculated based on the genetic code of the new DNA_{child} and the objective of S_{child} can be defined. The new S_{child} can therefore be interpreted as,

$$S_{child} = \left(DNA_{child} , \vec{O}_{child} \right)$$

The offspring is then mutated to allow for variation to occur. A random value within the range R is added to each DNA_{child} variable value.

$$R = \left(\text{(variableMin - variableValue)*mutationFactor , (variableMax - vairbaleValue)*mutationFactor} \right)$$

Any constrained (locked sliders) variables will not be mutated. The mutation factor can be selected interactively by means of a slider or can be randomly generated.

IV. Select Parents

Parents are selected from the population P_t using the same method as in **Step 2**.

V. Cross over and mutate P_t

The parents obtained from **Step 4** are crossed over and mutated to produce the new offspring population in the same manner as in **Step 3**.

VI. Combined population R_t

The current population P_t is concatenated with the new offspring population Q_t obtained in **Step 5** to form one list of solutions R_t of size 2N. Elitism is ensured as the dominant solutions from the previous generation are chosen for the next assuming that they are not dominated by any solutions within their offspring population.

$$R_t = P_t \cup Q_t$$

VII. Sort R_t for non-domination

The NSGA-II assumes that every solution S has a dominance rank attribute S_{rank} equivalent to the number of solutions whose objective values are larger or less than those of S, depending on whether the objective is of a maximisation or minimisation nature. Therefore, a non-dominated S is one having an S_{rank} equivalent to zero. All solutions whose S_{rank} is equivalent to zero are said to lie on the Pareto front (Deb *et al.* 2002). The algorithm minimises the cooling load whilst maximises the view value (Figure 50).

$$S_A = \left(Q_{Ax}, Q_{Ay}\right)$$

$$S_B = \left(Q_{Bx}, Q_{By}\right)$$

$$\left(Q_{Ax} > Q_{Bx}\right) \cap \left(Q_{Ay} > Q_{By}\right) \Rightarrow S_A \succ S_B \quad , S_{B\,rank} += 1$$

$$\left(Q_{Ax} < Q_{Bx}\right) \cap \left(Q_{Ay} < Q_{By}\right) \Rightarrow S_A \prec S_B \quad , S_{A\,rank} += 1$$

$$\left.\begin{array}{l}\left(Q_{Ax} < Q_{Bx}\right) \cap \left(Q_{Ay} > Q_{By}\right) \\ \left(Q_{Ax} > Q_{Bx}\right) \cap \left(Q_{Ay} < Q_{By}\right)\end{array}\right\} \Rightarrow S_{A\,rank} = S_{B\,rank} = 0$$

where,

Q_{Ax} and Q_{Bx} represent the objective values, $S_A \succ S_B$ represents S_B dominated by S_A, $S_B \succ S_A$ represents S_A dominated by S_B and $\left(Q_{Ax} > Q_{Bx}\right) \cap \left(Q_{Ay} > Q_{By}\right)$ represents the condition that Q_{Ax} has to be larger Q_{Bx} whilst Q_{Ay} also has to be larger than Q_{By} for S_B to be dominated by S_A

```
void sort (Solution [] list_solutions) {

  for (int i=0; i< N   ; i++)
  {
    Solution A = list_solutions[i];
    for (int j=i+1; j<N; j++)
    {
      Solution B = list_solutions[j];
      if (( A.objective.x > B.objective.x) && (A.objective.y < B.objective.y))
      {
        A.dominatedScore = A.dominatedScore + 1;
        B.dominatedSolutions.add(A);
        A.dominatingSolutions.add(B);
      }
      else
      {
        if ((A.objective.x < B.objective.x) && (A.objective.y > B.objective.y))
        {
          B.dominatedScore = B.dominatedScore + 1;
          A.dominatedSolutions.add(B);
          B.dominatingSolutions.add(A);
        }
      }
    }
  }
}
```

Figure 50: Non-dominated sorting method.

The combined population R_t is sorted for non-domination and each solution is given a rank.

VIII. Fill new population Q_{t+1}

The now sorted combined population R_t, is ordered from lowest S_{rank} to highest S_{rank}, so that the fronts are in order of domination. R_t is looped through and each solution is added to Q_{t+1} until the list reaches N solutions.

The first four fronts (F1 to F4) are colour coded to easily identify them (Figure 51). A trail of the solutions from the past generations are visualised as grey circles (Figure 51). The opacity of the grey circles is relative to the age of that solution.

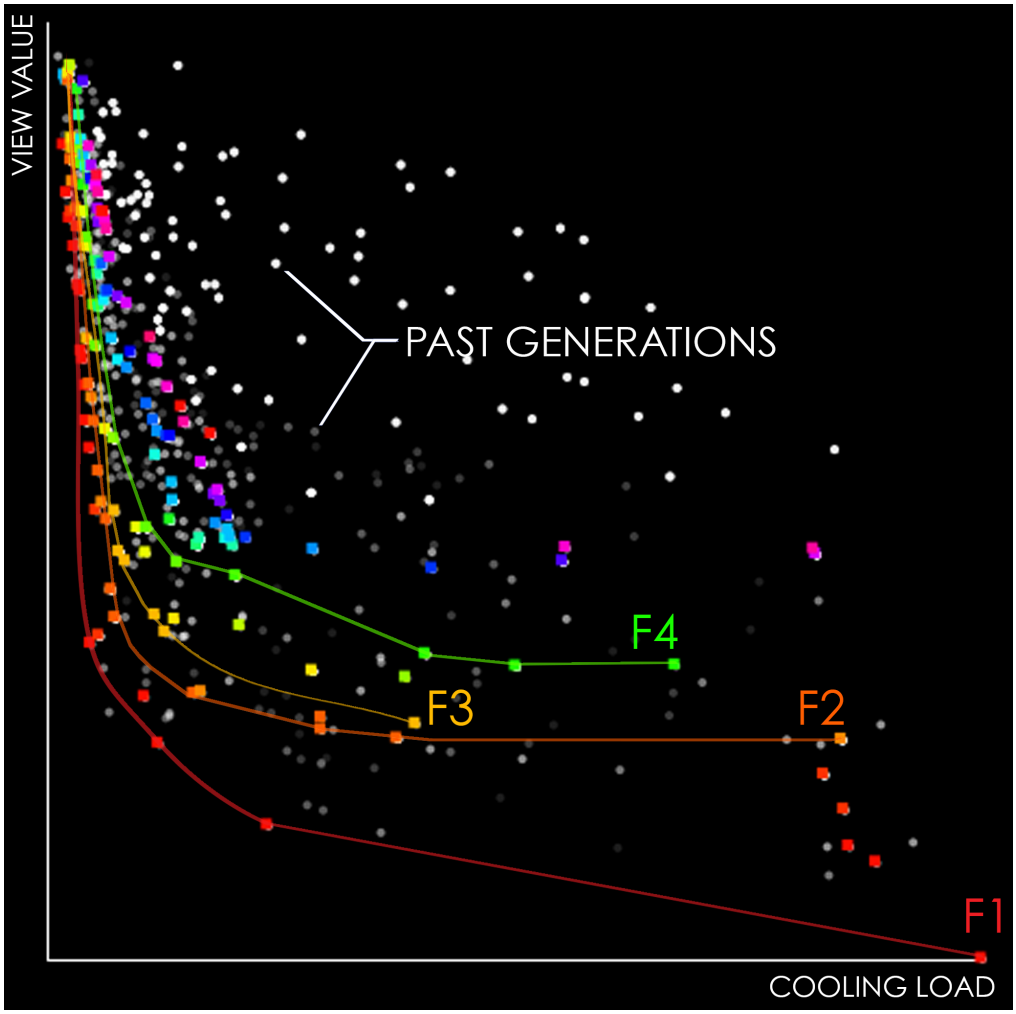

Figure 51: Colour coded fronts in the objective search space.

6.6. Testing the Optimiser

North View Test Exercise (Non Conflicting Objectives)

The GA was run for a building with a good view in a North orientation. As expected, the majority of the solutions on the Pareto front yielded large North facing windows (Figures 52 & 53). The relationship between the cooling load and view value objectives is not of a conflicting nature because North-facing windows do not admit heat from a Southern sun. Figure 52 visualises the third generation of a population size of 450 solutions. The corresponding cooling loads and view values were tabulated in Table 5.

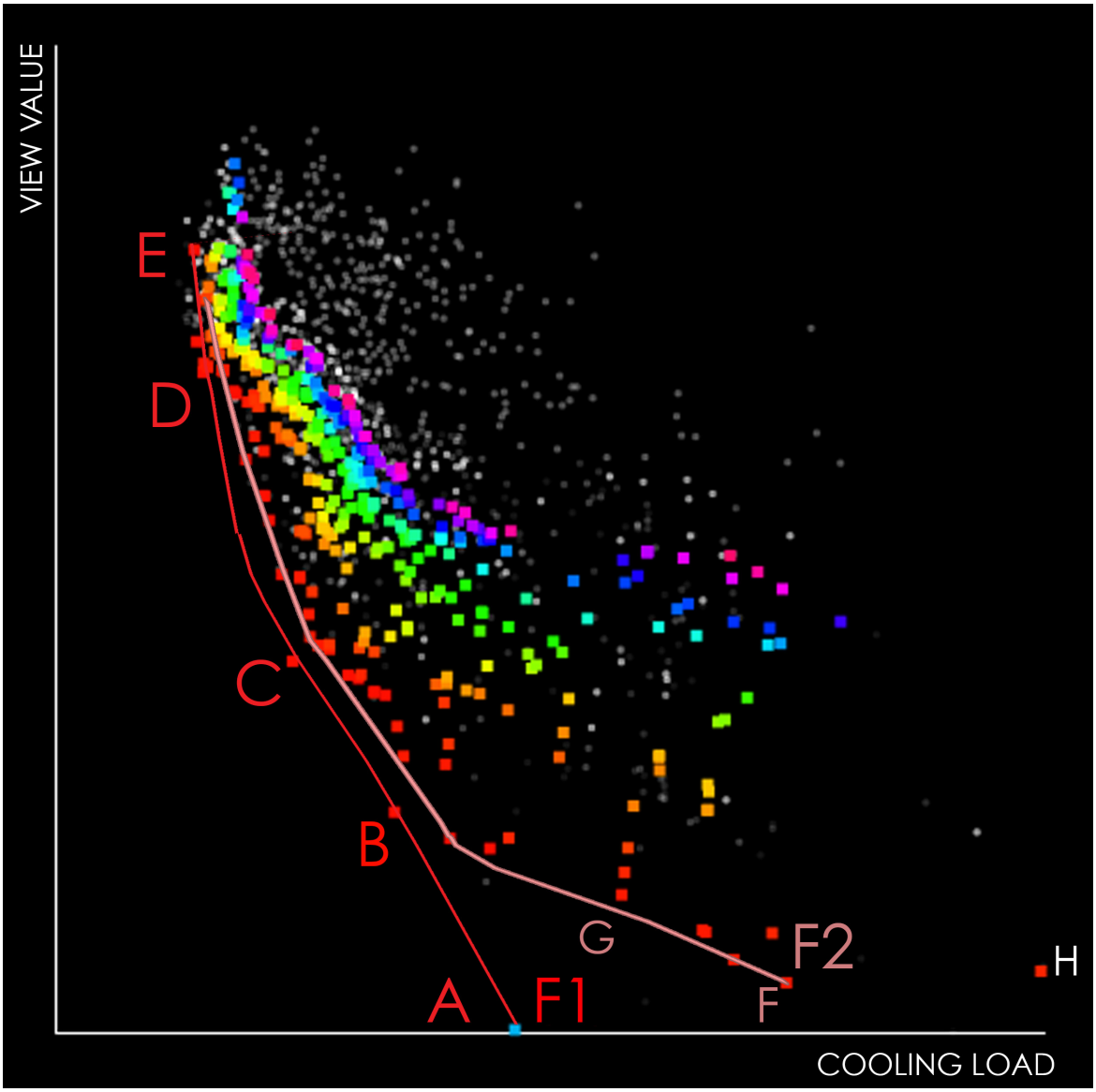

Figure 52: Solutions from a 3rd generation Pareto front of a North facing view.

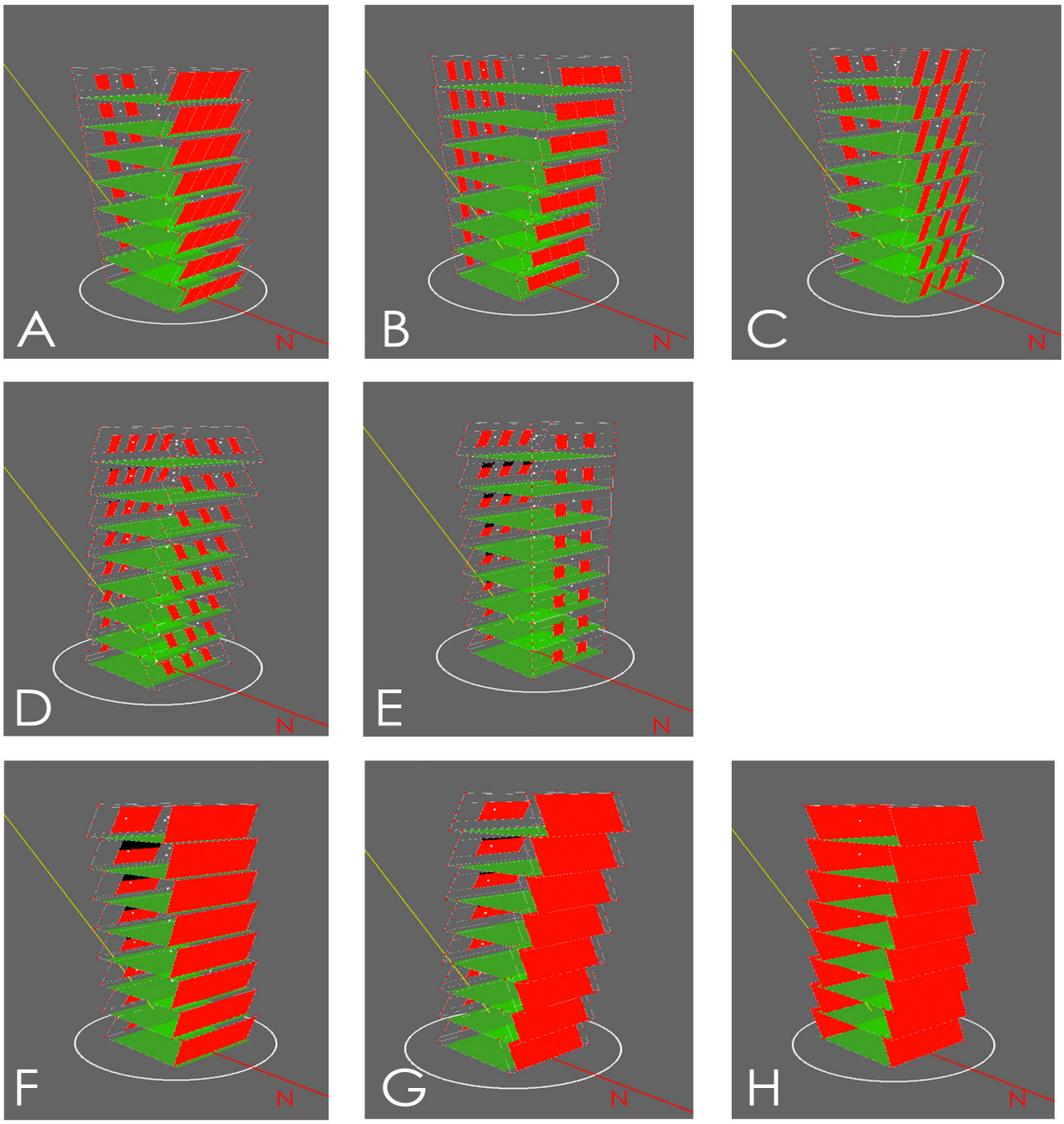

Figure 53: Pareto solutions (A toE) for a North facing view. F to H are solutions from the second front.

Solution	C (kWh)	V (€/month)
A	6760	40832
B	5001	31830
C	3509	25586
D	2203	13641
E	2074	8563
F	10731	38892
G	8325	35246
H	14454	38408

Table 5: Cooling loads and view values of the Pareto solutions in Figure 53.

South View Test Exercise (Conflicting Objectives)

The condominium scenario discussed in Chapter 4 was used as a test scenario for testing conflicting objectives. The view lies in a South orientation of the building, thus causing conflict with the cooling load due to large glazed facades. Three generations with a population of 450 were run.

Fully glazed South-facing walls such as in solutions A and B produce the highest cooling loads (Figure 54 and Table 6). However, the inclination of the facade can vary this value. A South-facing facade with an outward incline such as in solution A (Figure 55) causes a large angle of solar incidence which yields low radiation when compared to the same facade with an inward incline such as in solution C (Figure 55). A low angle of solar incidence means that the facade is exposed to high solar radiation. However, windows on inward inclined facades are partially shadowed by means of the produced overhangs which therefore directly reduces the cooling load.

The dimensions of the windows also effect the cooling load where minimising the width **WW** and height **WH** variables seem to reduce the cooling load. However this corresponds to a lower view value. This occurs mostly between solutions D and E on the Pareto front (Figure 54). Narrower and thinner windows cause interruptions, not making them suitable for landscapes or skylines (solution D). Although the South windows in solution C have a lower **WH** than those in solutions A and B, the window still yields a decent view value because the **WW** value is maximum thus creating an uninterrupted landscape window. Furthermore, the window is partially shadowed by the overhang due to the inward inclined facades. The combination of these elements allows such a solution to be a possible contender to satisfying the developer's aim yet consume less energy.

The Pareto front (Figure54) was sampled (A-E) and the corresponding objective values (per building per month) are tabulated in Table 6. Solutions F to H (Figure 55) were taken from the second front (F2) (Figure 54).

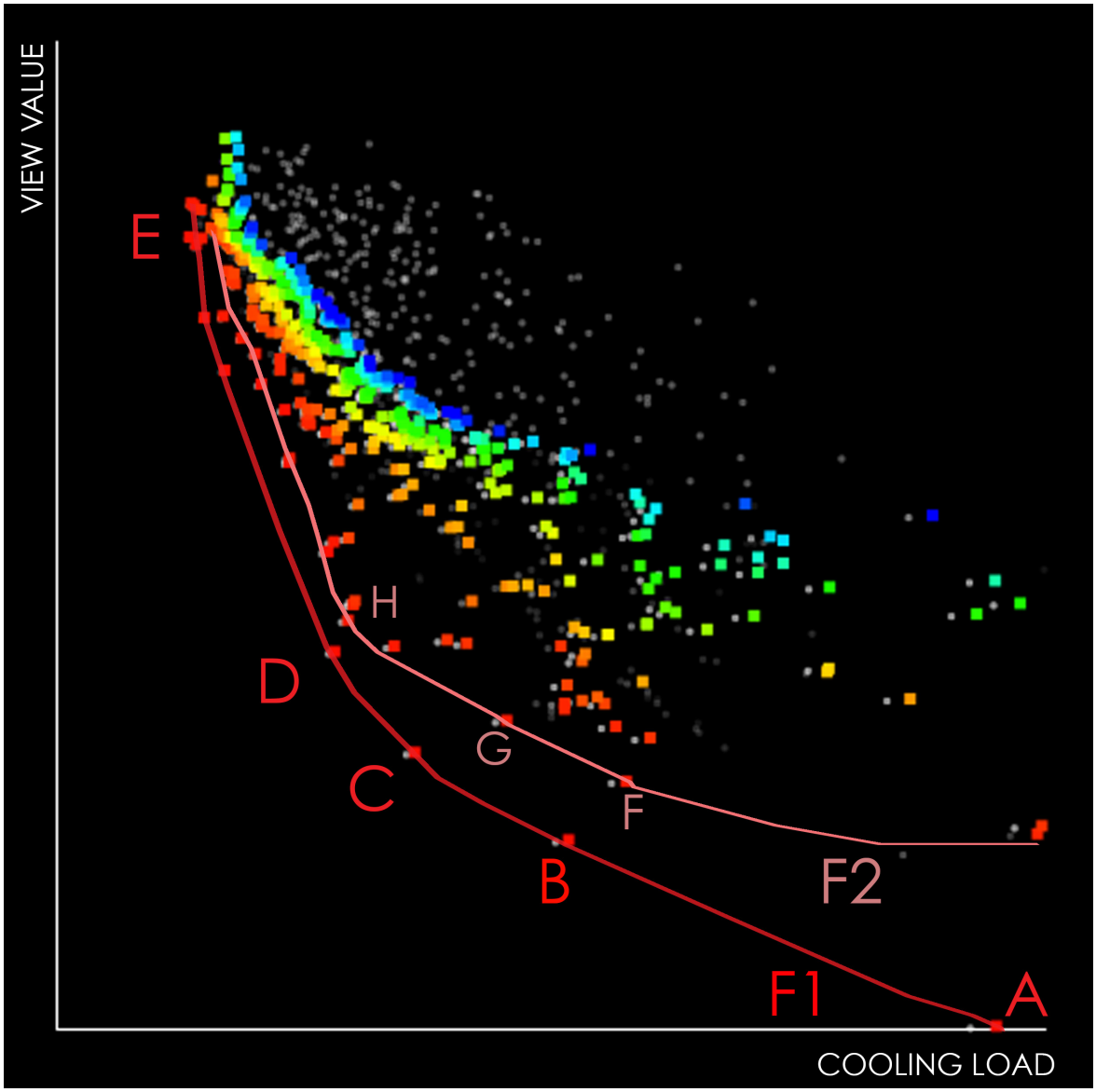

Figure 54: Third generations Pareto solutions (F1) for a South facing view. F2 is the second front.

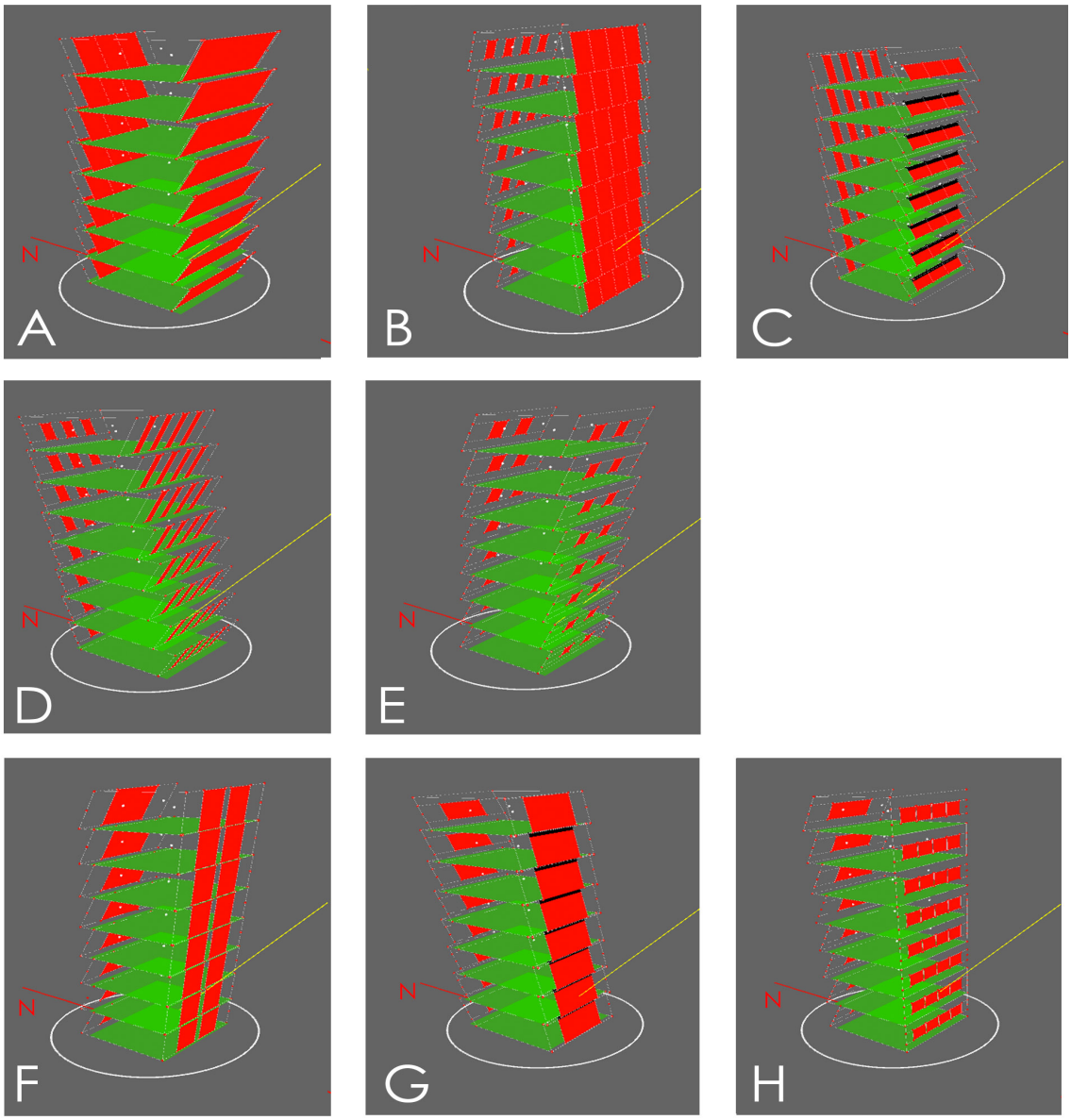

Figure 55: Pareto solutions (A toE) for a South facing view. F to H are solutions from the second front.

Solution	C (kWh)	V (€/month)
A	13102	45502
B	7158	36925
C	5021	32893
D	3907	28250
E	1890	9142
F	7958	34220
G	6298	31420
H	4092	--

Table 6: Cooling loads and view values of the Pareto solutions in Figure 55.

7. Case Study

7.1. Introduction

The generative design tool was tested on a realistic case study block of apartments which is also the reason to this research.

The building is located a few hundred metres away from the condominium discussed in Chapter 4. The current building is composed of all the issues this dissertation is tackling, mainly, large glazed South-East walls to take full advantage of the landmark view of Valletta (Figure 56).

Figure 56: South-East glazed facades of the existing apartment block.

South-East glazing coincides with the hot rising sun during the peak summer months. This causes large amounts of solar transmission into the space through the large glazed area and direct glare. The living room is situated in the front room, thus being directly effected by

these repercussions. Vertical blinds are therefore used for protection from the direct solar radiation and glare during the morning hours, thus obstructing the view.

A resident in this block of apartments was interviewed (Conti 2011) regarding the times of day and season the vertical blinds are actually used. The floor plans are almost identical on each floor, meaning the details in this interview are applicable to all floors. The resident stated that the South-East blinds are used between 9:00 and 12:00 during summer peak months and between 9:00 am and 14:00 during the winter months. The South-West blinds are used between 15:00 and 17:00 during the summer months and between 14:00 and 16:00 during the winter months.

It is being assumed that the blinds are used in the morning time because of the low altitude rising sun in the South-East. This transmits high intensity incident solar radiation through the glazing due to the low angle of incidence and also causes glare. During the winter, the rising sun is not as intense due to the longer travel path through the atmosphere. However it still causes unwanted glare as the angle of incidence of a rising sun is similar to the summer one (Figure 57). It is assumed that the blinds are used during the afternoon due to the high intensity radiation on the South-West facade during the summer months despite the high altitude.

Figure 57: Photo taken on 15th November at 10:34 am (South East Blinds drawn) (Santos 2011)

As explained earlier in Section 3.4, only the summer months are being considered. An important factor to note is the effect of the ambient radiation transmitted through the glazing. Generally, heat transfer through masonry construction has a large time-lag therefore the effects are not severe. However, since the facade is mostly glazed, the time-la g is assumed to be zero, thus contributing considerably to the ambient radiation components of the global radiation transmitted into the room. The same logic can be used for the winter time when large glazed walls directly contribute to the heating load due to heat loss. Although this is not as severe as the heat gains during the summer because the average winter temperature in the Maltese climate does not drop below 16° (MaltaWeather.com n.d.).

Figure 58 shows an internal photograph of one of the apartments in this building. This apartment is currently for sale and the photograph is displayed on a real-estate website. The clock seen in the image indicates the photo was taken at 16:15. This was further confirmed from the direction of shadows on the terrace. The photos were probably taken at this convenient time so as not to highlight the need to close the South-East blinds due to the direct sun and glare. This photograph clearly demonstrates the developer's aim translated into architecture.

Figure 58: Large glazed windows to frame the view (Engel & Volkers 2013)

7.2. Optimisation

The South-East facade is the crucial element of the building due to the reasons explained in section 6.2. This study will focus on optimising the South-East face of the building only, because the software tool currently does not allow windows on the side facades. The following variables were constrained in order to simulate the correct planning restrictions offered by the site.

Variable	Notation	Value
Floor height	***FH***	3m
Building height	***BH***	24m
Front facade inclination x direction	**IF***x*	0m
Back facade inclination x direction	**BF***x*	0m
Site length	**S***y*	10m
Site width	**S***x*	10m
Top floor relative length	**T***y*	0m
Top floor relative width	**T***x*	0m
Front facade number of windows	**FW***n*	$1 \leqq$ **FW***n* $\leqq 4$
Back facade number of windows	**BW***n*	$1 \leqq$ **BW***n* $\leqq 1$

The approximate dimensions of the site were determined (MEPA n.d.) (Figure 59 (left)) and input as constrained variable values **S***x* and **S***y*. The window face in the rectangular geometrical model was oriented towards the South-East by varying the North offset in the solar geometry panel (Figure 59, Figure 60). The latitude and longitude were set to 35.907185 and 14.508157 respectively, and the greenwich mean time (GMT) solar offset was set to 2 hours.

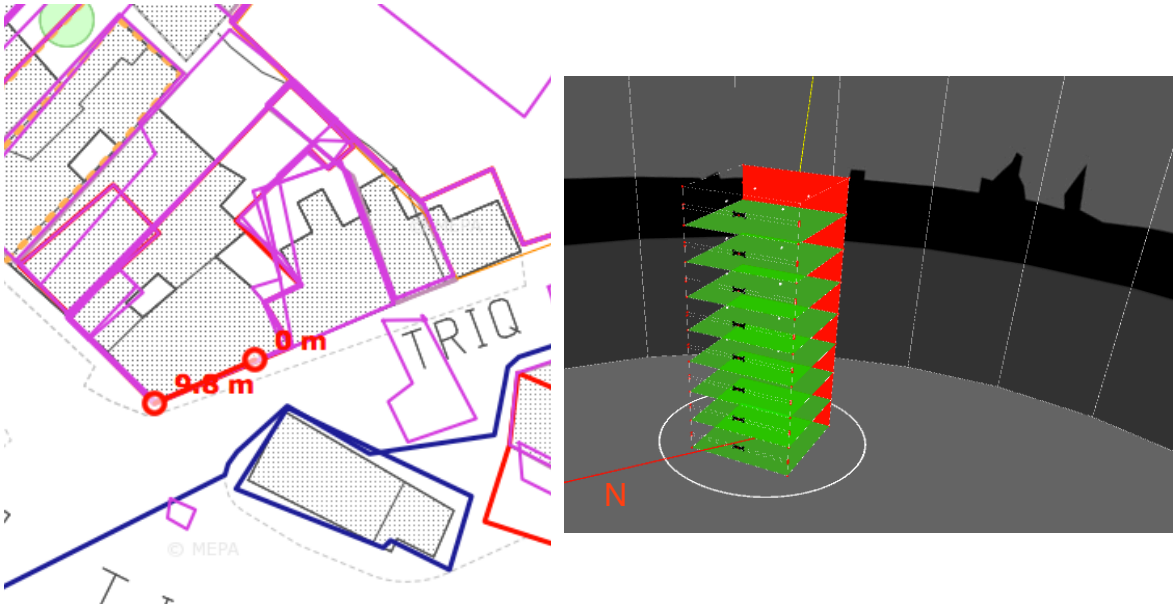

Figure 59: Planning map(left) (MEPA n.d.). Simulation geometry oriented towards the view accordingly (right).

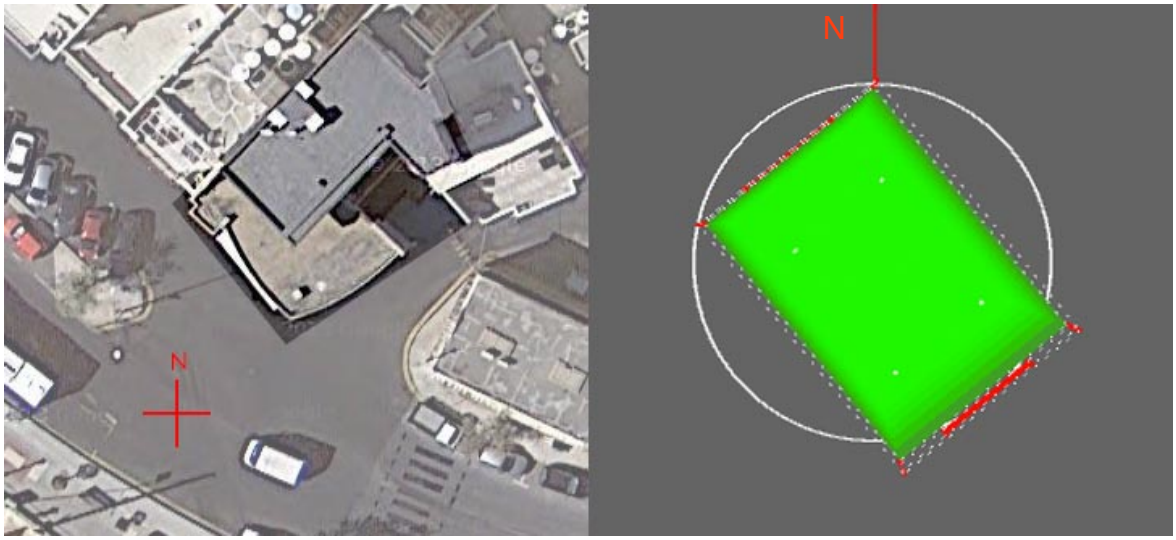

Figure 60: Simulating the existing dimensions (GoogleMaps 2013) by means of the simple geometric model.

The cooling load and view values were of the simplified geometric model were recorded for comparison at a later stage. The monthly cooling load for the entire building uses 11,160 kWh/month. This translates to 1395 kWh/month for each of the eight apartments, which is higher for a typical air-conditioned apartment during the summer months in Malta. However, this calculation assumes that the air-conditioner is running 24 hours a day. The total view value was € 27,617/month which is equivalent to € 3,452/month per apartment. This view component fits well in comparison to the apartments in the neighbouring condominium, sharing very similar elements.

The non-dominated Sorting Genetic Algorithm (GA) was run twice, once with an unconstrained number of windows and once with the number of windows constrained to 1. The width and height of the windows were unconstrained in both runs. Due to strict planning rules, projections outside of the site perimeter are not allowed thus constraining to avoid terraced overhangs. A population size of 450 was used in both cases which was found to allow a good exploration of the Pareto front.

7.3. Results

In both cases, the solutions with large glazed walls produced a lower cooling load than that of the simplified geometric model of the existing glazed walls. This indicates that either an inclined facade or an overhang will reduce the energy consumption yet retain a good view value when compared to the original view value. Furthermore, the sunny floor area obtained from an outward inclined facade such as in solutions G and H in Figure 64 is suitable for a sunny outdoor terrace, which perhaps increases the property value further.

The optimisation with an unconstrained number of windows still attempts to achieve a full glazed wall by maximising the window width variable consequently forming an uninterrupted window (solution C in Figure 62).

The lowest cooling load values were obtained from geometries with the smallest windows. The tilted facade further reduced the cooling load due to either shading or a high solar incident angle. As expected, the highest view values were obtained by means of fully glazed walls. The cooling load difference (Tables 7 & 8) between solution F (Figure 62) and solution L (Figure 64) is interesting to compare. They approximately share an equivalent total glazed area however the cooling load of L is drastically lower probably because the window height of F is not large enough to be shaded by the small overhangs. Since **T***y* and **Off***y* are constrained larger overhangs were not produced.

Long slit windows such as those in solution D (Figure 62) seem produce a high view value. This probably occurs due to allowing more of the sea and sky visible through the windows. The drastic increase in the view values of solutions F and D of an unconstrained number of windows demonstrates this effect. This is probably due to an increased visibility

of the vertical extremes of the view (sea and sky). In this exercise the sea was assigned with the grey tone score before the best thus increasing the view value drastically. Although high in value, this window configuration is not ideal for this skyline scenario because of the interruptions in between.

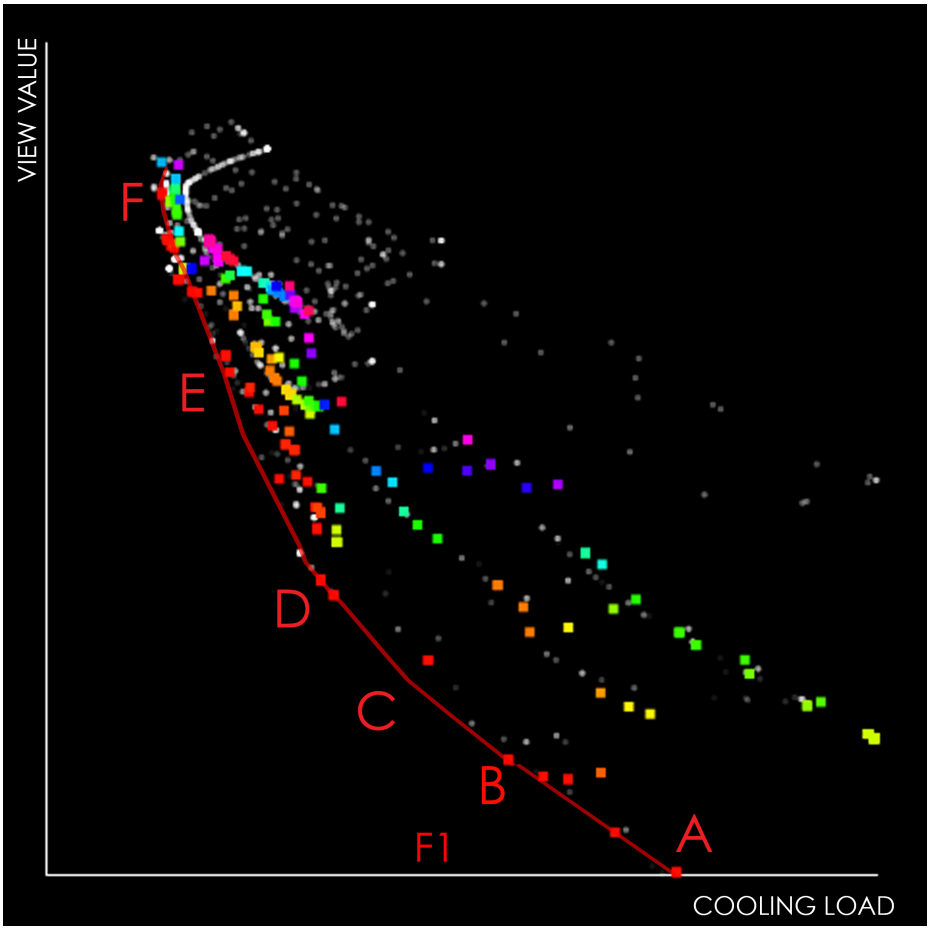

Figure 61: Pareto front (F1) of the third generation with an unconstrained number of windows.

Solution	C (kWh)	V (€/month)
A	5988	38430
B	4870	34910
C	4029	30083
D	3039	26926
E	1948	16115
F	1236	5917

Table 7: Cooling loads and view values of the Pareto solutions in Figure 61.

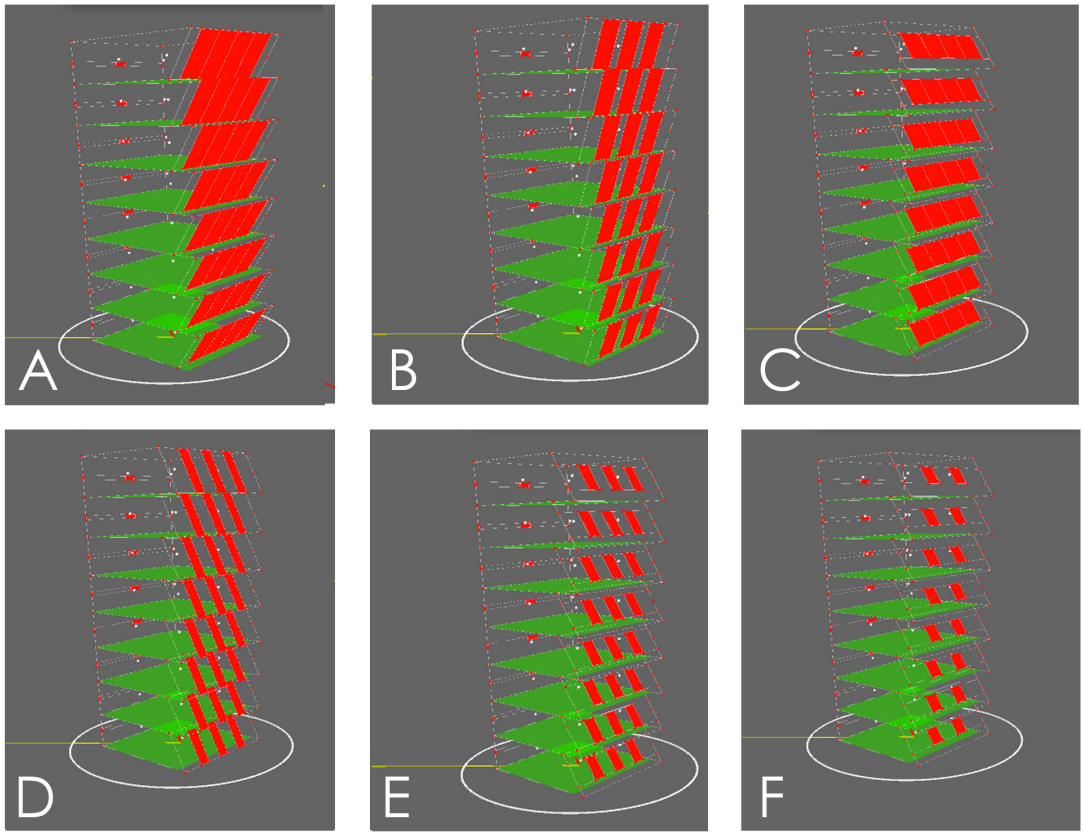

Figure 62: Pareto solutions with an unconstrained number of windows.

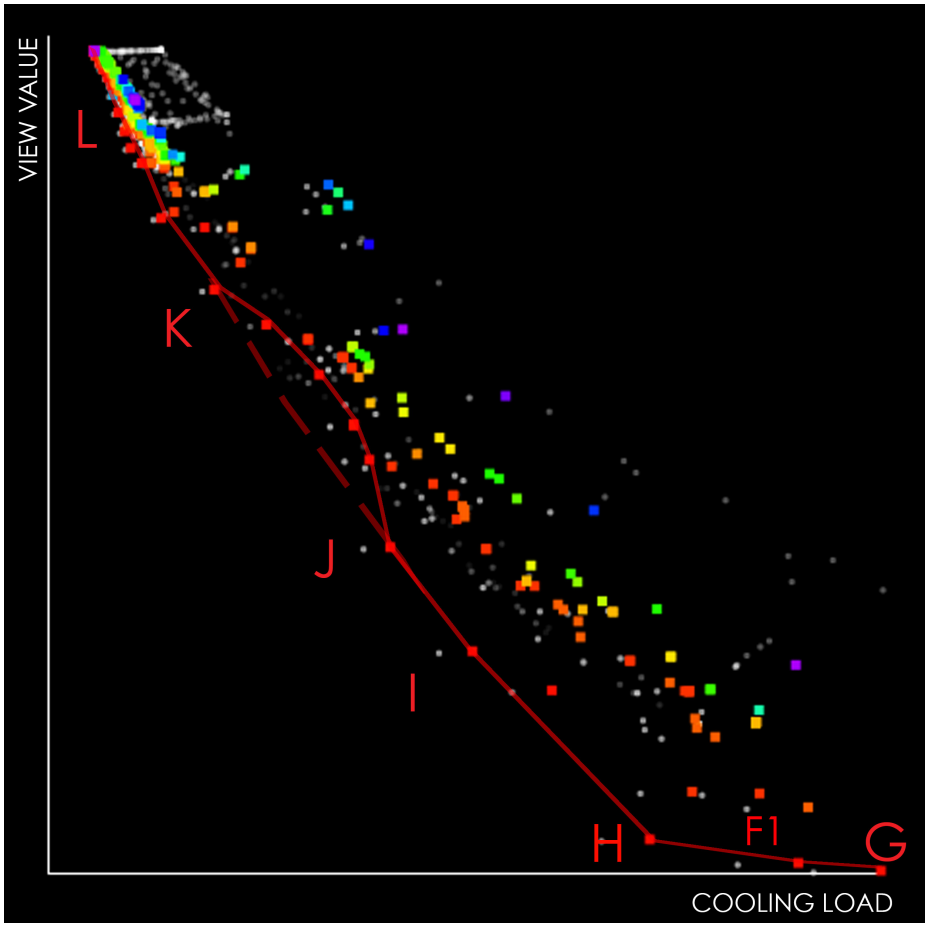

Figure 63: Pareto front (F1) of the third generation with the number of windows constrained.

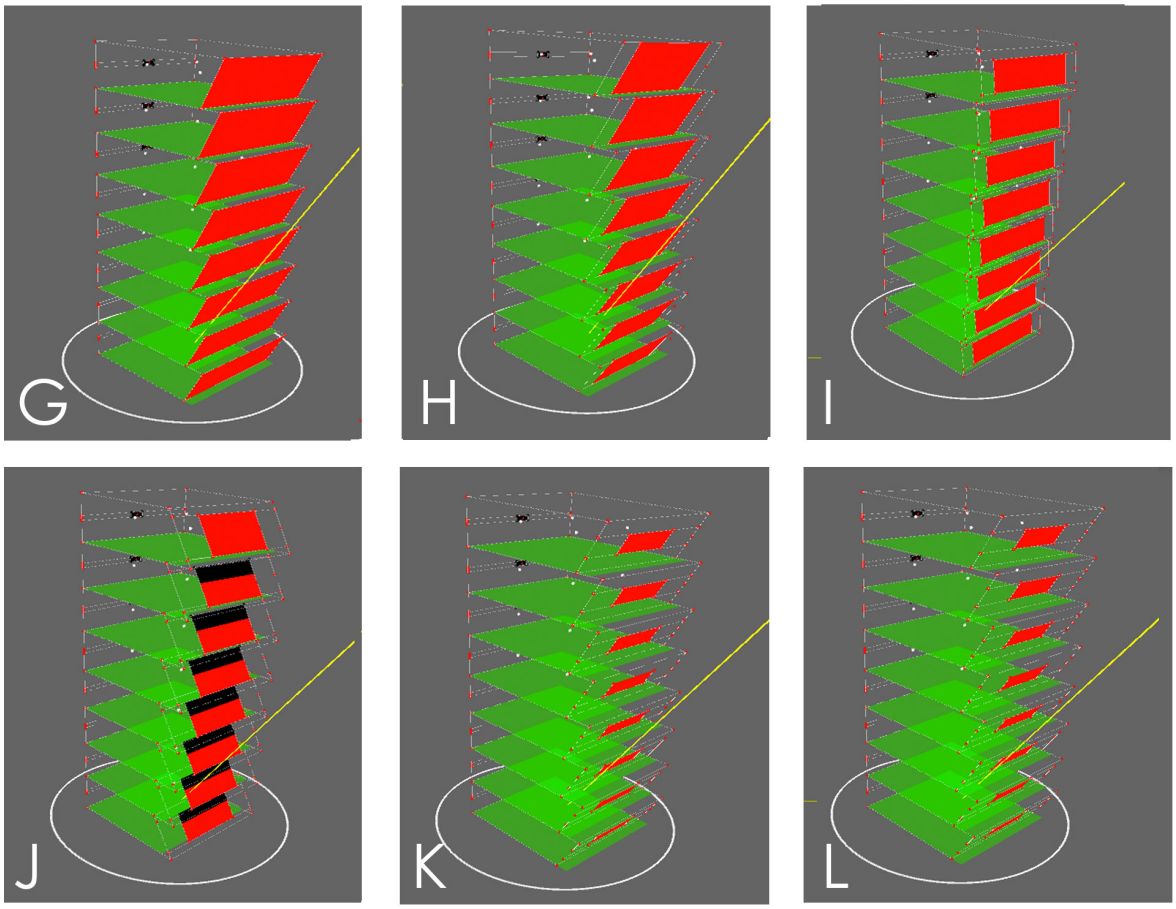

Figure 64: Pareto solutions with the number of windows constrained to 1.

Solution	C (kWh)	V (€/month)
G	8701	33875
H	6293	32689
I	4447	24991
J	3589	20784
K	1758	10364
L	705	2484

Table 8: Cooling loads and view values of the Pareto solutions in Figure 64.

7.4. Reflection on The Case Study Analysis

The results demonstrate that by slightly modifying the geometry of the existing building, potential high energy consumption of a proposed building can be avoided at an early design stage.

8. Conclusion

8.1. Overview

A generative design framework has been developed in the form of an interactive software tool. A simple building geometry simulating a block of developer's apartments was built and parametricised. The variables were chosen with the aim of allowing geometry that shades itself.

The solar position was calculated in order to determine the position of the sun at a given time and location. The position of the sun was then used to calculate the beam component of the global solar radiation. The exact radiation on the non-shaded area of the window was calculated by using a recursive raytracing routine. This checked each window vertex for ray intersection with the above floors and dynamically subdivided the window to calculate the precise radiation. The energy transmitted into the building through the windows took the this radiation and the ambient radiation into account. This was then added to the heat transfer through the roof construction to calculate the cooling load. Various cooling load calculation methods were reviewed and the ASHRAE Admittance method was selected and adapted to a non harmonic temperature variation. A list of typical peak summer temperatures for Malta were stored in an excel sheet and fed to the cooling load calculations.

A monetary value for the view was derived by extracting the component from the rental property of a few selected properties situated in a condominium. A smarter view evaluation method was developed to value a view based on it's contents and fenestration. An image of any selected view, scored prior to the simulation, can be uploaded to the software by the user and the tool is able to score each window based on what is seen from various positions on the apartment floor.

A weighted sum approach (Goldberg and Holland 1988) and a non-dominated Sorting Genetic Algorithm-II (Deb *et al.* 2002) were explored. NSGA-II was implemented because elitism is incorporated by carrying the non-dominated solutions to the next generation until they are dominated by other solutions. An interactive user-interface was developed to

allow the user to explore with the solution space by clicking on the plotted solutions and visualising the corresponding geometry.

The result is a generative software tool that allows the user to interact with the variables and visualise the corresponding geometry a built-in optimiser allows the user to select the population size, constrained variables and to interact with the solutions in the solutions space.

The generative tool has been applied to a case study of a building with large South-East facing glazed windows. The tool suggested tilted glazed walls that reduce the cooling load yet retain a good view value when compared to the current estimated view value. Such a tilt may be applied to buildings of a similar typology and view orientation. These buildings are very common in Malta and have the same design energy consequences.

8.2. Lessons Learned

The choice of variables proved to have great effect on the optimisation in terms of the relationship between the objectives.

Initially, the overhang geometry of the front facade and that of the back facade were controlled by two individual variables. This independence caused the optimisation to yield inhabitable (small) top floors as Pareto solutions. In turn, the very small top floor area increased the field of view of each of the *eyeball* positions on the floor due to their closer proximity to the window, thus increasing the view value which was not valid in such a small space. The independent variables were replaced by two variables controlling the dimensions of the top floor. This related the front and back facade and allowed control over the minimum top floor dimensions. Consequently, the overhangs changed linearly between the top floor and the fixed ground floor (fixed plot dimensions).

Fully glazed walls were only possible if the number of windows was one. The width of a window was controllable for only one window. This caused the optimisation to almost never produce fully glazed wall solutions as the probability was as low as 1/max number of windows. The width of a window was therefore amended to become relative to the

number of windows and the width of the wall. This allowed full glazed walls to be obtained by any number of windows. N windows of maximum width are equivalent to one window of wall height and wall width dimensions.

The spread of the random solutions in the initial population demonstrated to affect the variety of the results. Initially random variable values were generated from a built-in pseudo-random generator in Processing (Fry and C.Reas 2004). However, the initial random population seemed to cluster towards the upper left region of the solution space. This indicated inferior view values due to small window width and height randomly generated values. Normal distribution was therefore introduced to lower the probability of extreme values. This improved the population spread which consequently explored more geometrical combinations to reduce the cooling load. The implementation of a crowding distance calculation in the NSGA as proposed by Deb et al. (2002) may help avoid crowding and improve this variety.

8.3. Results

The window geometry can be seen to morph from one Pareto extreme to the other. The extreme minimised cooling load produces very small fenestration whilst the extreme maximised view, produces floor to ceiling windows of maximum width. In the case of unconstrained number of windows, the latter is equivalent to one window whose width and height correspond to the width and height of the wall.

The aim of the property developer is to yield profit by maximising the view. The developer's approach is not always easy to modify. The selected optimal multi-objective solution needs to therefore 'fully' satisfy the developer's singular objective, yet consider and minimise the cooling load. This provides an idea of the possible objective weightings. The developer's selection criteria could therefore translate to large glazed uninterrupted windows. The Pareto solution with the widest possible uninterrupted glazing and a minimised cooling load (when compared to the original load) could possibly be selected. This description corresponds to some of the Pareto results obtained in the case study test (Chapter 7).

We can conclude that an outward facade tilt can reduce the direct amount of incident solar radiation in the case of legal planning limitations, where floors cannot be projected outwards to create large overhangs, enough to shade at lEast half the window below. This limitation also applies to when property developers achieve the maximum possible volume of the site by not allowing terracing floors. An outward facade tilt is also suitable when inward tilts are not permissible due to limited habitable (constant floor to ceiling height) floor area. The external area caused by an outward tilt may be used as a sunny terrace. In the case of relaxed limitations, a combination of inward tilts and projected overhangs will shade large areas of the windows below.

An estate agency in Malta was contacted to enquire on the methods employed in real estate in order to evaluate the view. The author made reference to the properties within the 'Tigne Point' condominium mentioned in Chapter 4 and received the following reply:

"If a property in Tigne Point is facing Valletta, then it is facing South and would be very sunny. Another factor in higher value." (Bartoli 2013)

This highlights the issues in the traditional approach adopted by many in the real-estate and development industry. The adjective "sunny" is widely misinterpreted for a positive element in building as it is confused for "daylight" (diffused light).

8.4. Further Work

8.4.1. Variables

Future work will explore the possibilities of optimising the choice of variables such as work done by Bouchlaghem (2000).

8.4.2. Fenestration Geometry

The author intends to search for a more flexible approach to allow less restricted fenestration with the aim of framing objects in a view. A similar approach had been reviewed in Chapter 2 (Wright and Mourshed 2009), however the number of variables introduced is too large. Further fenestration shading approaches will also be explored.

8.4.3. View Distance

As discussed in Chapter 2, the distance of an object in a view can be significant to the view, regardless if it is generally labelled as positive or negative. The author would like to explore methods such as sterephotogrammetry to extract the distance from the photograph or by means of a Geographical Information System (GIS).

8.4.4. Ventilation and Daylight

Further developments could take the natural ventilation into consideration when calculating the cooling load. Furthermore, the penetration of daylight through the glazing could also be considered.

8.4.5. Computation

The proposed software tool involves several routines being calculated each time such as the raytracing routine. It would be beneficial to explore the possibility of the implementation of a parallel programming platform such as CUDA which would be ideal to assign jobs such as the ray tracing as they are independent and can be done in parallel.

8.4.6. Other

The developed software tool already allows interaction with the variables and solutions. An added advantage would allow the user to select a non dominated solution from the solution space and manually attempt to improve the objective value. If successful, the user may manually override the achieved solution into the front, and the population is resorted. The new non dominated solution would be carried onto the next generation unless dominated by a better solution.

The implementation of the above may produce a faster and smarter building optimisation tool to provide architects with quick solutions in the early stages of design. The aim is to achieve a number of solutions which maximise both objectives and which in turn still yield a high rental value for the apartments.

References

Agrawal, R.B., Deb, K. & Agrawal, R.B., 1994. Simulated binary crossover for continuous search space.

ASHRAE, 1979. *Cooling and heating load calculation manual.* Atlanta, Georgia: ASHRAE.

Baker, N. & Steemers, K., 1996. LT Method 3.0 — a strategic energy-design tool for Southern Europe. *Energy and Buildings,* 23(3), pp. 251-256, http://dx.doi.org/10.1016/0378-7788(95)00950-7.

Baldwin, S., 2013. Pyongyang from the Yanggakdo Hotel revoling restaurant. Skyscanner.

Bartoli, M., (mbartoli@franksalt.com.mt), 09th September 2013. *RE: View value evaluation in real estate.* Email to Z.X. Conti, (zackxconti@gmail.com).

Bouchlaghem, N., 2000. Optimising the design of building envelopes for thermal performance. *Automation in Construction,* 10(1), pp. 101-112, http://dx.doi.org/10.1016/S0926-5805(99)00043-6.

Bouchlaghem, N.M., 1996. A computer model for the design of window shading devices. *Building Research & Information,* 24(2), pp. 104-107, 10.1080/09613219608727509.

Brizlincot Parish Council, 2009. View 2 from Ashby Road.

Caldas, L., 2008. Generation of energy-efficient architecture solutions applying GENE_ARCH: An evolution-based generative design system. *Adv. Eng. Inform.,* 22(1), pp. 59-70, 10.1016/j.aei.2007.08.012.

Caldas, L. & Norford, L., 2003. Shape Generation Using Pareto Genetic Algorithms: Integrating Conflicting Design Objectives in Low-Energy Architecture. *International Journal of Architectural Computing,* 1(4), pp. 503-515, 10.1260/147807703773633509.

Caldas, L.G. & Norford, L.K., 2002. A design optimization tool based on a genetic algorithm. *Automation in Construction,* 11(2), pp. 173-184, http://dx.doi.org/10.1016/S0926-5805(00)00096-0.

CIBSE, 2006. *CIBSE Guide A: Environmental Design* CIBSE.

Coello, C.A.C., Lamont, G.B. & Van Veldhuisen, D.A., 2007. *Evolutionary algorithms for solving multi-objective problems.* Springer.

Conti, Z.X., 2011. *Parametric Integrated Design Process.* Bachelor of Engineering and Achitecture (Honours), University of Malta.

Day, A., Maidment, G. & Ratcliffe, M., 2000. Cooling degree-days and their applicability to building energy estimation. *CIBSE/AHRAE Conference.*

Deb, K., 2001. Multi-objective optimization. *Multi-objective optimization using evolutionary algorithms*, pp. 13-46,

Deb, K., Pratap, A., Agarwal, S. & Meyarivan, T., 2002. A fast and elitist multiobjective genetic algorithm: NSGA-II. *Evolutionary Computation, IEEE Transactions on,* 6(2), pp. 182-197, 10.1109/4235.996017.

Dubois, M.C. & Science, T.h.i.L.D.o.B., 1997. *Solar Shading and Building Energy Use: A Literature Review.* Lund University.

Duffie, J.A. & Beckman, W.A., 2013. *Solar Engineering of Thermal Processes.* Wiley.

Engel & Volkers, 2013. *Apartment, Sliema, Dining Area* [Online]. Available from: http://www.engelvoelkers.com/mt/east/sliema/east-sliema-apartment-w-01fy46-2423670.729748_exp/?startIndex=15&businessArea=residential&q=sliema&facets=bsnssr%3Aresidential%3B&pageSize=10&language=en&elang=en [Accessed].

Feinberg, J., 2012. *peasycam* [Online]. Available from: http://mrfeinberg.com/peasycam/ [Accessed 15th February 2013 2013].

Frank Salt Real Estate Malta, 2013. *Property Website* [Online]. Malta. Available from: www.franksalt.com.mt [Accessed 9th September 2013].

FrankSaltRealEstateMalta, 2013. *Property Website* [Online]. Malta. Available from: www.franksalt.com.mt [Accessed 9th September 2013].

Freemeteo, 2012. *Weather Forcast Valletta: Weather History: Daily Archive* [Online]. Available from: http://freemeteo.com/default.asp?pid=20&gid=2562305&sid=165970&la=1&lc=1&nDate=18/7/2012 [Accessed 15-03-2013 2013].

Fry, B. & C.Reas, 2004. *Processing* [Online]. Massachusetts institute of Technology. Available from: http://www.processing.org [Accessed].

Gagne, J.M.L. & Andersen, M., 2010. Multi-Objective FaÁade Optimization for Daylighting Design Using a Genetic Algorithm. *SimBuild 2010 - 4th National Conference of IBPSA-USA*. New York.

GeographyWorld, 2013. *Using Latitude and Longitude - Lesson 1* [Online]. Available from: http://geographyworldonline.com/tutorial/lesson1.html [Accessed 8th September 2013].

Goldberg, D. & Holland, J., 1988. Genetic Algorithms and Machine Learning. *Machine Learning,* 3(2-3), pp. 95-99, 10.1023/a:1022602019183.

GoogleMaps, 2013. *35.907185,14.508157* [Online]. Available from: https://maps.google.co.uk [Accessed 09th September 2013].

Gundimeda, H., 2005. Hedonic price method–A Concept Note. Madras School of Economics: Chennai.

Haddock, J., 2013. Birchills foundry/power station.

Honsberg, C. & Bowden, S., 2009. *PVCDROM* [Online]. Available from: http://pvcdrom.pveducation.org/index.html [Accessed 13th February 2013].

Hottel, H. & Woertz, B., 1942. Performance of flat-plate solar-heat collectors. *Journal Name: Trans. ASME (Am. Soc. Mech. Eng.); (United States); Journal Volume: 64*, p. Medium: X; Size: Pages: 91,

Hottel, H.C., 1976. A simple model for estimating the transmittance of direct solar radiation through clear atmospheres. *Solar Energy,* 18(2), pp. 129-134, http://dx.doi.org/10.1016/0038-092X(76)90045-1.

Ismail, F.S., Yusof, R. & Khalid, M., 2011. Self organizing multi-objective optimization problem. *International Journal of Innovative Computing, Information and Control,* 7(1), pp. 301-314,

JKGroup, 2013. *Real Estate Website - Apartments in Tigne* [Online]. Available from: www.jkproperties.com.mt [Accessed 10th September 2013].

Kahneman, D., 2011. *Thinking, fast and slow.* Macmillan.

Konak, A., Coit, D.W. & Smith, A.E., 2006. Multi-objective optimization using genetic algorithms: A tutorial. *Reliability Engineering & System Safety,* 91(9), pp. 992-1007, http://dx.doi.org/10.1016/j.ress.2005.11.018.

Lake, I.R., Lovett, A.A., Bateman, I.J. & Langford, I.H., 1998. Modelling environmental influences on property prices in an urban environment. *Computers, Environment and Urban Systems,* 22(2), pp. 121-136, http://dx.doi.org/10.1016/S0198-9715(98)00012-X.

Lartigue, B., Lasternas, B. & Loftness, V., 2013. Multi-objective optimization of building envelope for energy consumption and daylight. *Indoor and Built Environment*, 10.1177/1420326x13480224.

Liu, C.-a. & Wang, Y., 2008. A new dynamic multi-objective optimization evolutionary algorithm. *International Journal of Innovative Computing Information and Control,* 4(8), pp. 2087-2096,

MaltaWeather.com, n.d. *Malta's Climate* [Online]. Malta. Available from: http://www.maltaweather.com/information/maltas-climate/ [Accessed 11/10/13 2013].

Marion, W. & Wilcox, S., 1995. Solar radiation data manual for buildings. p. 248.

MEPA, M.E.P.A., n.d. *MEPA Map Server* [Online]. Available from: http://mapserver.mepa.org.mt/frame.php?site=malta_internet&lang=en&group=public&resol=2 [Accessed 15th September 2013].

Miller, B.L. & Goldberg, D.E., 1996. Genetic Algorithms, Selection Schemes, and the Varying Effects of Noise. *Evolutionary Computation,* 4(2), pp. 113-131, 10.1162/evco.1996.4.2.113.

Murata, T. & Ishibuchi, H., Year. MOGA: multi-objective genetic algorithms. In: Evolutionary Computation, 1995., IEEE International Conference on, Nov. 29 1995-Dec. 1 1995 1995. p. 289.

O'Callaghan, P.W. & Probert, S.D., 1977. Sol-air temperature. *Applied Energy,* 3(4), pp. 307-311, http://dx.doi.org/10.1016/0306-2619(77)90017-4.

Oracle, 2011. Java.

Perez, R., Ineichen, P., Seals, R., Michalsky, J. & Stewart, R., 1990. Modeling daylight availability and irradiance components from direct and global irradiance. *Solar Energy,* 44(5), pp. 271-289, http://dx.doi.org/10.1016/0038-092X(90)90055-H.

Prek, M. & Butala, V., 2010. Base Temperature and cooling degree days. *CLIMA 2010.* Antalya, Turket.

Ruivo, C.R., Ferreira, P.M. & Vaz, D.C., 2013. Prediction of thermal load temperature difference values for the external envelope of rooms with setback and setup thermostats. *Applied Thermal Engineering,* 51(1–2), pp. 980-987, http://dx.doi.org/10.1016/j.applthermaleng.2012.11.005.

Santos, F.d., 2011. Available from: http://www.panoramio.com/photo/47054386 [Accessed 15th September 2013].

Schlegel, A., 2012. processing library, controlP5. 2.0.4 ed.

Shea, K., Sedgwick, A. & Antonuntto, G., 2006. Multicriteria Optimization of Paneled Building Envelopes Using Ant Colony Optimization. In: I.C. Smith, ed. *Intelligent Computing in Engineering and Architecture.* Springer Berlin Heidelberg, pp. 627-636.

Shellard, J., 2006. Modelling Dimensions of Height and View at Melbourne's Docklands. *Pacific Rim Real Estate Society 12th Annual Conference.* New Zealand.

Spitler, J.D., McQuiston, F.C. & Lindsey, K.L., 1993. THE CLTD/SCL/CLF COOLING LOAD CALCULATION METHOD. *ASHRAE Transactions.* American Society of Heating, Refrigerating and Air-Conditioning Engineers, Inc, pp. 183-192.

Vassallo, J., 17th July 2013. *RE: The value of the view in the Tigne Point condominium.* Telephone Call to Z.X. Conti,

Wright, J. & Mourshed, M., 2009. Geometric optimization of fenestration. *Proceedings of the eleventh International IBPSA Conference (Building Simulation 2009)*. Glasgow, Scotland: © IBPSA, pp. 920-927.

Wright, J.A., Brownlee, A.E.I., Mourshed, M.M. & Wang, M., 2013. Multi-objective optimization of cellular fenestration by an evolutionary algorithm. *Journal of Building Performance Simulation*, pp. 1-19, 10.1080/19401493.2012.762808.

Yu, S.M., Han, S.S. & Chai, C.H., 2007. Modeling the value of view in high-rise apartments: a 3D GIS approach. *Environment and Planning B: Planning and Design,* 34(1), pp. 139-153,

Zitzler, E., Laumanns, M. & Thiele, L., 2001. SPEA2: Improving the Strength Pareto Evolutionary Algorithm.

Appendix A

A. Calculation of Global Solar Radiation

This appendix explains how the global solar radiation is calculated in terms of its components. It is necessary to determine the direction of the beam in order to determine its intensity at the specific location and time.

A.1. Direction of Beam Radiation

A.1.1. Calculating the elevation angle α

The elevation angle α is the angular height of the sun's position in the sky measured from the horizontal. This can be determined by,

$$\alpha = \sin^{-1}\left[\sin\delta\sin\varphi + \cos\delta\cos\varphi\cos(HRA)\right]$$

where,

φ is the latitude measured in degrees,

HRA is the hour angle ,

δ is the declination angle of the earth measured in degrees.

(Honsberg and Bowden 2009)

Declination δ is the tilt of the earth. This varies with the season where it reaches a maximum of 23.45 on June 21 and a minimum of -23.45 on December 22. δ is zero at the equinoxes (March 22 and September 23), positive during the Northern hemisphere summer and negative during the Northern hemisphere winter (Honsberg and Bowden 2009).

Figure 57 clearly visualises the relationship between the declination angle δ and the elevation α .

The declination angle δ is measured in degrees and may be calculated by,

$$\delta = \sin^{-1}\left\{\sin(23.45^{O})\sin\left[\frac{360}{365}(d-81)\right]\right\}$$

where, d is equivalent to the number of days passed since January 1st. θ_z in Figure 65 represents the solar zenith angle which can be expressed as $\alpha = 90^{\circ} - \theta_z$

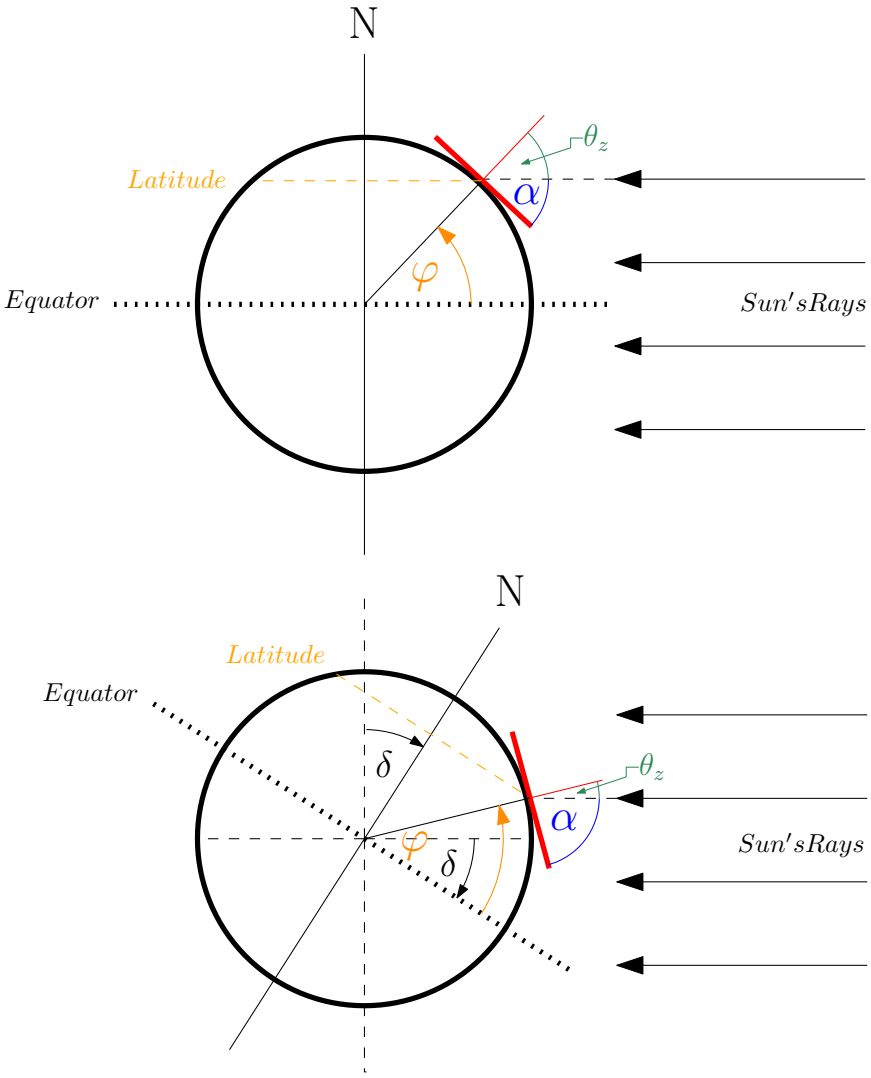

Figure 65: Declination angle explained.

The hour angle HRA can be defined as the conversion from local solar time into the angle of the sun's planar path 'travelled' in the sky (Figure 66). HRA at solar noon is equivalent to 0^{O} . Since the earth rotates at 15^{O} per hour, each hourly movement of the sun in the sky away from solar noon, corresponds to an angular motion of 15 degrees.

$$HRA = 15^{O}(LST - 12)$$

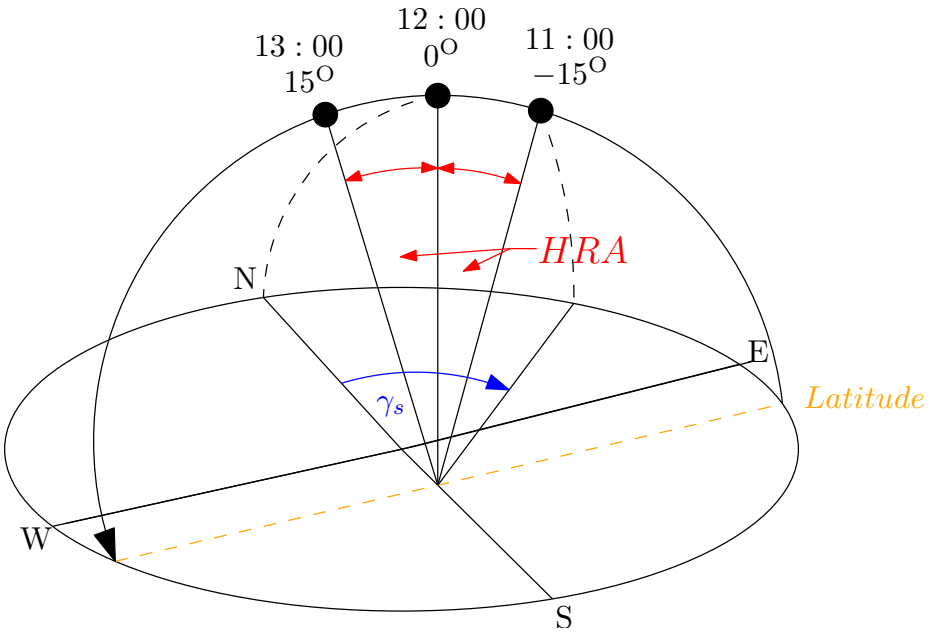

Figure 66: The HRA explained.

Local solar time LST is the corrected version of the local time LT where the correction factors consist of the time correction factor TC and local standard time meridian LSTM. LST is slightly longer than LT due to the eccentricity of the earth's orbit and due to adjustments such as time zones and daylight savings. The sun is highest in the sky at twelve noon LST (Honsberg and Bowden 2009).

$$LST = LT + \frac{TC}{60}$$

where,

$$TC = 4(Longitude - LSTM) + EoT$$

The local solar time meridian LSTM is a special longitude to which reference is made for particular time zone. This is similar to the Prime Meridian used for Greenwich Mean Time GMT. LSTM can be determined as follows,

$$LSTM = 15^{O}.\Delta T_{GMT}$$

The equation of time EoT is what corrects the eccentricity of the Earth's orbit and axial tilt is defined as,

$$EoT = 9.87\sin(2B) - 7.53\cos(B) - 1.5\sin(B)$$

where,

$$B = \frac{360}{365}(d - 81) \quad \text{(measured in degrees)}$$

Figure 67 visualises the plotted time correction EoT throughout the year (Honsberg and Bowden 2009). The non uniform shape of the curve indicates the eccentricity of the Earth's elliptical orbit.

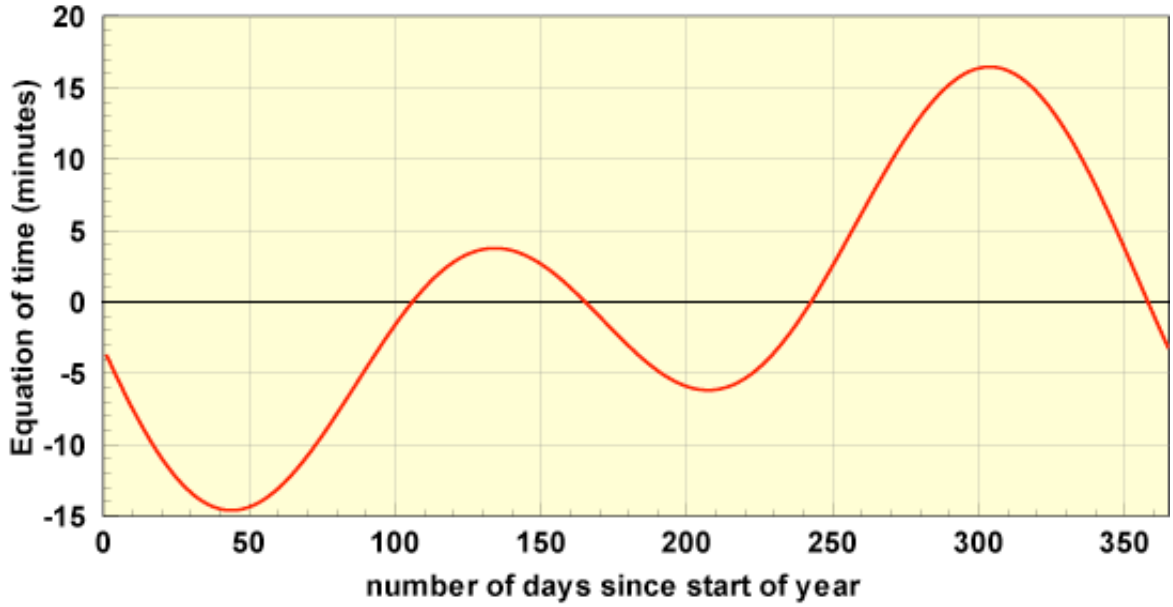

Figure 67: Plotted EoT (Honsberg and Bowden 2009)

The hour angle HRA can therefore be defined as,

$$HRA = 15^{O}\left\{\left(LT + \frac{\left(4\left(Longitude - \left(15^{O}.\Delta T_{GMT}\right)\right) + \left(9.87\sin\left(2\left(\frac{360}{365}(d-81)\right)\right) - 7.53\cos\left(\frac{360}{365}(d-81)\right) - 1.5\sin\left(\frac{360}{365}(d-81)\right)\right)\right)}{60}\right) - 12\right\}$$

A.1.2. Calculating The Latitude φ

The latitude φ is defined as the angular location of a position on the Earth's surface North or South of the equator (Duffie and Beckman 2013) (Figure 68). The North is regarded as positive.

Therefore,

$$-90^{O} \leq \varphi \leq 90^{O}$$

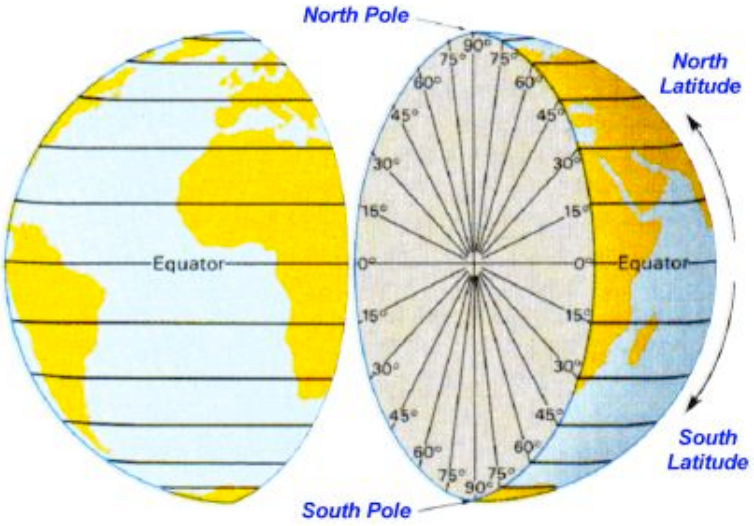

Figure 68: Latitude angles (GeographyWorld 2013)

The elevation angle α can therefore be calculated as a function of φ, δ and HRA.

Calculating The Azimuth Angle γ_s

The azimuth angle γ_s is the clockwise angle from the North to the position of the sun on the horizontal plane on the earth's surface and can be calculated by the following equation:

$$\gamma_s = \cos^{-1}\left[\frac{\sin\delta\cos\varphi - \cos\delta\sin\varphi(HRA)}{\cos\alpha}\right]$$

where,

before noon $(HRA < 0) \Rightarrow \gamma_s$

after noon $(HRA > 0) \Rightarrow 360^{O} - \gamma_s$

$$\vec{D} = (\sin\gamma_S i,\ \cos\gamma_S j,\ \sin\alpha k)$$

The direction vector $\vec{D}$ of the sun can therefore be defines as follows.

A.2. Global Solar Radiation

The global solar radiation incident on a surface I_{SG} is composed of three main components. These are the direct beam radiation I_B, the diffused sky radiation I_S and the reflected ground radiation I_R. Therefore, I_{SG} can be defined as,

$$I_{SG} = I_B \cos\theta + I_S + I_R$$

where,

θ is the angle of solar incidence between the direction of sun's rays (direct beam) to the normal of a horizontal surface.

A.2.1. Calculation of Direct Beam I_B

The direct beam component is equivalent to the intensity of the solar radiation post penetration of the atmosphere, right before it reaches a horizontal surface. The scattering and absorption of the extraterrestrial beam through the atmosphere vary with time due to the varying atmospheric conditions and air mass. Duffie & Beckman (2013) suggest to assume clear sky conditions. Hottel (1942) presents a model for calculating the clearly sky direct beam component on a horizontal surface which assumes clear atmospheric conditions. The climate in Malta suggests mostly clear skies during the summer months as considered in this dissertation thus, Hottel's (1942) model is suitable. This model suggest that direct beam I_B is composed of the product of the extra terrestrial radiation G_{ON} which refers to the radiation from the sun prior to penetrating the earth's atmosphere, the atmospheric transmittance τ_a which caters for the effects of scattering and absorption of the beam radiation as it penetrates the atmosphere, and the zenith angle θ_Z which is the angle between the direction of the beam and the normal of the horizontal surface ($\pi/2 - \alpha$). I_B is defined as,

$$I_B = G_{ON} \tau_A \cos\theta_Z$$

Duffie & Beckman (2013) present G_{ON} by the following equation.

$$G_{ON} = G_{SC}\left(1 + 0.033\cos\frac{360n}{365}\right)$$

where,

G_{ON} is the extraterrestrial radiation, measured on the plane perpendicular to the direction of the beam radiation on the *n*th day of the year (Duffie and Beckman 2013).

G_{SC} is the solar constant assumed as 1367 W/m^2 . This is the radiation leaving the sun. This value is said to vary slightly non-periodically however assumed as a constant (Figure 69).

This equation caters for the variation in G_{ON} flux which is caused by the variation in the distance between the sun and the earth due to the earth's elliptical orbit.

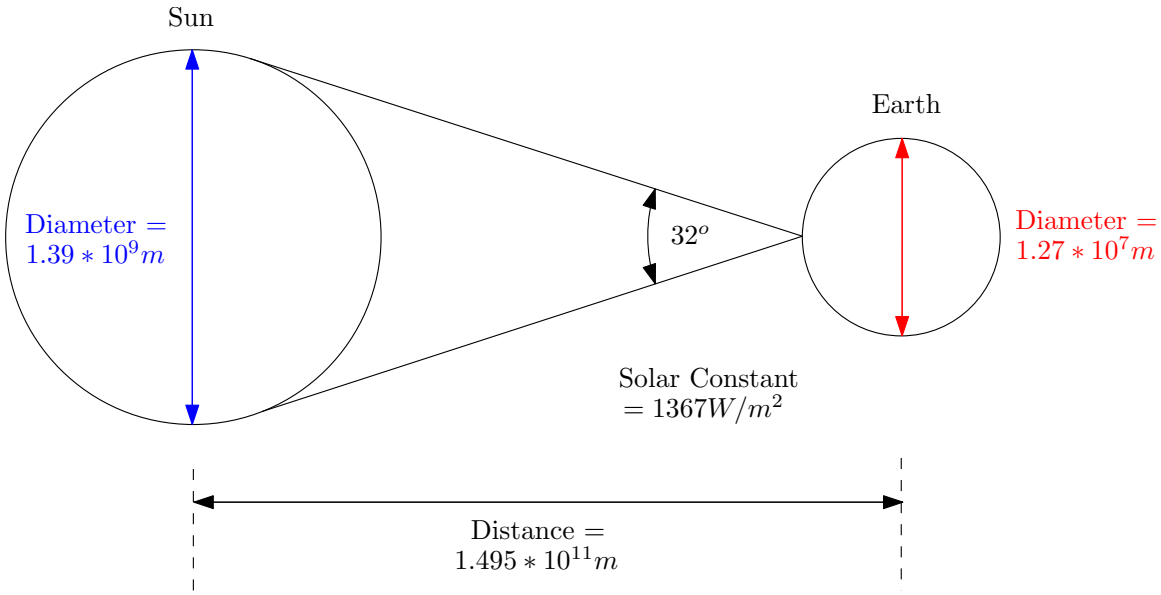

Figure 69: Sun-earth distance (adapted from Duffie and Beckman (2013)).

Hottel (1976) suggests the following quadratic equations for determining the atmospheric transmittance τ_a.

$$a_0 = 0.4237 - 0.00821(6 - A)^2$$
$$a_1 = 0.5055 + 0.00595(6.5 - A)^2$$
$$k - 0.2711 + 0.01858(2.5 - A)^2$$

where,

A is the altitude of the horizontal surface.

The coefficients of the above equations were derived from empirically obtained values for transmittance of solar radiation directly through the 1962 standard atmosphere to a surface at altitude A by means of the following relationship:

$$\tau_B = a_0 + a_1 \exp\left(\frac{-k}{\cos\theta_Z}\right)$$

The constants a_0 , a_1 and k cater for atmospheric visibility based on a value of 23km. These are given for altitude less than 2.5km (Hottel 1976) which is suitable for the Maltese geography. Correction factors are multiplied to a_0 , a_1 and k respectively in order to adapt to climate types (Table 9). The midlatitude climate correction factors were applied for Malta. However, these can be easily replaced to cater for other climates.

Climate Type	r_0	r_1	r_k
Tropical	0.95	0.98	1.02
Midlatitude summer	0.97	0.99	1.02
Subarctic summer	0.99	0.99	1.01
Midlatitude winter	1.03	1.01	1.00

[a] From Hottel (1976).

Table 9: Climate type correction factors (Hottel as cited in Duffie and Beckman

The direct beam component can therefore be calculated for any provided zenith angle θ_Z .

A.2.2. Calculation of Sky Radiation I_S

The sky radiation I_S caters for the diffused radiation from the sky. I_S can be determined by the following equation (Perez *et al.* 1990).

$$I_S = I_{DH}\left[0.5(1-F_1)(1+\cos\beta)+F_1\frac{a}{b}+F_2\sin\beta\right]$$

Where,

I_{DH} is the diffuse horizontal radiation,

F_1 is the circumsolar anisotropy coefficient, function of the sky. This refers to the glowing ring around the sun in the sky.

F_2 is the horizon/zenith anisotropy coefficient, function of sky condition

β is the tilt of the surface from the horizontal

a is the angle of the incident angle of the direct beam. If the angle is negative, a is 0

b is equivalent to $\cos\theta_Z$. If $\cos\theta_Z$ < 0.087, then b is 0.087

(Marion and Wilcox 1995)

The diffuse horizontal radiation I_{DH} component is the radiation from the sky (not from the direct beam) as a result of absorption and scattering of the direct beam. It is assumed for a horizontal surface. This can be calculated by the following equation.

$$I_{DH} = I_{GH} - I_B\sin(\alpha)$$

Where,

I_{GH} is the global horizontal radiation obtained by

$$I_{GH} = I_{DH} + I_B\cos\theta_Z$$

F_1 and F_2 are brightening coefficients

$$F_1 = f_{11} + f_{12}\Delta + \frac{\pi\theta_Z}{180} f_{13}$$

$$F_2 = f_{21} + f_{22}\Delta + \frac{\pi\theta_Z}{180} f_{23}$$

where ,

$$\Delta = I_{DH} \frac{AM}{G_{ON}}$$

The air mass *AM* can be defined as the length of the path travelled by the direct beam through the atmosphere. The air mass quantifies the reduction in the beam intensity due to absorption and scattering. Figure 70 visualises the relationship between the zenith angle θ_Z and the length of the path travelled through the atmosphere. This is why the intensity of the sun during the winter is lower than that in summer because the tilt in the earth (declination angle δ) produces a longer path to travel through the atmosphere thus more of the direct beam is absorbed. *AM* is determined by the following equation (Honsberg and Bowden 2009)

$$AM = \frac{1}{\cos\theta + 0.50572\left(96.07995 - \theta\right)^{-1.6364}}$$

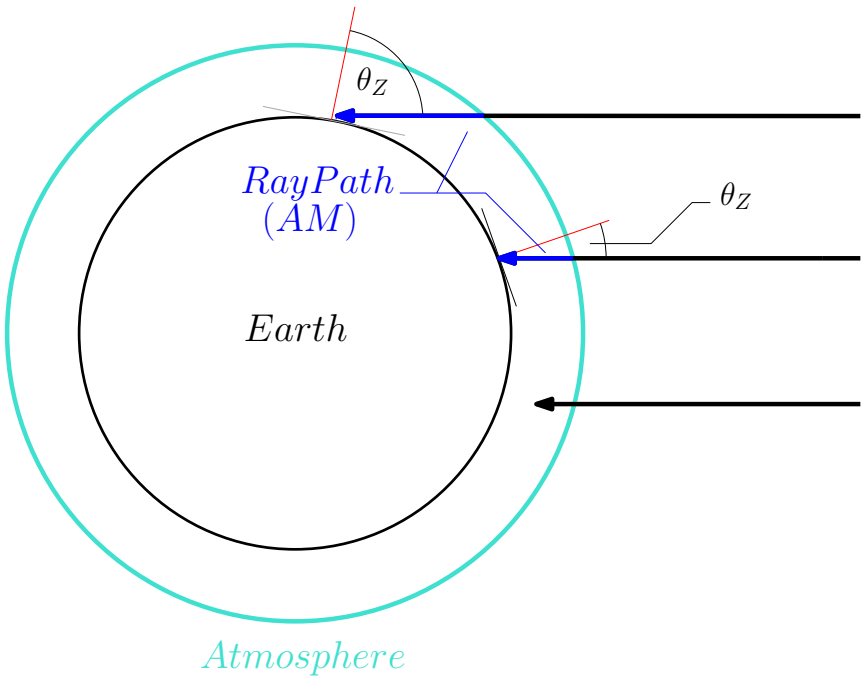

Figure 70: Air mass and zenith angle.

The *f* values are obtained from the following table (Table 10) and ε which is a function of the hour's diffuse radiation and normal incidence beam (Perez et al., as cited in Duffie and Beckman 2013).

Table 2.16.1 Brightness Coefficients for Perez et al. Anisotropic Sky[a]

Range of ε	f_{11}	f_{12}	f_{13}	f_{21}	f_{22}	f_{23}
0 - 1.065	–0.196	1.084	–0.006	–0.114	0.180	–0.019
1.065 - 1.230	0.236	0.519	–0.180	–0.011	0.020	–0.038
1.230 - 1.500	0.454	0.321	–0.255	0.072	–0.098	–0.046
1.500 - 1.950	0.866	–0.381	–0.375	0.203	–0.403	–0.049
1.950 - 2.800	1.026	–0.711	–0.426	0.273	–0.602	–0.061
2.800 - 4.500	0.978	–0.986	–0.350	0.280	–0.915	–0.024
4.500 - 6.200	0.748	–0.913	–0.236	0.173	–1.045	0.065
6.200 - ↑	0.318	–0.757	0.103	0.062	–1.698	0.236

[a] From Perez et al. (1988).

Table 10: Brightness Coefficients (Perez *et al.* 1990)

A.2.3. Calculation of Ground Reflected Radiation I_R

I_R is the radiation reflected from the ground from the sky. I_R is a function of the global horizontal radiation I_H , the tilt of the surface β and the albedo ρ which is the ground reflectivity. ρ varies for different materials. A value of 0.12 corresponding to concrete is being assumed as the ground material for the building typology being considered in this dissertation.

$$I_R = 0.5\rho\, I_H(1-\cos\beta)$$

Therefore, I_T can be determined for any solar incident angle $\cos\theta$, on any surface,

$$\because \quad I_{SG} = I_B\cos\theta + I_S + I_R$$